The PHILOSOPHICAL MAGAZINE

FIRST PUBLISHED IN 1798

L. 44 SEVENTH SERIES No. 358 November 1953

A Journal of Theoretical Experimental and Applied Physics

PRICE 15s. 0d.
Annual Subscription £8 0s. 0d. payable in advance

D AND PUBLISHED BY TAYLOR & FRANCIS LTD., RED LION COURT, FLEET ST., LONDON E.C.4

CXXVII. *Nuclear Reactions Produced by the Bombardment of Boron by Low Energy Alpha-Particles*

By E. S. Shire, J. R. Wormald, G. Lindsay-Jones, A. Lundén and A. G. Stanley
Cavendish Laboratory, Cambridge*

[Received July 9, 1953]

Abstract

Boron targets have been bombarded by helium nuclei of energy between 1 and 2 Mev. Resonances for production of gamma-rays and protons from the reactions $^{10}B(\alpha p)^{13}C^*$, of protons from $^{10}B(\alpha, p)^{13}C$, and of deuterons from $^{10}B(\alpha d)^{12}C$ were observed at 1·13, 1·24, 1·39, 1·51, 1·64, 1·68 and 1·83 Mev. Resonances for neutrons from the $^{10}B(\alpha n)^{13}N$ reaction were detected at 1·51, 1·64 and 2·05 Mev. Angular distributions of the particles emitted were measured at 1·13, 1·51, 1·64, 1·68 and 1·83 Mev and spins and parities of 4^-, 3^-, 4^+, 4^- and 4^+ tentatively assigned to the corresponding ^{14}N levels. Spins and parities of $3/2^-$ and $5/2^+$ were confirmed for the second and third excited levels of ^{13}C. Reaction cross sections and reduced level widths were obtained for alpha-particle energies of 1·51 and 1·64 Mev. A resonance in the $^{11}B(\alpha p)^{14}C$ reaction was found at 1·58 Mev alpha-particle energy.

§ 1. Introduction

We have studied the reactions which occur when boron is bombarded with singly charged helium ions of energy between 1 and 2 Mev. ^{10}B is of particular interest as a target for alpha-particle bombardment in this energy region because the compound nucleus formed can break up in a number of different ways; by emission of neutrons to form ^{13}N, deuterons to form ^{12}C, or protons to form ^{13}C, either in the ground state or in one of the first three excited states. By measuring the angular distributions of the emitted particles we have been able to obtain spins and parities of certain states of the ^{14}N nucleus and of the four lowest states of ^{13}C.

Talbott and Heydenburg (1953) have studied the gamma-rays from $^{13}C^*$ produced in the reaction $^{10}B(\alpha, p\gamma)^{13}C^*$ and have found several resonances at alpha-particle energies below 3 Mev. The production of protons and deuterons from the reactions $^{10}B(\alpha p)^{13}C$ and $^{10}B(\alpha d)^{12}C$ has been studied for alpha-particles of 7·45 and 6·64 Mev energy by Creagan (1949) and Perkin (1950) who reported a number of proton groups

* Communicated by the Authors.

corresponding to various levels in the residual ^{13}C nucleus. Neutrons from $^{10}B(\alpha n)^{13}N$ were found by Rogers *et al.* (1952) who used polonium alpha-particles, and steps in the thick target yield were observed by Heydenburg (see Ajzenberg and Lauritsen 1952 a) at $E_\alpha = 1{\cdot}5$, $2{\cdot}3$ and $2{\cdot}7$ MeV.

§ 2. Experimental Method and Apparatus

We made all measurements with a beam of singly charged helium ions produced by our electrostatic generator. We did not attempt to obtain very accurate absolute measurements of the energy of these ions but we believe their energy was homogeneous and constant to about 1 kev during any one measurement. The radio-frequency ion-source gave a very steady beam of a few microamps of target current.

We used thin targets of separated boron isotopes about $5\,\mu g\ cm^{-2}$ thick on thick copper or silver backing. They were normally run at about 150°C to prevent carbon deposits.

2.1. *Gamma-ray Measurements*

To obtain gamma-ray intensities we used both a sodium-iodide crystal with a photo-multiplier, and a Geiger counter. The former was usually employed to obtain gamma-ray yield curves, but the latter was more stable over long periods of time and was usually used as a monitor during experiments on particle angular distributions. We analysed the gamma-radiation by using the crystal and multiplier in conjunction with a pulse-analyser of the type described by Hutchinson and Scarrott (1951), calibrating the system by radiations from radioactive sources and from known (p, γ) and (α, nγ) reactions.

2.2. *Charged Particle Measurements*

Charged particles were observed with three kinds of apparatus. To detect long-range protons we used a proportional counter, short-range particles being stopped by an aluminium foil equivalent to 18 cm of air. For protons of shorter range and for deuterons we used either an analysing magnet fitted with a zinc-sulphide screen and photo-multiplier, or a double ionization chamber. The magnetic analyser had 54° inflexion focusing with an energy resolution of about 8% and a solid angle of acceptance of 4×10^{-4} steradian.

The ionization chamber, which we filled with pure argon to about one atmosphere pressure, is shown in outline in fig. 1. Electrons, produced by protons, P, entering the chamber through the window, W, were accelerated through the grid, G. The two sets of small pulses arising from electrons intercepted by electrodes C_1 and C_2 were amplified about twenty times and then mixed in opposition. By suitable adjustment of the relative amplification of the two sets of pulses we were able to arrange that only protons stopping opposite C_1 gave an output pulse; longer range particles passed both C_1 and C_2 producing no output.

We used mica foils to alter the range in the chamber of particles to be recorded and moved C_1 and C_2 parallel to themselves to provide the fine adjustment necessary to bring the end of the range opposite the gap between C_1 and C_2. We were sometimes able to separate the second fastest group of protons from faster and slower groups by connecting the electrodes C_1 and C_2 effectively in parallel instead of in opposition, or by using one electrode only. The slower groups were then stopped before reaching C_1 while the fastest group of protons gave pulses small enough for adjustment of the scaler discriminating voltage to exclude them. The advantage of this ionization chamber over the magnetic-analyser lay mainly in the larger solid angle which could be used, though its energy resolution was not as good.

Fig. 1

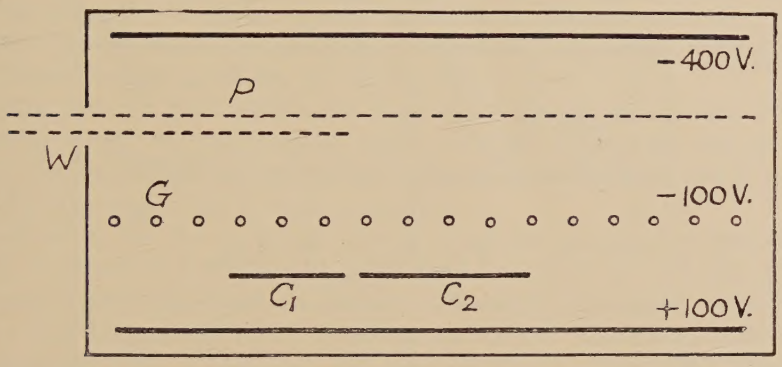

Differential ionization chamber. For details see text.

2.3. *Neutrons*

To detect neutrons we used a zinc-sulphide-plastic phosphor and a photo-multiplier as described by Hornyak (1952), setting the discriminator bias high enough to prevent detection of gamma-rays of energy less than 6 MeV. We placed this detector in line with the incident alpha-particle beam so that it subtended a solid angle of about three steradians. To enable us to compare the neutron yield with the yield of other particles, R. Edge found the absolute cross section of the $^{10}B(\alpha n)^{13}N$ reaction for an alpha-particle energy of 1·51 MeV by measuring the production of radioactive manganese when the neutrons were absorbed in sodium permanganate solution.

2.4. *Angular Distributions*

We measured the angular distributions of charged particles by mounting the proportional counter, the ionization chamber or the magnetic-analyser so that each could be moved over an angular range of 20° to 160° relative to the incident helium-ion beam without shutting down the electrostatic generator. We could not as a rule work at angles forward of 90°. Most

distributions were measured with only the most suitable detector for that distribution, but a few measurements were made both with the magnetic-analyser and with the ionization chamber.

§ 3. Experimental Results

3.1. *Resonances and Yields*

(i) *Gamma-ray Intensities*

Figure 2 (*a*) shows the yield curve which was obtained with a ^{10}B target for gamma-rays emitted at 90° to the incoming alpha-particles.

Fig. 2

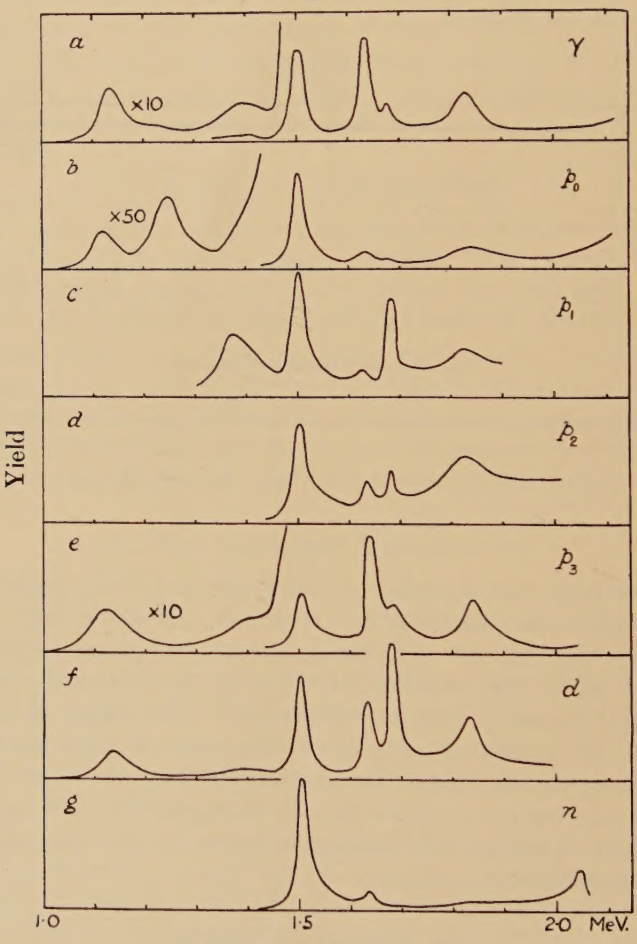

Alpha-particle energy.

Yield curves for ^{10}B. The vertical scales are different for each particle. For absolute yields see table 1.

Resonances occur at 1·13, 1·39, 1·51, 1·64, 1·68 and 1·83 MeV (all ±0·01 MeV). The resonance at 1·13 MeV was previously found by

G. A. Jones (private communication) and those at 1·51, 1·63, 1·68 and 1·83 MeV by Talbott and Heydenburg (1953). We found no gamma-rays when we repeated the experiments with a separated ^{11}B target.

(ii) *Protons*

With the magnetic-analyser we found four groups of protons from the $^{10}B(\alpha p)^{13}C$ reaction, corresponding to Q values of 4·13, 1·00, 0·41 and 0·27 MeV (all $\pm 0{\cdot}02$ MeV). These groups will be referred to as p_0 p_1 p_2 p_3 respectively. They arise from reactions in which the residual ^{13}C nucleus is left in its ground state or in one of the first three excited states at 3·13, 3·72, 3·86 MeV. Our values are in agreement with those quoted by Ajzenberg and Lauritsen (1952 a). We made a careful search at the 1·51 and 1·64 MeV resonances for a proton group which has been occasionally reported (Ajzenberg and Lauritsen 1952 b), with $Q=3{\cdot}3$ MeV corresponding to a level in ^{13}C at about 0·7 MeV, but we could not find it. If such a group exists its intensity is less than 7% of the intensity of the corresponding p_0 group, which is itself weak.

Figure 2 shows yield curves for the various proton groups obtained by counting at 90° to the incident alpha-particles. We used the proportional counter for the p_0 group, the ionization chamber for the p_1 group and the magnet for the p_2 and p_3 groups.

Resonances for the p_0 group appear at all the gamma-ray resonances except 1·39 MeV and there is an additional resonance at 1·24 MeV, where the gamma-rays are weak or absent. We could not detect resonances for the p_1 group at 1·13 and 1·24 MeV but observed marked resonances for the energies 1·39, 1·51, 1·64, 1·68 and 1·83 MeV. The solid angle of acceptance of the magnetic-analyser was too small for us to measure the p_2 yield curve below 1·4 MeV, but we observed resonances at the 1·51, 1·64, 1·68 and 1·83 MeV. Resonances for the p_3 group occur at the energies which give gamma-ray resonances. This group is much the strongest for energies from 1·5 to 2 MeV.

Similar experiments with a thin ^{11}B target showed only one pronounced resonance for the emission of protons at an alpha-particle energy of $1{\cdot}58\pm 0{\cdot}03$ MeV. Figure 3 shows the yield curve obtained by means of the proportional counter. The energy of the emitted protons, measured by means of the magnetic-analyser, corresponds to a Q value of $0{\cdot}85\pm 0{\cdot}02$ MeV which is to be compared with the value of $0{\cdot}75\pm 0{\cdot}01$ MeV measured by Frye and Wiedenbeck (1951) from experiments using polonium alpha-particles. Since the analysis of the particles emitted from our ^{10}B targets showed no sign of this group, we are satisfied that our results for ^{10}B have not been disturbed by traces of ^{11}B in the ^{10}B targets.

(iii) *Deuterons from the* $^{10}B(\alpha d)^{12}C$ *Reaction*

Figure 2 (*f*) shows the yield curve we obtained with the magnet for deuterons at 90°. Resonances occur at all the energies given earlier for

protons or gamma-rays except at 1·24 MeV. That this group did consist of deuterons was confirmed by the change in energy when the analyser was moved from 90° to 160° or when a thin foil was placed between target and analyser. The measured Q value of this group is $1{\cdot}39 \pm 0{\cdot}01$ MeV in reasonable agreement with the value 1·35 MeV calculated from masses (Ajzenberg and Lauritsen 1952 a).

Fig. 3

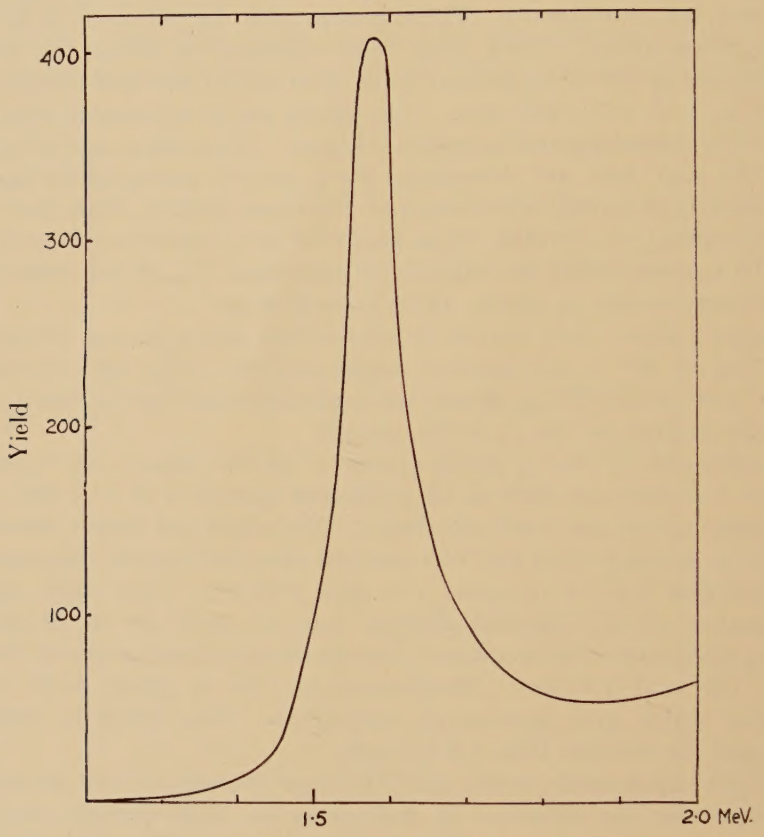

Alpha-particle energy.

Yield curve for $^{11}B(\alpha p)^{14}C$.

(iv) *Neutrons from the* $^{10}B(\alpha n)^{13}N$ *Reaction*

Figure 2 (*g*) shows the yield curve for neutrons measured at 0° to the incident beam. Definite resonances were observed only at 1·51 MeV and at 1·64 MeV in the region below 1·9 MeV and there appears to be a third resonance at 2·05 MeV.

(v) *Relative Intensities of Different Particle Groups at each Resonance*

At 1·51 MeV alpha-particle energy the intensities of proton and deuteron groups were sufficient for us to measure all of them with the magnetic-analyser. We then obtained the intensity of each group at

other resonances relative to its intensity at 1·51 MeV from the appropriate yield curve. Our results are shown in table 1. The relative values for the 1·51 MeV resonance are accurate to about 10%, but the errors for the weaker groups may be considerably larger.

Table 1. Number of Particles, per milli-coulomb of He^+ Ions Incident on a Nominal 5 μg cm^{-2} Target, Emitted at 90° in Laboratory Space into a Solid Angle of 4×10^{-4} steradian

E_α (MeV)	d	p_0	p_1	p_2	p_3
1·13	260	5	21*	13*	230
1·24	(35)	9	5*	9*	(30)
1·39	90	(7)	85	10*	(190)
1·51	930	620	170	660	3300
1·64	720	100	35	280	6500
1·68	1200	(50)	110	350	2600
1·83	560	140	60	450	2900

Figures enclosed in brackets indicate that a clear resonance was not observed. Figures marked with an asterisk were obtained by measurement only at the energies given in column 1 and not from yield curves.

(vi) *Gamma-ray Energies*

Gamma-rays may be expected from transitions in the ^{14}N nucleus formed by capture of an alpha-particle or from transitions between the four lowest states of ^{13}C (see fig. 4). We could distinguish only one gamma-ray energy above 0·5 MeV at 3·73±0·06 MeV. Within the accuracy of our measurements this may be ascribed to transitions from the second or third excited level of ^{13}C, or from both, to the ground state. We were not able to detect the small amount of 3·1 MeV radiation which the existence of the p_1 group of protons shows must have been present. Radiation due to alpha-particle capture must have been weak in comparison with that from the excited ^{13}C nucleus.

Below 0·5 MeV pulses due to gamma-radiation of energy 0·21±0·03 MeV were superimposed on a broad background of small pulses arising from the presence of the 3·7 MeV radiation. By making measurements with and without a lead sheet 0·11 cm thick in front of the scintillation counter it was possible to obtain the relative intensities of the 0·2 MeV and 3·7 MeV radiations. It is reasonable to assume that the 0·2 MeV radiation arises from transitions between the second and third excited levels in ^{13}C. With this assumption, and after correcting our experimental results for the different efficiencies of the counter for 0·2 MeV and for 3·7 MeV radiation, for the measured anisotropy of the gamma-radiation, and for the 3·7 MeV radiation following the emission of p_2 protons from the ^{14}N nucleus, we estimated that about 30% of the ^{13}C nuclei in the 3·9 MeV level reached the ground state by way of the 3·7 MeV level.

3.2. *Angular Distributions*

(i) *Charged Particles*

We measured the angular distributions of the charged particle groups only at resonances that were sufficiently strong relative to the tails of adjacent resonances for us to consider the whole yield to be due, at least to a first approximation, to a single level of the compound nucleus, ^{14}N. We have analysed our results, after correcting to centre-of-mass coordinates, in the form

$$N_\theta = 1 + a\cos^2\theta + b\cos^4\theta,$$

except for the case of the p_0 group at 1·83 MeV where an additional term $k\cos\theta$ was necessary.

Table 2 gives the values of a, b and k we have obtained.

(ii) *Neutrons*

The intensity of these at 1·51 MeV and 90° was 3·5 times that at 0°. Errors of measurement were large and this figure is consistent with a distribution the same as that for p_0 protons from the mirror reaction.

§ 4. Comparison of Experimental Results with Theoretical Predictions

4.1. *Theoretical Angular Distributions*

If we assume that only one level of the compound nucleus, ^{14}N, is involved for a given type of reaction the theoretical angular distribution of emitted particles relative to the incident alpha-particles is given by

$$N(\theta) = \sum_{j_z j_z'} \Big| \sum_{l} (2l+1)^{1/2} f_r(l) \langle jj_z l0 \,|\, JJ_z\rangle \Big|^2 \times \Big| f_s(l') \langle JJ_z \,|\, j'j'_z l'm'\rangle Y_{l'}^{m'}(\theta, 0) \Big|^2. \quad \ldots\ldots\ldots \quad (1)$$

j is the resultant spin of alpha-particle and target nucleus, ^{10}B, and is thus always 3. J is the total angular momentum of the compound nucleus and j' the combined spin of the residual particles. $f_r(l)$ and $f_s(l')$ are complex factors describing the probability amplitudes associated with orbital momenta, l and l', of the incident and emitted particles. $\langle jj_z l0 \,|\, JJ_z\rangle$ and $\langle JJ_z \,|\, j'j'_z l'm'\rangle$ are transformation coefficients (Condon and Shortley 1951) and $Y_{l'}^{m'}(\theta, 0)$ is a spherical harmonic (cf. Seed and French 1952). Since both the proton and the neutron have spins 1/2 and the corresponding residual nuclei, ^{13}C and ^{13}N, spins not zero, j' may in general, though not always, take two values. When this is so, the observed angular distribution will be the sum of two functions $N(\theta)$, one multiplied by a factor, the spin-channel factor, which can only be predicted by assuming a specific type of coupling between spin and orbital momentum. Table 3 gives theoretical values of $N(\theta)$ calculated on the assumption that only the lowest values of l and l' permitted by conservation of momentum and parity take part.

4.2. *Assignment of Spins and Parities*

Rotblat (1951) has shown from a study of the $^{12}C(dp)^{13}C$ reaction that the ground state and the excited levels occurring in ^{13}C at 3·09, 3·68 and 3·89 MeV above the ground state have spins and parities $1/2^-$; $1/2^+$; $3/2^-$ or $1/2^-$; $5/2^+$ or $3/2^+$ respectively, while the ground state of ^{12}C is known to be 0^+. If we compare tables 2 and 3 for the emission of p_0

Fig. 4

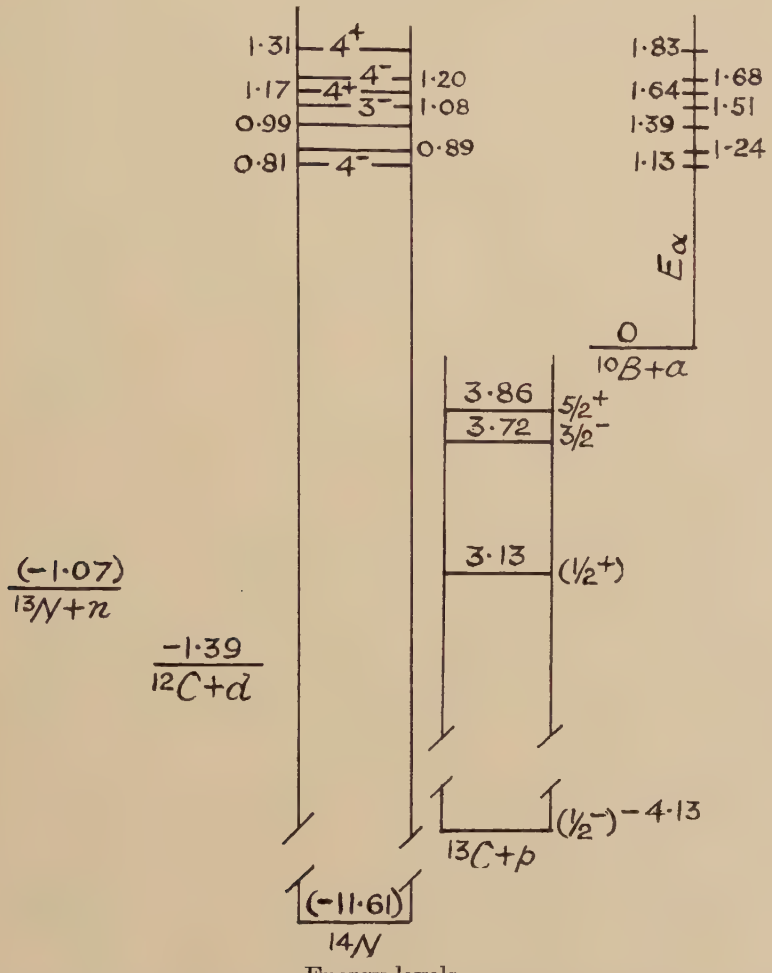

Energy levels.

Energies are plotted vertically in MeV. Bombarding energies are plotted to scale in centre-of-mass coordinates and indicated in laboratory co-ordinates. Figures in brackets are taken from Ajzenberg and Lauritsen (1952 a).

protons and deuterons we can tentatively assign spins and parities of 4^-, 3^-, 4^+, 4^-, 4^+ to the ^{14}N resonances formed at 1·13, 1·51, 1·64, 1·68 and 1·83 MeV bombarding energy. For the 1·68 MeV level a better fit for the deuterons could be obtained by assuming $(J, P)=1^-$ (P=parity),

Table 2. Angular Distributions of Charged Particles

E_α (MeV)	p_0	p_1	p_2	p_3	d
1·13 (4⁻)	$a^+=+0{\cdot}57\pm0{\cdot}09$			$a=+0{\cdot}72\pm0{\cdot}06$	$a=+1{\cdot}25\pm0{\cdot}02$
1·24	$a^+=-0{\cdot}39\pm0{\cdot}08$				
1·51 (3⁻)	$a^+=-0{\cdot}93\pm0{\cdot}04$	$a=-0{\cdot}81\pm0{\cdot}04$ $a^*=-0{\cdot}80\pm0{\cdot}02$	$a=-0{\cdot}80\pm0{\cdot}02$ $a^*=-0{\cdot}83\pm0{\cdot}02$	$a=+0{\cdot}52\pm0{\cdot}02$ $a^*=+0{\cdot}55\pm0{\cdot}03$	$a=-0{\cdot}92\pm0{\cdot}03$ $a^*=-0{\cdot}94\pm0{\cdot}05$
1·64 (4⁺)	$a^+=+3{\cdot}18\pm0{\cdot}24$ $b^+=-3{\cdot}54\pm0{\cdot}54$	$a^*=+3{\cdot}33\pm0{\cdot}5$ $b^*=-2{\cdot}8\ \pm0{\cdot}6$		$a=-2{\cdot}16\pm0{\cdot}11$ $b=+2{\cdot}52\pm0{\cdot}16$	$a=+2{\cdot}77\pm0{\cdot}20$ $b=-2{\cdot}87\pm0{\cdot}30$
1·68 (4⁻)		$a^*=+0{\cdot}93\pm0{\cdot}06$			$a=+1{\cdot}09\pm0{\cdot}02$
1·83 (4⁺)	$k^+=-0{\cdot}5$ $a^+=+0{\cdot}9$ $b^+=-1{\cdot}3$	$a^*=+1{\cdot}46\pm0{\cdot}4$ $b^*=-2{\cdot}7\ \pm1{\cdot}0$		$a=-0{\cdot}78\pm0{\cdot}17$ $b=+1{\cdot}18\pm0{\cdot}23$	$a=+1{\cdot}33\pm0{\cdot}24$ $b=-1{\cdot}91\pm0{\cdot}39$

Values of a, b and k in $N(\theta)=1+k\cos\theta+a\cos^2\theta+b\cos^4\theta$. b and k were zero unless a value is given. Measurements taken with magnetic analyser except those marked + and *, for which the proportional counter and ionization chamber were used respectively. All measurements have been corrected so as to refer to centre-of-gravity space. Figures in brackets in column 1 are our assignments of spin and parity for the ^{14}N levels concerned.

		$l=1$			$l=2$			
j'		$J=2^-$	$J=3^-$	$J=4^-$	$J=1^+$	$J=2^+$	$J=4^+$	$J=5^+$
0^-	l'	2	—	4	1	—	—	5
(p_0)	a	+0·50	—	+1·67	+0·50	—	—	−0·26
	b	0	—	0	0	—	—	+2·74
0^+	l'	—	3	—	—	2	4	—
(p_1)	a	—	−1·0	—	—	−0·40	+8·00	—
	b	—	0	—	—	−0·60	−9·00	—
1^-	l'	2	2	4	1	1	3	5
(p_0, p_2)	a	+0·23	−0·90	+1·31	−0·20	−0·67	+4·77	+0·32
	b	0	0	0	0	0	−5·32	+1·84
1^+	l'	1	3	3	0	2	4	4
(p_1, d)	a	+0·33	−0·82	+1·46	0	−0·86	+2·93	+0·05
	b	0	0	0	0	+0·43	−3·21	+2·25
2^-	l'	0	2	2	1	1	3	3
(p_2)	a	0	−0·29	+1·17	+0·04	+1·20	−0·85	+0·42
	b	0	0	0	0	0	+1·08	+1·62
2^+	l'	1	1	3	2	0	2	4
(p_3)	a	−0·27	−0·69	+0·73	−0·20	0	+2·10	+1·16
	b	0	0	0	0	0	−2·27	+0·37
3^-	l'	2	0	2	3	1	1	3
	a	−0·23	0	+0·09	−0·20	−0·23	+0·09	+1·71
	b	0	0	0	0	0	0	−1·01
3^+	l'	1	1	1	2	2	2	2
(p_3)	a	+0·09	+1·80	+0·73	+0·06	+0·84	−2·38	+0·81
	b	0	0	0	0	+0·07	+2·79	+0·83

Theoretical values of a and b in $N(\theta)=1+a\cos^2\theta+b\cos^4\theta$. For definitions of l, l', J, j' see text.
All distributions are isotropic for $l=0$.

formed by f-wave alpha-particles, but this is unlikely as such a resonance level could emit neutrons and p_0 protons with $l'=0$, resulting in a broad level and prolific emission of protons and neutrons, contrary to our observations. Comparison of the theoretical and observed p_3 distributions confirms the above assignments and definitely rules out the assignment $3/2^+$ to the excited level at 3·89 MeV in the ^{13}C nucleus. The experimental p_1 distributions for the 1·51 and 1·64 resonances fit the theoretical distributions quite well if a suitable choice of spin-channel factor is made. For the 1·68 and 1·83 MeV resonances the fit is better for $(J, P)=4^-$ and 4^+ respectively than for the other values of J listed in table 3. With a suitable choice of spin-channel factor the experimental p_2 distribution for the 1·51 MeV resonance agrees with that predicted theoretically for $(J, P)=3^-$ for the ^{14}N level and $3/2^-$ for the 3·68 MeV level of ^{13}C. The p_2 distribution does not rule out $1/2^-$ for this level of ^{13}C though the agreement between the predicted distribution and our observations is not as good as when $3/2^-$ is chosen.

There is, however, evidence for preferring $3/2^-$ to $1/2^-$ in the existence of the 0·2 MeV gamma-radiation which we detected (§ 3.1 (vi) above). The transition from the third excited level $(5/2^+)$ of ^{13}C at 3·9 MeV to the ground state $(1/2^-)$ involves $\Delta J=2$ and change of parity, so that magnetic quadrupole radiation may be expected. If the second excited level at 3·7 MeV were $1/2^-$ the 0·2 MeV radiation arising from transitions between the third and second excited states would also be magnetic quadrupole, about 10^7 times weaker than the radiation of 3·9 MeV energy (Blatt and Weisskopf 1952). The 0·2 MeV radiation would have been much too weak for us to detect. On the other hand, if the second excited level is $3/2^-$, the 0·2 MeV radiation will be electric dipole, comparable in intensity with the 3·9 MeV radiation. The branching ratio we observed was 0·3, in good agreement with this assumption. The evidence from the 0·2 MeV radiation thus strongly supports our assignment $3/2^-$ to the second excited level of ^{13}C.

Figure 4 gives the energy level scheme relevant to our experiments and summarizes our results.

4.3. *Discussion of Assignments Made*

Comparison of tables 2 and 3 shows that for our assignments of spin and parity to the ^{14}N levels the experimental and theoretical values of the coefficients a and b of $\cos^2\theta$ and $\cos^4\theta$, though always of the right sign and right order of magnitude frequently differ by more than the experimental error. We think these discrepancies can be accounted for by our neglect, in the theory, of values of l and l' higher than the minimum values permitted by angular momentum and parity conservation and by neglect of interference between levels. Interference is clearly shown in the case of the p_0 proton distribution produced by 1·83 MeV alpha-particles. We have not included in table 3 distributions for a compound nucleus state with $(J, P)=3^+$. If such levels had been formed by

alpha-particles of $l=0$ only, all the emitted particles would have had an isotropic distribution. We found no level where this was the case. If a mixture of $l=0$ and $l=2$ alpha-particles formed a 3^+ level, anisotropic distributions would be possible, but we have not been able to fit such distributions to our observations.

Experiments, which will be reported separately, on the angular correlation between gamma-rays and emitted particles agree with predictions based on our assignments of spins and parities, though the processes concerned are too complex for us to deduce spins or parities from such correlations alone.

4.4. *Reaction Cross Sections and Level Widths*

From the yield curves, the angular distributions of the emitted particles, and the target thicknesses we were able to estimate the reaction cross sections in many cases. Owing to the difficulty of estimating the thicknesses of the targets used, and their gradual deterioration under bombardment

Table 4. Cross Sections and Partial Widths

E_α (MeV)	Particle (x)	σ_x (10^{-27}cm^2)	Γ_x (kev)	γ_x^2 (10^{-13} kev cm)	$\frac{2M_a\gamma_x^2}{3\hbar^2}$ (%)	γ_x^2 (10^{-13} kev cm)	$\frac{2M_a\gamma_x^2}{3\hbar^2}$ (%)
1·51	α	—	1·7	470	10	240	6·0
	p_0	4·7	0·62	4·3	0·022	1·7	0·012
	p_1	1·3	0·17	340	1·7	41	0·29
	p_2	5·3	0·70	190	0·94	44	0·31
	p_3	42	5·6	140	0·72	66	0·47
	d	7·0	0·93	20	0·28	18	0·26
	n	32	4·3	68	0·34	26	0·19
1·64	α	—	1·0	620	14	330	8·2
	p_0	0·98	0·18	8·2	0·042	1·7	0·012
	p_1	0·46	0·085	6100	31	380	2·7
	p_2	2·4	0·44	3400	18	420	3·0
	p_3	52	9·6	2700	14	680	4·9
	d	11	2·0	330	4·5	270	3·9
	n	3·2	0·59	150	0·75	23	0·16

Columns 5 and 6 give reduced widths assuming reaction radii 3·41, 4·86 and $5{\cdot}06\times10^{-13}$ cm for emission of nucleon, alpha-particle and deuteron. Columns 7 and 8 give reduced widths assuming radii 4·86, 5·43 and $5{\cdot}15\times10^{-13}$ cm.

Table 5. Widths of Resonances

E_α (MeV)	1·13	1·24	1·39	1·51	1·64	1·68	1·83
Γ (kev)	43±4	36±5	50±5	14±4	14±4	5±2	21±4

Widths have been corrected for target thickness and centre-of-mass motion.

our results, which are given in table 4, are subject to considerable error, but are, we believe, correct to about a factor of two. We obtained total widths Γ from our yield curves by correcting the observed widths for target thickness and centre of gravity movement. Our results are shown in table 5.

In the case of the 1·51 and 1·64 MEV resonances, for which we are reasonably confident of our spin and parity assignments, we have estimated partial widths Γ_x for the various reactions on the assumption that the cross section, σ_x, for a reaction can be obtained from the Wigner one-level formula

$$\sigma_x = \frac{\lambda^2}{4\pi} \frac{2J+1}{(2s+1)(2i+1)} \cdot \frac{\Gamma_\alpha \Gamma_x}{(E_0-E_\alpha)^2+(\Gamma/2)^2} \quad . \quad . \quad . \quad (2)$$

where J is the angular momentum of the compound nucleus, $s(=0)$ and $i(=3)$ the spins of alpha-particle and ^{10}B nucleus respectively and Γ_α the partial width for alpha-particles. Since $\Gamma=\Gamma_\alpha+\Sigma\Gamma_x$ we must solve an equation of the form

$$\Gamma_\alpha(\Gamma-\Gamma_\alpha) = \frac{\pi\Gamma^2(2s+1)(2i+1)}{\lambda^2(2J+1)} \Sigma\sigma_x. \quad . \quad . \quad . \quad . \quad (3)$$

This leads to two values of Γ_α and hence to two values of each of the other partial widths. In table 4 we have chosen the more plausible smaller value of Γ_α and hence the larger of the two possible values for each of the other partial widths. Since we could observe no capture gamma-radiation we have put $\Gamma_\gamma=0$ in the above calculations.

In table 4 we also give the reduced width γ_x^2 of a level from the relation $\Gamma_x=2kP_x\gamma_x^2$ and the corresponding value of $\Theta^2=2M a\gamma_x^2/3\hbar^2$ where M and a are the appropriate reduced mass and reaction radius (Teichman and Wigner 1952). We obtained P_x for charged particles from the tables of Bloch *et al.* (1951) and P_x for neutrons from the formulae given by Blatt and Weisskopf (1952).

In table 4 we have given γ_x^2 and Θ_x^2 for two sets of values of a ; one (columns 5 and 6) for $a=1{\cdot}45\times 13^{1/3}\times 10^{-13}$ cm for nucleons, $1{\cdot}45\times(12^{1/3}+1{\cdot}2)\times 10^{-13}$ cm for deuterons and $1{\cdot}45\times(10^{1/3}+1{\cdot}2)\times 10^{-13}$ cm for alpha-particles ; the other (columns 7 and 8) for $a=1{\cdot}45\times(A_1^{1/3}+A_2^{1/3})\times 10^{-13}$ cm where A_1 and A_2 are the atomic weights (^{16}O=16) of the particles concerned.

4.5. *Discussion of Level Widths*

As can be seen from table 4 the value of Θ^2 for a given reaction is sensitive to the reaction radius, a. For both sets of radii used in table 4 however, Θ^2 is noticeably smaller for the p_0 protons than for the other groups of protons. It is also considerably smaller than Θ^2 for neutrons whereas, since p_0 protons and neutrons are produced by mirror reactions, much the same value of Θ^2 might have been expected for the two cases. We think that the difference between Θ^2 for p_0 protons and for neutrons cannot be accounted for by experimental error, though since the relevant

cross sections were measured by very different kinds of experiment some possibility of such an explanation remains. If we compare our values of Θ^2 for protons with that of 12% calculated by Teichman and Wigner (1952) for protons in the $^{13}C(p\gamma)^{14}N$ reaction at 550 kev bombarding energy and nearly the same reaction radius, we see the decrease in Θ^2 which is to be expected theoretically (Teichman and Wigner, *ibid.*) with increasing excitation energy, 12·7 Mev in our case compared with 8·06 Mev for the $^{13}C(p\gamma)^{14}N$ reaction.

§ 5. Conclusion

Our results enable us to confirm the assignments J, $P=1/2^-$ and $1/2^+$ made by Rotblat (1951) for the ground state and lowest excited state of ^{13}C. They enable us to select $5/2^+$ from his assignment $5/2^+$ or $3/2^+$ for the level at 3·86 Mev, and $3/2^-$ rather than $1/2^-$ for the level at 3·72 Mev. These values of spins and parities of the four lowest levels in ^{13}C are in accord with a simple application of the shell theory. The ground state consists of a ^{12}C core (i.e. a complete 1s shell and a complete $p_{3/2}$ sub-shell) plus a single $p_{1/2}$ neutron. We can excite the system with the least possible energy by promoting the odd neutron to the next shell, a process which would require about 4 Mev and give two levels $2s_{1/2}$ and $d_{5/2}$; or else we can break the closed $p_{3/2}$ shell and obtain a nucleon, which we then pair with the $p_{1/2}$ neutron, a rearrangement which needs the energy for lifting a nucleon from $p_{3/2}$ to $p_{1/2}$, plus the difference in pairing energy between $(p_{3/2})^2$ and $(p_{1/2})^2$. Thus we would expect the following low-lying levels: $d_{5/2}$ and $s_{1/2}$ ($5/2^+$ and $1/2^+$), $(p_{3/2})^{-1}(p_{1/2})^2$ ($3/2^-$), $p_{1/2}$ (ground state) ($1/2^-$) and we would expect all other levels to be higher. These predictions agree with what we have inferred from our experiments. With our assignments the three lowest excited levels correspond exactly with those of the mirror nucleus ^{13}N as reported by Jackson and Galonsky (1953) from measurement of the elastic scattering of protons by carbon. For a more detailed discussion see Inglis (1953).

It is not possible to draw any very definite conclusions at present from our measurements of reduced widths for the various reactions which occur when ^{10}B is bombarded with alpha-particles, but it would appear to be well worth while to measure the widths for competing reactions for more cases. We intend to do this and also to repeat under better conditions our comparison of Θ^2 for p_0 protons and neutrons.

Acknowledgments

We wish to thank Dr. A. P. French, Mr. J. M. C. Scott and Mr. A. M. Lane for a number of helpful discussions and the Atomic Energy Research Establishment, Harwell, for preparing separated isotope targets for us. Three of us (G. L.-J., A. G. S. and J. R. W.) wish to thank the Department of Scientific and Industrial Research and our Colleges for financial assistance while this work was being done. One of us (A. L.) is similarly indebted to the British Council.

References

Ajzenberg, F., and Lauritsen, T., 1952 a, *Rev. Mod. Phys.*, **24,** 367 ; 1952 b, *Ibid.*, **24,** 360.

Blatt, J. M., and Weisskopf, V. F., 1952, *Theoretical Nuclear Physics* (New York : Wiley).

Bloch, I., Hull, M. M. Jr., Broyles, A. A., Bouricius, W. G., Freeman, B. E., and Breit, G., 1951, *Rev. Mod. Phys.*, **23,** 147.

Condon, E. U., and Shortley, G. H., 1951, *The Theory of Atomic Spectra* (Cambridge : University Press).

Creagan, R. J., 1949, *Phys. Rev.*, **76,** 1769.

Frye, G. M., and Wiedenbeck, M. L., 1951, *Phys. Rev.*, **82,** 960.

Hornyak, W. F., 1952, *Rev. Sci. Instrum.*, **23,** 264.

Hutchinson, G. W., and Scarrot, G. G., 1951, *Phil. Mag.*, **42,** 792.

Inglis, D. R., 1953, *Rev. Mod. Phys.*, **25,** 421.

Jackson, H. L., and Galonsky, A. I., 1953, *Phys. Rev.*, **89,** 370.

Perkin, J. L., 1950, *Phys. Rev.*, **79,** 175.

Rogers, M., Odencrantz, F. K., and Plain, G. J., 1952, *Phys. Rev.*, **85,** 756(A).

Rotblat, J., 1951, *Phys. Rev.*, **83,** 1271.

Seed, J., and French, A. P., 1952, *Phys. Rev.*, **88,** 1007.

Talbott, F. L., and Heydenburg, N. P., 1953, *Phys. Rev.*, **90,** 186.

Teichman, T., and Wigner, E. P., 1952, *Phys. Rev.*, **87,** 123.

CXXVIII. *Stable Dislocations in the Common Crystal Lattices*

By F. C. Frank
H. H. Wills Physical Laboratory, University of Bristol*
and
J. F. Nicholas
Division of Tribophysics, C.S.I.R.O., Melbourne, Australia†

[Received July 2, 1953]

Abstract

On the assumption that the energy per unit length of a dislocation line is proportional to the square of the Burgers vector, the stability of dislocations in simple cubic, face-centred cubic, diamond, hexagonal close-packed, and body-centred cubic lattices is discussed. It is shown that in each of these lattices, there is only a finite number of Burgers vectors which correspond to stable perfect dislocations; these vectors are enumerated. Imperfect dislocations are discussed for those lattices in which they can occur and the finite sets of Burgers vectors corresponding to isolated stable imperfect dislocations are found. Stable extended dislocations, consisting of arrays of imperfect dislocations separated by areas of translation-twin surface, are discussed but there is no limit to the number of these that is geometrically possible.

§ 1. Introduction

The Burgers vector of a perfect dislocation may be any lattice vector: that of an imperfect dislocation may be any lattice vector, added to a vector characteristic of the translation-twin surface or surfaces attached to the dislocation. Therefore, in principle, there is an infinity of possible Burgers vectors for the dislocations of a given lattice. However, if one neglects the crystal anisotropy and the small variations of energy with the orientation of the Burgers vector relative to the direction of the dislocation line, the energy per unit length of a dislocation may be taken as proportional to the square of the magnitude of its Burgers vector (Nabarro 1952). Therefore, if the Burgers vector, $\mathbf{b}$ (of magnitude b), of a dislocation is equal to the sum of two other possible Burgers vectors, say $\mathbf{b}_1$ and $\mathbf{b}_2$, and $b^2 > b_1^2 + b_2^2$, i.e. $\mathbf{b}_1 \cdot \mathbf{b}_2 > 0$, then the dissociation of the dislocation, according to $\mathbf{b} \rightarrow \mathbf{b}_1 + \mathbf{b}_2$, lowers the energy. The original dislocation is then unstable against such a dissociation and, when this principle is used

* Communicated by the Authors.
† Temporarily at H. H. Wills Physical Laboratory, University of Bristol.

consistently, the number of possible Burgers vectors corresponding to stable dislocations becomes finite. Because the dislocation energy is not exactly proportional to b^2, dislocations which are stable in one orientation may be unstable in another, particularly when $\mathbf{b}_1 \cdot \mathbf{b}_2$ is small, but such a complication will be neglected in this paper. We shall also ignore the fact that even a moderate stress may dissociate a weakly stable dislocation since a stress will, in general, exert different forces on the two component dislocations.

In the sections which follow, we treat the stability principle as exact and apply it to different lattices to find all the possible Burgers vectors which correspond to stable dislocations. For each lattice, we first choose three primitive vectors, $\mathbf{a}_1$, $\mathbf{a}_2$, $\mathbf{a}_3$, and form all possible combinations,

$$\mathbf{b}=n_1\mathbf{a}_1+n_2\mathbf{a}_2+n_3\mathbf{a}_3$$

where the n_i are integral or zero. These are the possible Burgers vectors for perfect dislocations. For each different vector, we then consider all possible decompositions into two other vectors, say $\mathbf{b}_1$ and $\mathbf{b}_2$, with $\mathbf{b}=\mathbf{b}_1+\mathbf{b}_2$ and calculate the maximum value of $b^2-(b_1^2+b_2^2)$. If this is negative the perfect dislocation corresponding to $\mathbf{b}$ is listed as stable, if zero as doubtfully stable and if positive as unstable. The treatment for imperfect dislocations is similar and the details will be given as the various cases arise.

§ 2. Simple Cubic Lattice

In the simple cubic lattice (e.g. caesium chloride), primitive vectors are (1, 0, 0), (0, 1, 0), and (0, 0, 1), the unit of length being the lattice constant. From these we may construct :

(*a*) 6 vectors : (1, 0, 0) etc. (where etc. implies permutations and changes of sign), for which $b^2=1$. These are the displacements from a lattice point to its nearest neighbours.

(*b*) 12 vectors : (1, 1, 0) etc., for which $b^2=2$. These are the displacements from a lattice point to its second nearest neighbours.

(*c*) 8 vectors : (1, 1, 1) etc., for which $b^2=3$. These are the displacements from a lattice point to its third nearest neighbours.

Dislocations of type (*a*) are stable but the stability of type (*b*) against dissociation into pairs of type (*a*), or of type (*c*) against dissociation into one each of types (*a*) and (*b*) or into three of type (*a*), is in doubt. Any dislocation whose Burgers vector has a component greater than 1 is unstable.

There are no imperfect dislocations in this lattice.

§ 3. Face-Centred Cubic Lattice

In the face-centred cubic lattice, taking the customary unit cell to define a Cartesian reference system and using the lattice constant as unit of length, we find a set of primitive vectors to be $(0, \frac{1}{2}, \frac{1}{2})$, $(\frac{1}{2}, 0, \frac{1}{2})$, and

$(\frac{1}{2}, \frac{1}{2}, 0)$. From these the Burgers vectors corresponding to stable perfect dislocations will be derived in § 3.1. However, as is well known, the face-centred cubic lattice can also be regarded as built of close-packed layers of atoms in (111) planes. The projections of these layers along the [111] axis occupy three different sets of positions and in this way the layers may be labelled as a, b, or c. The perfect lattice is then characterized by one of the continuing sequences : . . . abcabc . . . or . . . cbacba . . . Though many metals crystallize in this system a comparable number do so in the hexagonal close-packed system which is characterized by a layer structure such as . . . ababab . . . while others, e.g. Ca, La, Tl, Co, and some Cu-rich Cu/Si alloys, occur in either of these structures or indeed in structures with random arrangements somewhere between these two regular sequences. Furthermore, growth and recrystallization twins corresponding to the sequence . . . abcbacba . . . are prevalent in most face-centred cubic metals. The common feature of all these structures. that no two successive layers are alike, implies that every atom has twelve nearest neighbours, six in its own layer and three in each of the layers immediately above and below. It is customarily assumed that, to a good first approximation, the lowest energy states are determined by this simple rule alone. Therefore, any surface at which there is an anomaly in the stacking without a breach of this rule satisfies the conditions for a translation-twin surface (Frank 1951 a) and in face-centred cubic lattices there will be imperfect dislocations associated with the edges of such a surface. The actual energy of the surface probably arises from the reflection of electron waves at the change of lattice pattern but so far no reliable estimate of its magnitude is available.

3.1. *Perfect Dislocations*

From the primitive vectors, $(0, \frac{1}{2}, \frac{1}{2})$, $(\frac{1}{2}, 0, \frac{1}{2})$, and $(\frac{1}{2}, \frac{1}{2}, 0)$, we can construct :

(*a*) 12 vectors : $(0, \frac{1}{2}, \frac{1}{2})$ etc., for which $b^2=\frac{1}{2}$. These are the displacements from a lattice point to its nearest neighbours.

(*b*) 6 vectors : (1, 0, 0) etc., for which $b^2=1$. These are the displacements from a lattice point to its second nearest neighbours.

Dislocations of type (*a*) are stable but the stability of a dislocation of type (*b*) against dissociation into a pair of type (*a*), e.g.

$$(1, 0, 0) \rightarrow (\tfrac{1}{2}, \tfrac{1}{2}, 0) + (\tfrac{1}{2}, -\tfrac{1}{2}, 0)$$

is in doubt. All further combinations are unstable.

3.2. *Imperfect and Extended Dislocations*

3.2.1. *Isolated imperfect dislocations on one plane*

We may generate a translation-twin on (111) in two ways, viz. (i) by removing a layer of atoms, say a, and closing up the gap by the displacement normal to (111) which brings the c and b layers into contact or (ii)

by inserting a plane of atoms, say b, between c and a layers which have been separated by the necessary normal displacement. These processes give rise to sequences (i) . . . abcbcabc . . . and (ii) . . . abcbabc . . . and the translation-twins so formed are intrinsic and extrinsic respectively in the sense defined by Frank (1951 a). The first involves one breach of the stacking rules and the second two, but both involve the same kind of anomaly in second nearest neighbour relationships between two pairs of layers. We cannot tell at present which has the higher surface energy, nor do we know whether one occurs more commonly than the other. These forms of stacking fault are illustrated in figs. 1 (*a*) and (*b*).

If a bounded translation-twin is formed, i.e. if only part of a layer is removed or added (fig. 1 (*c*)), then we must have imperfect dislocations at the boundaries. These can be classified into four sets according to which type of twin is present and according to which boundary is being considered, i.e. the left or right hand one when looking at the layers in

Fig. 1

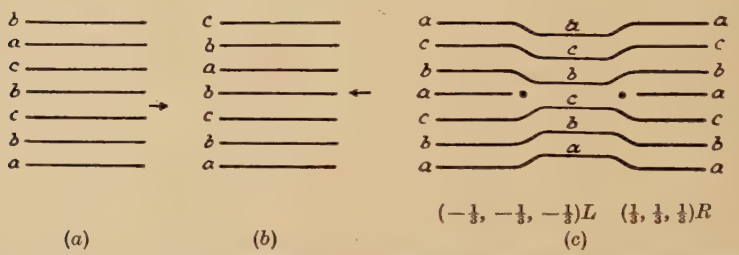

Stacking faults in a face-centred cubic lattice forming (*a*) an intrinsic and (*b*) an extrinsic translation-twin surface. The arrows show where the layer has been removed or inserted to generate these structures. A bounded faulted region with its associated imperfect dislocations is shown in (*c*). (In figs. 1–6 the [111] direction is vertically upwards in the plane of the paper.)

a standard way. We shall define this standard way by taking the [111] direction as ' top '. The sets will then be denoted by L and R for the dislocations associated with twins of type (i) and λ and ρ for those associated with twins of type (ii). Other translation twins of the extrinsic type may be generated by inserting three or more extra (111) planes, but the boundaries of these are necessarily groups of dislocations, not single ones, so that a consideration of all possible stable dislocations of the four sets above is sufficient.

We shall use the convention that the circuits involved in defining Burgers vectors are taken in a clockwise sense. Since the displacement of the b-layer in a translation of type (i) above is $(-\frac{1}{3}, -\frac{1}{3}, -\frac{1}{3})$, typical Burgers vectors of dislocations of the L and R sets are $(-\frac{1}{3}, -\frac{1}{3}, -\frac{1}{3})L$ and $(\frac{1}{3}, \frac{1}{3}, \frac{1}{3})R$. Similarly, for the other sets we have $(\frac{1}{3}, \frac{1}{3}, \frac{1}{3})\lambda$ and $(-\frac{1}{3}, -\frac{1}{3}, -\frac{1}{3})\rho$. All other Burgers vectors of these sets can then be found by combining these vectors with true lattice translations. Clearly

we need consider only one set, say the L set, and the others are then easily deducible. For stability, we must first test each L dislocation against dissociation into a perfect dislocation and another L dislocation. Then further, since the removal of one layer is equivalent to the insertion of two, we must test each L dislocation against dissociation into two λ dislocations, and conversely, since the insertion of one layer is equivalent to the removal of two, we must test each λ dislocation against dissociation into two L dislocations. Obviously, the same argument holds for the R and ρ dislocations.

For the L set, we can construct the following vectors which correspond to all dislocations which are not unstable against dissociations involving perfect dislocations :

(*a*) 3 vectors : $(\frac{1}{6}, \frac{1}{6}, -\frac{1}{3})L$, $(\frac{1}{6}, -\frac{1}{3}, \frac{1}{6})L$, and $(-\frac{1}{3}, \frac{1}{6}, \frac{1}{6})L$, with $b^2=\frac{1}{6}$. These represent displacements from a lattice point to the nearest twin lattice positions in the (111) plane.

(*b*) 1 vector : $(-\frac{1}{3}, -\frac{1}{3}, -\frac{1}{3})L$, with $b^2=\frac{1}{3}$. This is the displacement normal to (111) described above.

(*c*) 3 vectors : $(\frac{2}{3}, \frac{1}{6}, \frac{1}{6})L$, $(\frac{1}{6}, \frac{2}{3}, \frac{1}{6})L$ and $(\frac{1}{6}, \frac{1}{6}, \frac{2}{3})L$ with $b^2=\frac{1}{2}$.

Of these, types (*a*) and (*b*) are stable while type (*c*) are stable against the dissociation

$$(\tfrac{2}{3}, \tfrac{1}{6}, \tfrac{1}{6})L \rightarrow (\tfrac{1}{2}, \tfrac{1}{2}, 0)+(\tfrac{1}{6}, -\tfrac{1}{3}, \tfrac{1}{6})L$$

provided $(\frac{1}{2}, \frac{1}{2}, 0)$ cannot dissociate further. However, if the dislocation line lies in the $(1\bar{1}\bar{1})$ or $(\bar{1}1\bar{1})$ planes, as well as in the (111) plane, i.e. in $[01\bar{1}]$ or $[10\bar{1}]$, then the $(\frac{1}{2}, \frac{1}{2}, 0)$ dislocation can further dissociate (as described below) and the stability of $(\frac{2}{3}, \frac{1}{6}, \frac{1}{6})L$ becomes doubtful. Further, dislocations of this type are doubtfully stable against dissociations into two λ dislocations, one of type (*a*) and one of type (*b*), e.g.

$$(\tfrac{2}{3}, \tfrac{1}{6}, \tfrac{1}{6})L \rightarrow (\tfrac{1}{3}, -\tfrac{1}{6}, -\tfrac{1}{6})\lambda+(\tfrac{1}{3}, \tfrac{1}{3}, \tfrac{1}{3})\lambda$$

and this is independent of the orientation of the dislocation line.

Some of these imperfect dislocations have already been described in the literature, type (*a*) being ' half-dislocations ' of the Heidenreich–Shockley type and type (*b*) being the original ' sessile ' dislocations of Frank (1949). Type (*c*) are a new type of sessile dislocation.

Figure 1 (*c*) shows L and R dislocations of type (*b*) while fig. 2 shows the arrangement of layers about dislocations of all the L and λ types. The dissociations of the type (*c*) dislocations are also shown.

In order to enumerate all the imperfect dislocations of the above types, we must distinguish between the planes which can form the translation-twin surface. There are four essentially different ones, viz. $(1\bar{1}\bar{1})$, $(\bar{1}1\bar{1})$, $(\bar{1}\bar{1}1)$, and (111), and we will denote these by a, b, c, and d. Then any of these imperfect dislocation sets may be described by a symbol of the form D_i where D denotes one of L, R, λ, or ρ, and i denotes one of a, b, c, or d. The dislocations we have specified above are those of the set L_d. If we use (h, k, l) to denote the Burgers vector of a typical

imperfect dislocation, then it is clear that, corresponding to the set $(h, k, l)L_i$, we have the sets $(-h, -k, -l)R_i$, $(-h, -k, -l)\lambda_i$, and $(h, k, l)\rho_i$. Further, we can easily see that, corresponding to the set $(h, k, l)D_{\bar{d}}$, we have the sets $(h, -k, -l)D_a$, $(-h, k, -l)D_b$, and $(-h, -k, l)D_c$. Table 1 gives the changes necessary to derive the Burgers vectors of any set from those of the L_d set.

Fig. 2

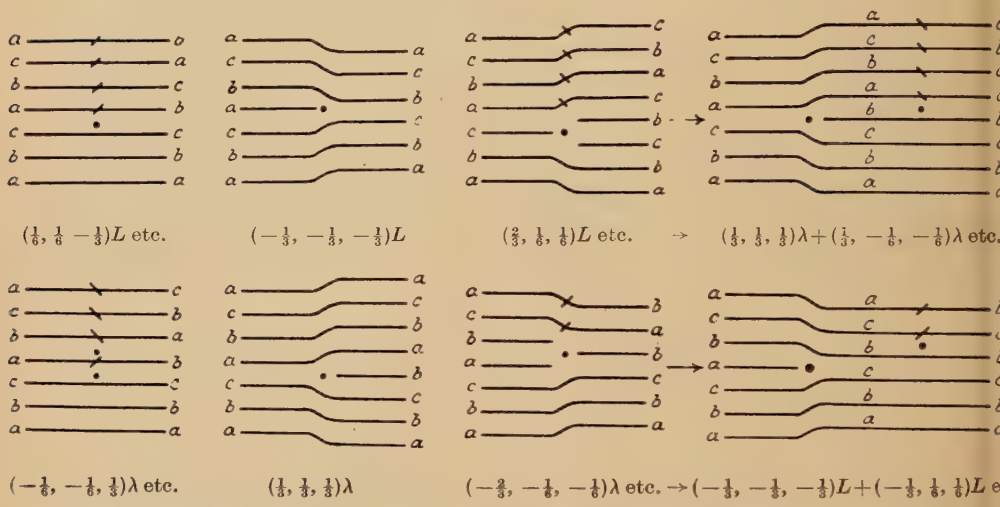

Layer structures about dislocations of L and λ types in a face-centred cubic structure. ● indicates the projection of the dislocation line while the sloping lines indicate that a change must be made in the nomenclature of the plane on passing from the unslipped to the slipped region (see Frank 1950). The dissociations of the doubtfully stable dislocations with $b^2=\frac{1}{2}$ are also shown.

Table 1

	a	b	c	d
L, ρ R, λ	$(h, -k, -l)$ $(-h, k, l)$	$(-h, k, -l)$ $(h, -k, l)$	$(-h, -k, l)$ $(h, k, -l)$	(h, k, l) $(-h, -k, -l)$

When all twinning planes are considered we have 64 stable and 48 doubtfully stable imperfect dislocations of this kind.

If, on the one plane, we have adjoining regions of intrinsic and extrinsic translation-twin surface, the boundary line between the regions will be the line of an imperfect dislocation. Such dislocations can be considered as combinations of two of the imperfect dislocations described above so that they can be denoted by a symbol of the form D_iD_i'. The conditions for their existence imply that the only occurring combinations are $L_i\rho_i$ and $R_i\lambda_i$. Considering first the $L_d\rho_d$ group we find that a typical Burgers

vector is $(\frac{1}{3}, \frac{1}{3}, \frac{1}{3})$, i.e. a vector of the R_d type. Therefore, the new dislocation group can be correlated with the known R_d group and it is easily seen that the stable dislocations of the two groups will have the same vectors. However, such a dissociation as

$$(-\tfrac{2}{3}, -\tfrac{1}{6}, -\tfrac{1}{6})L_d\rho_d \rightarrow (-\tfrac{1}{3}, -\tfrac{1}{3}, -\tfrac{1}{3})L_d + (-\tfrac{1}{3}, \tfrac{1}{6}, \tfrac{1}{6})\rho_d$$

(analogous to the doubtfully stable dissociation of $(\frac{2}{3}, \frac{1}{6}, \frac{1}{6})L$ above), although it involves no change in dislocation energy, does reduce the area of translation-twin surface and hence the total energy. Therefore, dislocations of this type will be classed as unstable. In a similar way, the $R_d\lambda_d$ group may be correlated with the L_d group. Ultimately therefore, on any plane we have four stable dislocations of $L_i\rho_i$ type and four of $R_i\lambda_i$ type, making in all 32 stable imperfect dislocations of this combined type. Strictly, the dissociations $L \rightarrow \lambda + \lambda$ etc., described above (and in fig. 2) should have been described as $L \rightarrow \lambda + L\rho$ etc. Such a change does not alter the argument.

3.2.2. *Extended dislocations*

When imperfect dislocations can exist, stable perfect dislocations in some orientations become unstable since the dissociation of a perfect dislocation into two imperfect ones can lead to a reduction in energy. In such a dissociation a new area of translation-twin surface is created between the two imperfect dislocations and the surface energy associated with this limits the separation of the component dislocations. Such a dissociation is described as an extension and the combination of imperfect dislocations and translation-twin surface as an extended dislocation.

Each dislocation with a Burgers vector of $(\frac{1}{2}, \frac{1}{2}, 0)$ type has eight modes of extension, two in each octahedral plane. Those in the two planes containing its Burgers vector may occur spontaneously, and permit glide. Those in the other two octahedral planes will not occur without an additional stress as they do not involve a reduction in energy; since one of the component dislocations is sessile, these extensions will anchor the dislocation. For the $(\frac{1}{2}, -\frac{1}{2}, 0)$ dislocation the extensions are:

$$(\tfrac{1}{6}, -\tfrac{1}{6}, \tfrac{1}{3})L_a + (\tfrac{1}{3}, -\tfrac{1}{3}, -\tfrac{1}{3})R_a \text{ and } (\tfrac{1}{3}, -\tfrac{1}{3}, -\tfrac{1}{3})\lambda_a + (\tfrac{1}{6}, -\tfrac{1}{6}, \tfrac{1}{3})\rho_a;$$
$$(\tfrac{1}{3}, -\tfrac{1}{3}, \tfrac{1}{3})L_b + (\tfrac{1}{6}, -\tfrac{1}{6}, -\tfrac{1}{3})R_b \text{ and } (\tfrac{1}{6}, -\tfrac{1}{6}, -\tfrac{1}{3})\lambda_b + (\tfrac{1}{3}, -\tfrac{1}{3}, \tfrac{1}{3})\rho_b;$$
$$(\tfrac{1}{3}, -\tfrac{1}{6}, \tfrac{1}{6})L_c + (\tfrac{1}{6}, -\tfrac{1}{3}, -\tfrac{1}{6})R_c \text{ and } (\tfrac{1}{6}, -\tfrac{1}{3}, -\tfrac{1}{6})\lambda_c + (\tfrac{1}{3}, -\tfrac{1}{6}, \tfrac{1}{6})\rho_c;$$
$$(\tfrac{1}{6}, -\tfrac{1}{3}, \tfrac{1}{6})L_d + (\tfrac{1}{3}, -\tfrac{1}{6}, -\tfrac{1}{6})R_d \text{ and } (\tfrac{1}{3}, -\tfrac{1}{6}, -\tfrac{1}{6})\lambda_d + (\tfrac{1}{6}, -\tfrac{1}{3}, \tfrac{1}{6})\rho_d.$$

Figure 3 shows the two modes of extension of the $(\frac{1}{2}, -\frac{1}{2}, 0)$ dislocation in (111). The extensions in $(\bar{1}\bar{1}1)$ would be similar. The first mode is that of Shockley and Heidenreich (1948). The energies involved in the two modes are presumably slightly different, but a change from one to the other must involve an activation energy so that both should occur. Neither type is able to climb but both are free to glide in the (111) plane, and cause the same slip by their motions. There is no obvious macroscopic observation by which they could be distinguished. Figure 4

shows the extensions of a $(\frac{1}{2}, \frac{1}{2}, 0)$ dislocation in (111). These are equivalent to the extensions of $(\frac{1}{2}, -\frac{1}{2}, 0)$ in either $(1\bar{1}\bar{1})$ or $(\bar{1}1\bar{1})$.

The perfect dislocations of (1, 0, 0) type can be dissociated, with a lowering of energy, into two imperfect dislocations, one of $(\frac{2}{3}, \frac{1}{6}, \frac{1}{6})$ type and one of $(\frac{1}{3}, -\frac{1}{6}, -\frac{1}{6})$ type, in whatever octahedral plane the dislocation line may lie. Therefore, all dislocations of (1, 0, 0) type lying in a {111} plane become unstable when imperfect dislocations can be formed. Since the dislocations of $(\frac{2}{3}, \frac{1}{6}, \frac{1}{6})$ type are sessile, such an extension renders the dislocation incapable of glide. The extension in (111) is illustrated in fig. 5.

Fig. 3

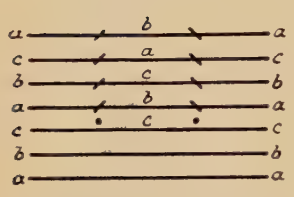

$(\frac{1}{6}, -\frac{1}{3}, \frac{1}{6})L + (\frac{1}{3}, -\frac{1}{6}, -\frac{1}{6})R$
$= (\frac{1}{2}, -\frac{1}{2}, 0)$

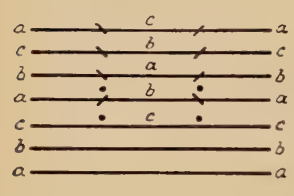

$(\frac{1}{3}, -\frac{1}{6}, -\frac{1}{6})\lambda + (\frac{1}{6}, -\frac{1}{3}, \frac{1}{6})\rho$
$= (\frac{1}{2}, -\frac{1}{2}, 0)$

Fig. 4

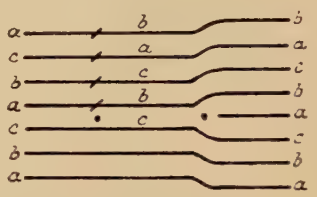

$(\frac{1}{6}, \frac{1}{6}, -\frac{1}{3})L + (\frac{1}{3}, \frac{1}{3}, \frac{1}{3})R$
$= (\frac{1}{2}, \frac{1}{2}, 0)$

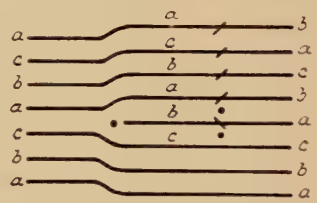

$(\frac{1}{3}, \frac{1}{3}, \frac{1}{3})\lambda + (\frac{1}{6}, \frac{1}{6}, -\frac{1}{3})\rho$
$= (\frac{1}{2}, \frac{1}{2}, 0)$

Fig. 5

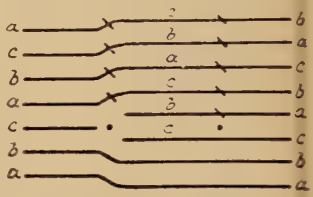

$(\frac{2}{3}, \frac{1}{6}, \frac{1}{6})L + (\frac{1}{3}, -\frac{1}{6}, -\frac{1}{6})R$
$= (1, 0, 0)$

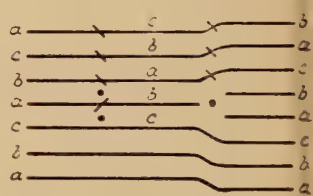

$(\frac{1}{3}, -\frac{1}{6}, -\frac{1}{6})\lambda + (\frac{2}{3}, \frac{1}{6}, \frac{1}{6})\rho$
$= (1, 0, 0)$

Fig. 3. Possible modes of extension in (111) of a dislocation with a Burgers vector of $(\frac{1}{2}, -\frac{1}{2}, 0)$.

Fig. 4. Possible modes of extension in (111) of a dislocation with a Burgers vector of $(\frac{1}{2}, \frac{1}{2}, 0)$.

Fig. 5. Possible modes of extension in (111) of a dislocation with a Burgers vector of (1, 0, 0).

There are certain groups of more than two imperfect dislocations, in which the elastic interactions between members of the group are repulsive, but the stacking faults connecting them prevent an unlimited expansion of the group, which as a whole constitutes a perfect dislocation of the lattice. Such groups can also be classified as extended dislocations : their Burgers vectors are necessarily relatively large. Figure 6 shows examples of such extended dislocations with resultant Burgers vectors of $(1, -\frac{1}{2}, -\frac{1}{2})$, $(1, -1, 0)$, $(1, \frac{1}{2}, \frac{1}{2})$, and $(1, 1, 1)$. In the first two examples the components are glissile, and so the complete groups can glide. The

second two examples are sessile. The most likely processes for production of extended dislocations are processes of combination of dislocations in complex crystal slip. Those in which the components are sessile can only attain their equilibrium configuration at temperatures which permit vacancy diffusion to occur. Clearly there is no limit to the number and complexity of geometrically possible extended dislocations.

Fig. 6

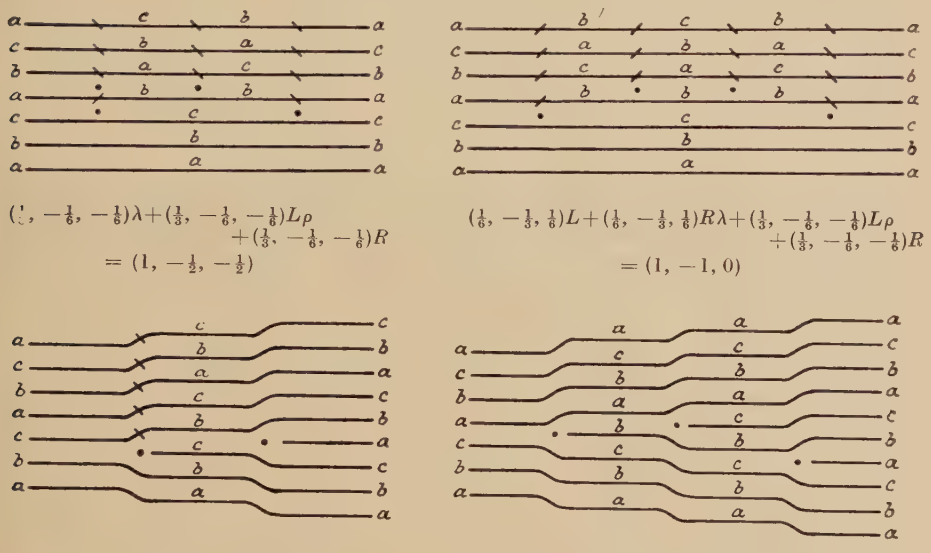

More complex extended dislocations in a face-centred cubic lattice.

3.2.3. *Combinations of two imperfect dislocations on different planes*

If we have two imperfect dislocations on different {111} planes these may combine together to form a new type of dislocation, the dislocation line of which must lie in the ⟨110⟩ direction common to the two {111} planes. Following a suggestion by Nabarro, Thompson (1953) has described these as 'stair-rod' dislocations. Obviously we have a large number of possible combinations as we have to define one of L, R, λ, ρ, and one of a, b, c, d, for each combining imperfect dislocation. We, therefore, have to denote each such dislocation by a symbol of the form D_iD_j' where D and D' may or may not be different but i and j must be different. Since, however, D_iD_j' and $D_j'D_i$ are indistinguishable there are only 96 different sets. Among these there are only two really distinct types, any set being simply derivable from one of these. The basic two that we shall consider are L_aL_b and L_aR_b.

Treating L_aL_b first, a vector typical of the combination is $(0, 0, \frac{2}{3})$. We now combine this with true lattice vectors and test each resulting

vector for stability against decomposition either into a different L_aL_b vector and a true lattice vector or into one L_a vector and one L_b vector. An additional condition for instability in the latter case is that at least one of the dislocations corresponding to the component vectors should be glissile. Under these conditions, we find the following combinations :

(*a*) 1 vector : $(0, 0, -\frac{1}{3})L_aL_b$, having $b^2=1/9$.

(*b*) 4 vectors : $(\frac{1}{2}, 0, \frac{1}{6})L_aL_b$, $(-\frac{1}{2}, 0, \frac{1}{6})L_aL_b$, $(0, \frac{1}{2}, \frac{1}{6})L_aL_b$, and $(0, -\frac{1}{2}, \frac{1}{6})L_aL_b$, having $b^2=5/18$.

(*c*) 2 vectors : $(\frac{1}{2}, -\frac{1}{2}, -\frac{1}{3})L_aL_b$ and $(-\frac{1}{2}, \frac{1}{2}, -\frac{1}{3})L_aL_b$, having $b^2=11/18$.

Types (*a*) and (*b*) are stable while type (*c*) is doubtfully stable against the decomposition

$$(\tfrac{1}{2}, -\tfrac{1}{2}, -\tfrac{1}{3})L_aL_b \rightarrow (\tfrac{1}{2}, -\tfrac{1}{2}, 0)+(0, 0, -\tfrac{1}{3})L_aL_b$$

since the dislocation line must lie in the intersection of the *a* and *b* planes, i.e. along $[1\bar{1}0]$ and hence cannot lie in either the $(\bar{1}\bar{1}1)$ or (111) plane, i.e. the $(\frac{1}{2}, -\frac{1}{2}, 0)$ dislocation cannot lower its energy by extension. All further combinations are unstable.

For the type L_aR_b, a vector typical of the combination is $(\frac{1}{3}, -\frac{1}{3}, 0)$

Fig. 7

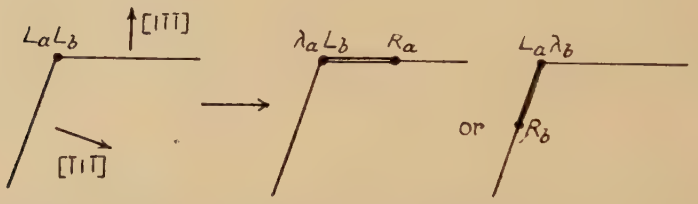

Possible modes of dissociation of a combined dislocation of L_aL_b type. A single line indicates a translation-twin surface of intrinsic type, a double line one of extrinsic type. The positions of the dislocations are indicated by dots.

and, by combination with true lattice vectors and stability tests similar to those above, we find the following combinations :

(*a*) 1 vector : $(-\frac{1}{6}, \frac{1}{6}, 0)L_aR_b$, having $b^2=1/18$.

(*b*) 1 vector : $(\frac{1}{3}, -\frac{1}{3}, 0)L_aR_b$, having $b^2=2/9$.

Types (*a*) and (*b*) are both stable but all further combinations are unstable.

However, we can now find further dissociations for the dislocations of L_aL_b type since, as shown in fig. 7, such dislocations can dissociate either into one $L_a\lambda_b$ and one R_b dislocation or into one λ_aL_b and one R_a dislocation. Then dissociations such as the following can occur :

$$(\tfrac{1}{2}, 0, \tfrac{1}{6})L_aL_b \rightarrow (\tfrac{1}{3}, \tfrac{1}{6}, \tfrac{1}{6})R_a+(\tfrac{1}{6}, -\tfrac{1}{6}, 0)\lambda_aL_b$$

and

$$(\tfrac{1}{2}, -\tfrac{1}{2}, -\tfrac{1}{3})L_aL_b \rightarrow (\tfrac{1}{3}, -\tfrac{1}{3}, 0)L_a\lambda_b+(\tfrac{1}{6}, -\tfrac{1}{6}, -\tfrac{1}{3})R_b$$

so that the only stable dislocation of the L_aL_b type is one with a Burgers vector of $(0, 0, -\frac{1}{3})$. We can, of course, have the corresponding dissociations, $L_aR_b \rightarrow R_a+\lambda_aR_b$, etc., but these do not lead to instability of dislocations having Burgers vectors of the types (*a*) and (*b*) above.

To find the corresponding vectors for the other sets, we use the following rules :

(1) If $(h, k, l)L_aL_b$ and $(H, K, L)L_aR_b$ are any Burgers vectors belonging to either stable or unstable dislocations, then the corresponding vectors for other intersections are :

$$(h, l, k)L_aL_c,\ (l, -k, -h)L_bL_c,\ (-l, k, -h)L_aL_d,\ (-h, -l, k)L_bL_d, \text{ and } (-h, k, -l)L_cL_d\ ;$$

$$(H, L, K)L_aR_c, (L, -K, -H)L_bR_c, (-L, K, -H)L_aR_d, (-H, -L, K)L_bR_d, \text{ and } (-H, K, -L)L_cR_d.$$

(2) If $(h, k, l)D_iD_j'$ is a Burgers vector, then (h, k, l) is still a possible vector when any L in the symbol is replaced by ρ and/or any R by λ, or conversely. Further, $(-h, -k, -l)$ is a possible vector when every L or ρ is replaced by R or λ and simultaneously every R or λ by L or ρ.

Table 2 lists all the vectors corresponding to stable stair-rod dislocations. It is interesting to note that since the dislocation lines of these must lie in the intersection of the two planes concerned, all the stable dislocations are of edge type and all are, of course, sessile.

Table 2

	ab	*ac*	*bc*	*ad*	*bd*	*cd*
$LL, L\rho, \rho L, \rho\rho$	$(0, 0, -\frac{1}{3})$	$(0, -\frac{1}{3}, 0)$	$(-\frac{1}{3}, 0, 0)$	$(\frac{1}{3}, 0, 0)$	$(0, \frac{1}{3}, 0)$	$(0, 0, \frac{1}{3})$
$RR, R\lambda, \lambda R, \lambda\lambda$	$(0, 0, \frac{1}{3})$	$(0, \frac{1}{3}, 0)$	$(\frac{1}{3}, 0, 0)$	$(-\frac{1}{3}, 0, 0)$	$(0, -\frac{1}{3}, 0)$	$(0, 0, -\frac{1}{3})$
$LR, L\lambda, \rho R, \rho\lambda$	$(-\frac{1}{6}, \frac{1}{6}, 0)$ $(\frac{1}{3}, -\frac{1}{3}, 0)$	$(-\frac{1}{6}, 0, \frac{1}{6})$ $(\frac{1}{3}, 0, -\frac{1}{3})$	$(0, -\frac{1}{6}, \frac{1}{6})$ $(0, \frac{1}{3}, -\frac{1}{3})$	$(0, \frac{1}{6}, \frac{1}{6})$ $(0, -\frac{1}{3}, -\frac{1}{3})$	$(\frac{1}{6}, 0, \frac{1}{6})$ $(-\frac{1}{3}, 0, -\frac{1}{3})$	$(\frac{1}{6}, \frac{1}{6}, 0)$ $(-\frac{1}{3}, -\frac{1}{3}, 0)$
$RL, R\rho, \lambda L, \lambda\rho$	$(\frac{1}{6}, -\frac{1}{6}, 0)$ $(-\frac{1}{3}, \frac{1}{3}, 0)$	$(\frac{1}{6}, 0, -\frac{1}{6})$ $(-\frac{1}{3}, 0, \frac{1}{3})$	$(0, \frac{1}{6}, -\frac{1}{6})$ $(0, -\frac{1}{3}, \frac{1}{3})$	$(0, -\frac{1}{6}, -\frac{1}{6})$ $(0, \frac{1}{3}, \frac{1}{3})$	$(-\frac{1}{6}, 0, -\frac{1}{6})$ $(\frac{1}{3}, 0, \frac{1}{3})$	$(-\frac{1}{6}, -\frac{1}{6}, 0)$ $(\frac{1}{3}, \frac{1}{3}, 0)$

3.2.4. *Combinations of three or more imperfect dislocations*

When we consider combinations of three imperfect dislocations, various cases can be distinguished. First, if all three lie in different planes, then clearly the dislocation line can have only point size and any analysis of stability is meaningless. Secondly, if all three lie in the one plane, they can be considered in pairs and no new results are found. However, further investigation is needed in the cases where two of the dislocations lie in one plane, one belonging to an intrinsic and one to an extrinsic translation twin, and the third lies in an intersecting plane.

An example of such a combination is $L_a\rho_a L_b$ for which a typical vector is $(-\frac{1}{3}, \frac{1}{3}, 0)$, i.e. a vector of the R_aL_b type. Thus we have the same combinations with lattice vectors in both these cases and it can easily be shown that any such combination of three imperfect dislocations has vectors identical with those of a two-dislocation combination. This correlation implies that we need treat only the combinations $L_a\rho_a L_b$ and $L_a\rho_a R_b$ which have vectors identical with the combinations R_aL_b and R_aR_b, respectively. The stability of any three-fold combination must, however, be tested against dissociations not only into a perfect dislocation and another dislocation of similar type but also, as shown in fig. 8, into a simple imperfect dislocation and a different sort of combination. For instability in the latter case, we need the further condition that the simple imperfect dislocation is glissile. When account is taken

Fig. 8

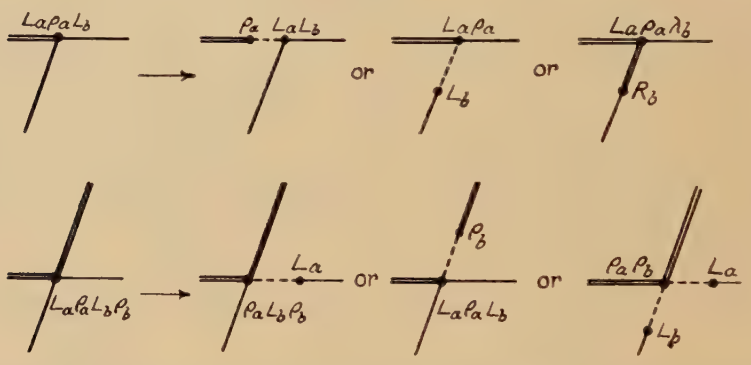

Possible modes of dissociation of combined dislocations of $L_a\rho_a L_b$ and $L_a\rho_a L_b\rho_b$ types (orientation of diagrams as in fig. 7). A dotted line indicates a plane across which no fault exists after the dissociation.

of all such dissociations, the stable combinations in the $L_a\rho_a L_b$ and $L_a\rho_a R_b$ sets are found to be exactly those of the R_aL_b and R_aR_b sets. The vectors corresponding to stable three-dislocation combinations can therefore be found by considering the vectors of the corresponding two-dislocation combination in table 2.

Four imperfect dislocations can meet in a line only when we have one of intrinsic and one of extrinsic type occurring on each of two planes, e.g. $L_a\rho_a L_b\rho_b$. This combination has Burgers vectors equal to those of the R_aR_b combination and in a similar manner to that described above all such four-fold combinations can be correlated with two-fold ones so that again we need consider only two cases, viz. $L_a\rho_a L_b\rho_b$ and $L_a\rho_a R_b\lambda_b$. These can dissociate in such ways as are shown in fig. 8 and, when the stability tests are applied, we find the corresponding Burgers vectors to be those of the stable R_aR_b and R_aL_b sets. A particularly interesting dissociation is

$$(0, 0, -\tfrac{2}{3})L_a\rho_a L_b\rho_b \rightarrow (\tfrac{1}{6}, \tfrac{1}{3}, -\tfrac{1}{6})L_a + (-\tfrac{1}{6}, -\tfrac{1}{3}, -\tfrac{1}{6})L_b + (0, 0, -\tfrac{1}{3})\rho_a\rho_b,$$

in which the total dislocation energy is unaltered. However, as shown in fig. 8, the area of translation-twin surface is reduced and hence the total energy. We may therefore class this combined dislocation as unstable.

For any given pair of planes, there are four possible types of four-dislocation combination, so that we have 24 sets in all. The Burgers vectors of the stable dislocations can be found from table 2.

3.3. *Use of Thompson's Notation*

Thompson (1953) has developed a convenient notation for describing the Burgers vectors of dislocations in a face-centred cubic lattice. This is based on the geometry of a regular tetrahedron having faces parallel to the four {111} planes used above. If we construct a tetrahedron with the points $(0, \frac{1}{2}, \frac{1}{2})$, $(\frac{1}{2}, 0, \frac{1}{2})$, $(\frac{1}{2}, \frac{1}{2}, 0)$, and $(0, 0, 0)$, as the vertices A, B, C, and D, then the outward drawn normals to the faces opposite these points are in the $[1\bar{1}\bar{1}]$, $[\bar{1}1\bar{1}]$, $[\bar{1}\bar{1}1]$, and $[111]$ directions so that these faces represent the a, b, c, and d planes respectively.

The Burgers vectors of the perfect dislocations can then be described as follows :

(a) those of the $(0, \frac{1}{2}, \frac{1}{2})$ type are represented by the joins DA, etc., the choice of letters and order sufficing to cover the twelve cases ;

(b) those of the $(1, 0, 0)$ type are represented by the symbol AB/CD and its permutations. This symbol means either the sum of the vectors AC and BD or, geometrically, a vector equal to twice the join of the midpoints of AB and CD. Since $AB/CD=AB/DC=BA/CD=-CD/AB$, etc., there are only six distinct permutations for this symbol.

To describe the imperfect dislocations it is necessary to introduce the points α, β, γ, and δ at the centres of the faces a, b, c, and d. The presence of one of these letters in the symbol for a dislocation implies that the dislocation includes an imperfect component on the corresponding plane.

The single imperfect dislocations of L_d type are represented by :

(a) δA, δB, δC with $b^2=\frac{1}{6}$;

(b) δD with $b^2=\frac{1}{3}$;

(c) $D\delta/AB$, $D\delta/BC$, $D\delta/CA$ with $b^2=\frac{1}{2}$.

Dislocations of the R_d type are represented by a reversal of the order of the letters but, of course, no distinction can be made between L and ρ or R and λ so that this notation is not as descriptive as the one used in § 3.2 though it is much more compact. For the dislocations on other planes, an obvious change of lettering can be made.

The dissociations of the type (c) dislocations correspond to the forms :

$$D\delta/AB \rightarrow DA+\delta B,$$

and

$$D\delta/AB \rightarrow C\delta+D\delta,$$

where the geometrical proof of the second needs the use of the formula

$$A\delta+B\delta+C\delta=0.$$

The dissociations of perfect dislocations of $(\frac{1}{2}, \frac{1}{2}, 0)$ type follow one of the patterns

$$AB \rightarrow A\alpha + \alpha B$$

or

$$AB \rightarrow A\delta + \delta B,$$

the choice depending on which plane contains the dislocation line. For the combinations of imperfect dislocations, we have :

L_aL_b type : (*a*) $\alpha\beta/CD$ with $b^2=1/9$;
(*b*) $\alpha\beta/AC$, $\alpha\beta/AD$, $\alpha\beta/BC$, $\alpha\beta/BD$ with $b^2=5/18$;
(*c*) $\beta A/\alpha\alpha$, $\alpha B/\beta\beta$ with $b^2=11/18$.

L_aR_b type : (*a*) $\alpha\beta$ with $b^2=1/18$;
(*b*) $A\alpha/B\beta$ with $b^2=2/9$.

The instabilities of the last two groups of the L_aL_b type result from dissociations such as :

$$\alpha\beta/AC \rightarrow D\beta + \alpha\beta$$

and

$$\beta A/\alpha\alpha \rightarrow A\alpha/B\beta + A\beta.$$

3.4. *Associated Lattices*

The analysis in § 3.1 was based solely on the assumption of a lattice having primitive vectors of $(0, \frac{1}{2}, \frac{1}{2})$, $(\frac{1}{2}, 0, \frac{1}{2})$, and $(\frac{1}{2}, \frac{1}{2}, 0)$. It can therefore be applied not only to metals such as aluminium or copper which have the simple face-centred cubic structure but also to substances which have other atoms in the unit cell and yet still preserve the symmetry of the face-centred cubic structure, e.g. NaCl, α-ZnS (zincblende), CaF_2 (fluorite). Further, it can be applied without change to the diamond lattice since this corresponds to a face-centred cubic lattice with extra atoms displaced by $(\frac{1}{4}, \frac{1}{4}, \frac{1}{4})$ from the original set and the two sets of atoms are distinguishable by the orientations of their neighbours. Therefore such a displacement as $(\frac{1}{4}, \frac{1}{4}, \frac{1}{4})$ is not a permissible Burgers vector for a dislocation. It would in fact produce a configuration in which one carbon atom was linked equidistantly either to six others at the corners of a flattened octahedron or to four others in a plane. Therefore the stable perfect dislocations of all these structures are of the types (*a*) and (*b*) described in § 3.1.

However, these complex structures do differ in their twinning properties so that, before applying the analysis of § 3.2 to them, we must first consider their layer structures. In diamond the layer structure is . . . aabbccaabbcc . . . and in fluorite it is . . . aαabβbcγcaαa . . . If the layer doublets and triplets in these structures are manipulated like the single layers of the elementary face-centred cubic structure, each carbon atom in diamond is still surrounded by four equidistant carbon atoms and each ion in fluorite preserves its number of nearest neighbours of like and unlike sign. The prevalence of twins in both these substances

confirms the possibility of this manipulation. Zincblende with a layer structure of . . . aαbβcγaα . . . differs from these in that the layer pairs are polar in character but their sequence can still be manipulated in the same way. A great range of ' stacking-fault ' structures is known for carborundum which has the same structure. The regular periodicity of these must be attributed to the dislocation systems on which their growth is based (Frank 1951 b).

On the other hand, in NaCl with a layer sequence of . . . aγbαcβaγb . . . no such manipulation is possible. In this sequence any three successive letters are unlike in respect of their positions in their respective alphabets and Latin and Greek letters alternate. Hence each layer is determined by the two preceding ones. Accordingly, twins are not observed and there should be no stacking faults. Therefore, all dislocations in a NaCl-type lattice must be perfect.

§ 4. Hexagonal Close-packed Lattice

In the hexagonal close-packed lattice (e.g. magnesium, β–ZnS (wurtzite)) the primitive unit cell contains two like atoms whose environments differ in orientation. The displacement from one to the other is therefore not a permissible Burgers vector for a dislocation line surrounded by good crystal (cf. diamond in § 3.4). We shall use a Cartesian reference system with the interatomic distance in the basal plane as unit of length. A set of primitive vectors is then (1, 0, 0), $(-\frac{1}{2}, \frac{1}{2}\sqrt{3}, 0)$, and (0, 0, K), where K is the axial ratio, c/a, which is equal to $\sqrt{(8/3)}$ for the packing of hard spheres. These primitive vectors are parallel to the first, second, and fourth axes when the hexagonal structure is referred to the more usual four-axed system.

4.1. *Perfect Dislocations*

From the primitive vectors given in § 4, we can construct :

(*a*) 6 vectors : $(\pm 1, 0, 0)$ and $(\pm\frac{1}{2}, \pm\frac{1}{2}\sqrt{3}, 0)$ with $b^2=1$. These are the displacements from one lattice point to its nearest neighbours in the basal plane.

(*b*) 2 vectors : $(0, 0, \pm K)$ with $b^2=K^2\sim 8/3$. These are the displacements from one lattice point to its second nearest neighbours.

(*c*) 12 vectors : $(\pm 1, 0, \pm K)$ and $(\pm\frac{1}{2}, \pm\frac{1}{2}\sqrt{3}, \pm K)$ with $b^2=1+K^2 \sim 11/3$. These are the displacements from one lattice point to its third nearest neighbours.

Dislocations of types (*a*) and (*b*) are stable while those of type (*c*) are of doubtful stability against dissociation into one of type (*a*) and one of type (*b*). All other combinations of the primitive vectors correspond to unstable dislocations.

It should be noticed that the displacements to the nearest neighbours not in the basal plane are excluded as Burgers vectors for the reason given in § 4.

4.2. *Imperfect Dislocations*

Considered as a structure of layers parallel to the basal plane, the perfect lattice has the sequence . . . abab . . . where the a- and b-layers are close-packed planes which have projections on the basal plane of (0, 0)+base lattice vectors and $(\frac{1}{2}, \frac{1}{6}\sqrt{3})$+base lattice vectors respectively, the perpendicular distance between layers being $\frac{1}{2}K$. To obtain imperfect dislocations we must consider c-layers which project onto $(\frac{1}{2}, -\frac{1}{6}\sqrt{3})$+base lattice vectors, and analysis on the same lines as for the face-centred cubic structure (§ 3) indicates that these can be introduced into the structure at intervals without greatly affecting the energy. Obviously the sequences . . . bcbcbc . . . and acacac . . . also represent perfect close-packed hexagonal lattices. In order to classify the various types of translation-twin that can occur, we will use the convention due to Frank (1951 b) of describing any of the successions a to b, b to c, or c to a

Fig. 9

Possible stacking faults in a hexagonal close-packed lattice. (The [001] direction is vertically upwards in the plane of the paper in figs. 9–11.)

as △, and their opposites as ▽. On this basis, hexagonal close-packing produces a sequence . . . △▽△▽△ . . . and any translation-twin will introduce a finite number of extra △'s or ▽'s. Thus a twin that produces two extra △ successions is denoted by (2△), and so on.

Four different types of intrinsic translation-twins are possible and these are denoted by (1△), (1▽), (2△), and (2▽) (see fig. 9). Of these, the first two involve only one breach of the rule that next nearest neighbour layers should be alike while the second pair involve two such breaches. This suggests that the former ones may involve a smaller energy increase but, on the other hand, the latter ones can be formed by a single act

of basal slip and hence they may occur more frequently. Further, translation twins of the extrinsic type may be formed by separating two layers by $\frac{1}{2}K$ and then inserting a c-layer. These are of the types $(3\triangle)$ and $(3\triangledown)$ shown in fig. 9. As these involve two breaches of the next nearest neighbour rule and cannot be formed by one basal slip they may be rare. More complex extrinsic twins may be formed but they can all be considered as combinations of these simpler types so that our list of imperfect dislocations will include only those which bound the six types of twin already introduced.

Since the Burgers vector of the dislocation at the left boundary of a translation-twin surface may be equal to any translation of the upper portion which will generate the twin and that of the right boundary may be the negative of any of these, we can write down possible vectors for the bounding dislocations. A typical set is :

$(\frac{1}{2}, \frac{1}{6}\sqrt{3}, \frac{1}{2}K)L(1\triangle)$	$(-\frac{1}{2}, -\frac{1}{6}\sqrt{3}, -\frac{1}{2}K)R(1\triangle)$
$(-\frac{1}{2}, -\frac{1}{6}\sqrt{3}, -\frac{1}{2}K)L(1\triangledown)$	$(\frac{1}{2}, \frac{1}{6}\sqrt{3}, \frac{1}{2}K)R(1\triangledown)$
$(-\frac{1}{2}, -\frac{1}{6}\sqrt{3}, 0)L(2\triangle)$	$(\frac{1}{2}, \frac{1}{6}\sqrt{3}, 0)R(2\triangle)$
$(\frac{1}{2}, \frac{1}{6}\sqrt{3}, 0)L(2\triangledown)$	$(-\frac{1}{2}, -\frac{1}{6}\sqrt{3}, 0)R(2\triangledown)$
$(0, 0, \frac{1}{2}K)L(3\triangle), L(3\triangledown)$	$(0, 0, -\frac{1}{2}K)R(3\triangle), R(3\triangledown).$

The most general boundary vector then consists of a combination of the appropriate one of these with a true lattice vector and the dislocations corresponding to all such combinations must be tested for stability against dissociation. Moreover, as in the face-centred cubic case, in addition to the dissociation into a perfect dislocation plus another imperfect dislocation of the same type, we can also have dissociations into two imperfect dislocations of different types. Such possible dissociations are :

$$D(1\triangle)\rightarrow D(2\triangle)+D(1\triangledown) \text{ or } D(3\triangle)+D(2\triangledown),$$
$$D(2\triangle)\rightarrow D(1\triangle)+D(1\triangle) \text{ or } D(3\triangle)+D(1\triangledown),$$
$$D(3\triangle)\rightarrow D(2\triangle)+D(1\triangle).$$

For these dissociations to occur without delay at least one of the component dislocations must be glissile, i.e. the third index of its Burgers vector must be zero. This implies that at least one of the components must be of $(2\triangle)$ or $(2\triangledown)$ type so that the dissociations given for $D(2\triangle)$ must be considered further and this is done below.

On the above conditions, we find the following stable sets (illustrated in fig. 10) :

(*a*) 3 vectors : $(\pm\frac{1}{2}, -\frac{1}{6}\sqrt{3}, 0)$, $(0, \frac{1}{3}\sqrt{3}, 0)$ as $L(2\triangle)$ or $R(2\triangledown)$, together with their negatives as $L(2\triangledown)$ or $R(2\triangle)$, making 12 in all having $b^2=\frac{1}{3}$. These are the displacements to the nearest twin lattice positions in the basal plane.

(*b*) 2 vectors : $(0, 0, \pm\frac{1}{2}K)$ as $L(3\triangle)$, $R(3\triangle)$, $L(3\triangledown)$, or $R(3\triangledown)$, making 8 in all having $b^2=\frac{1}{4}K^2\sim\frac{2}{3}$. These are the normal displacements from one layer to the next.

Fig. 10

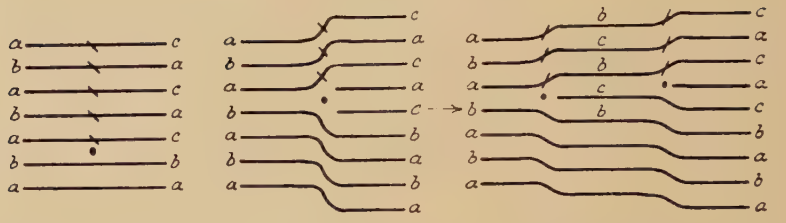

$\left(\frac{1}{2}, -\frac{1}{2\sqrt{3}}, 0\right) L(2\triangle)$ etc. $\left(\frac{1}{2}, -\frac{1}{2\sqrt{3}}, K\right) L(2\triangle)$ $\rightarrow$ $\left(\frac{1}{2}, \frac{1}{2\sqrt{3}}, \frac{K}{2}\right) L(1\triangle)$

or $\left(0, -\frac{2}{\sqrt{3}}, 0\right) L(2\triangle)$ etc. or $\left(0, -\frac{2}{\sqrt{3}}, K\right) L(2\triangle)$ or $\left(0, -\frac{1}{\sqrt{3}}, \frac{K}{2}\right) L(1\triangle)$

$+ \left(0, -\frac{1}{\sqrt{3}}, \frac{K}{2}\right) L(1\triangle)$

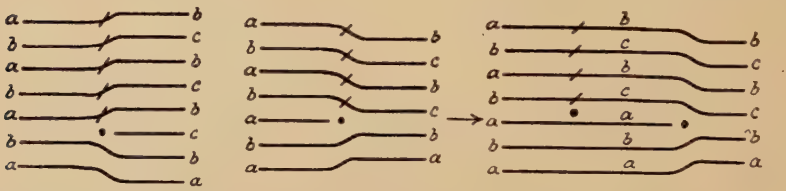

$\left(\frac{1}{2}, \frac{1}{2\sqrt{3}}, \frac{K}{2}\right) L(1\triangle)$ etc. $\left(\frac{1}{2}, \frac{1}{2\sqrt{3}}, -\frac{K}{2}\right) L(1\triangle) \rightarrow \left(\frac{1}{2}, \frac{1}{2\sqrt{3}}, 0\right) L(2\triangledown)$

$+ \left(0, 0, -\frac{K}{2}\right) L(3\triangle)$

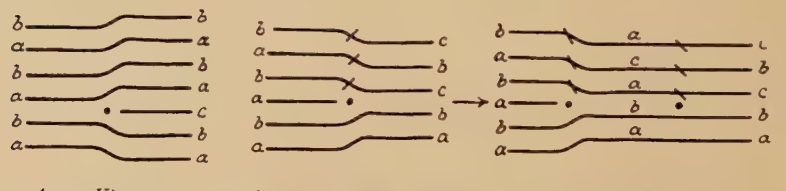

$\left(0, 0, \frac{K}{2}\right) L(3\triangle)$ $\left(0, \frac{2}{\sqrt{3}}, -\frac{K}{2}\right) L(1\triangle) \rightarrow \left(0, \frac{1}{\sqrt{3}}, \frac{K}{2}\right) L(1\triangledown)$

$+ \left(0, \frac{1}{\sqrt{3}}, 0\right) L(2\triangle)$

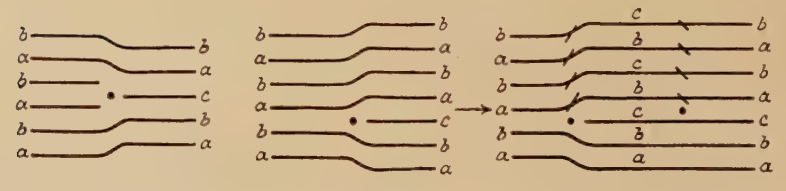

$\left(0, 0, -\frac{K}{2}\right) L(3\triangle)$ $\left(1, 0, \frac{K}{2}\right) L(3\triangle) \rightarrow \left(\frac{1}{2}, \frac{1}{2\sqrt{3}}, \frac{K}{2}\right) L(1\triangle)$

$+ \left(\frac{1}{2}, -\frac{1}{2\sqrt{3}}, 0\right) L(2\triangle)$

Layer structures about some L type dislocations in a hexagonal lattice, together with various dissociations.

(*c*) 6 vectors : $(\pm\frac{1}{2}, \frac{1}{6}\sqrt{3}, \pm\frac{1}{2}K)$, $(0, -\frac{1}{3}\sqrt{3}, \pm\frac{1}{2}K)$ as $L(1\triangle)$ or $R(1\triangledown)$, together with their negatives as $L(1\triangledown)$ or $R(1\triangle)$, making 24 in all having $b^2=\frac{1}{3}+\frac{1}{4}K^2\sim 1$. These are the displacements to nearest neighbour atoms not in the same basal plane.

(*d*) 3 vectors : $(0, -\frac{2}{3}\sqrt{3}, 0)$, $(\pm 1, \frac{1}{3}\sqrt{3}, 0)$ as $L(2\triangle)$ or $R(2\triangledown)$, together with their negatives as $L(2\triangledown)$ or $R(2\triangle)$, making 12 kinds in all having $b^2=4/3$.

(*e*) 6 vectors : $(\pm\frac{1}{2}, -\frac{1}{6}\sqrt{3}, \pm K)$, $(0, \frac{1}{3}\sqrt{3}, \pm K)$ as $L(2\triangle)$ or $R(2\triangledown)$, together with their negatives as $L(2\triangledown)$ or $R(2\triangle)$, making 24 kinds in all having $b^2=\frac{1}{3}+K^2\sim 3$.

(*f*) 6 vectors : $(0, -\frac{2}{3}\sqrt{3}, \pm K)$, $(\pm 1, \frac{1}{3}\sqrt{3}, \pm K)$ as $L(2\triangle)$ or $R(2\triangledown)$, together with their negatives as $L(2\triangledown)$ or $R(2\triangle)$, making 24 kinds in all having $b^2=4/3+K^2\sim 4$.

Types (*a*) and (*b*) are stable while type (*c*) are doubtfully stable against dissociations of the type :

$$(\tfrac{1}{2}, \tfrac{1}{6}\sqrt{3}, \tfrac{1}{2}K)L(1\triangle) \rightarrow (0, 0, \tfrac{1}{2}K)L(3\triangle)+(\tfrac{1}{2}, \tfrac{1}{6}\sqrt{3}, 0)L(2\triangledown).$$

Types (*d*), (*e*), and (*f*) are all doubtfully stable against dissociations into one perfect dislocation and one imperfect dislocation of type (*a*). Furthermore, the latter two types are unstable against dissociations of the types :

$$(\tfrac{1}{2}, -\tfrac{1}{6}\sqrt{3}, K)L(2\triangle) \rightarrow (\tfrac{1}{2}, \tfrac{1}{6}\sqrt{3}, \tfrac{1}{2}K)L(1\triangle)+(0, -\tfrac{1}{3}\sqrt{3}, \tfrac{1}{2}K)L(1\triangle)$$

and

$$(0, -\tfrac{2}{3}\sqrt{3}, K)L(2\triangle) \rightarrow 2(0, -\tfrac{1}{3}\sqrt{3}, \tfrac{1}{2}K)L(1\triangle),$$

but these dissociations can only occur by a process involving dislocation climb since the component dislocations are sessile (see fig. 10). Since, however, this climb involves only a small amount of local diffusion of vacancies or interstitial atoms, it should occur quite easily and we will class dislocations of types (*e*) and (*f*) as unstable. This analysis gives in all 20 stable and 36 doubtfully stable imperfect dislocations. However, it must be noted that, by a rotation of the original cartesian axes through 60° about [001], we get an equivalent reference system in which $\triangle$ has become $\triangledown$ and vice versa. Therefore, the distinction between the $\triangle$ and $\triangledown$ sets, though it has been convenient in the above, really depends only on the original choice of reference system. In fact, then, there are only 10 different Burgers vectors corresponding to stable and 18 corresponding to doubtfully stable imperfect dislocations in the hexagonal lattice. Unlike the face-centred cubic case, there is here only one plane parallel to which we can get translation-twin surfaces so that no complexity arises from the interaction of two imperfect dislocations on different planes.

The ordinarily stable perfect dislocations become unstable against extension into two or more imperfect dislocations when the dislocation line lies in the basal plane. Possible extensions are given below and illustrated in fig. 11.

$$(1, 0, 0) \rightarrow (\tfrac{1}{2}, -\tfrac{1}{6}\sqrt{3}, 0)L(2\triangle)+(\tfrac{1}{2}, \tfrac{1}{6}\sqrt{3}, 0)R(2\triangle) \text{ or } (\tfrac{1}{2}, \tfrac{1}{6}\sqrt{3}, 0)L(2\triangledown)$$
$$+(\tfrac{1}{2}, -\tfrac{1}{6}\sqrt{3}, 0)R(2\triangledown),$$

$$(0, 0, K) \rightarrow (\tfrac{1}{2}, \tfrac{1}{6}\sqrt{3}, \tfrac{1}{2}K)L(1\triangle)+(-\tfrac{1}{2}, -\tfrac{1}{6}\sqrt{3}, \tfrac{1}{2}K)R(1\triangle).$$

$$(1, 0, K) \rightarrow (\tfrac{1}{2}, \tfrac{1}{6}\sqrt{3}, \tfrac{1}{2}K)L(1\triangle)+(\tfrac{1}{2}, -\tfrac{1}{6}\sqrt{3}, \tfrac{1}{2}K)R(1\triangle).$$

The first of these occurs spontaneously and presumably such extended dislocations are the dislocations involved in basal slip in hexagonal lattices. The other extensions involve dislocation climb and hence cannot occur spontaneously. Further, these dislocations become incapable of glide when they are extended.

Fig. 11

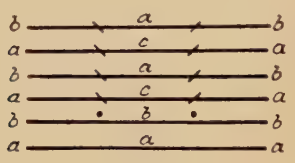

$$\left(\tfrac{1}{2}, -\frac{1}{2\sqrt{3}}, 0\right)L(2\triangle) + \left(\tfrac{1}{2}, \frac{1}{2\sqrt{3}}, 0\right)R(2\triangle) = (1, 0, 0)$$

or

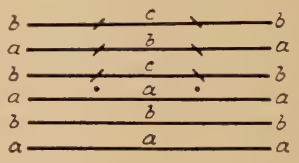

$$\left(\tfrac{1}{2}, \frac{1}{2\sqrt{3}}, 0\right)L(2\triangledown) + \left(\tfrac{1}{2}, -\frac{1}{2\sqrt{3}}, 0\right)R(2\triangledown)$$

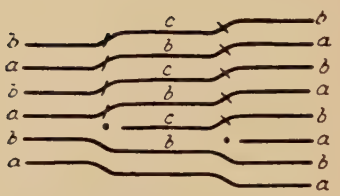

$$\left(\tfrac{1}{2}, \frac{1}{2\sqrt{3}}, \frac{K}{2}\right)L(1\triangle) + \left(-\tfrac{1}{2}, -\frac{1}{2\sqrt{3}}, \frac{K}{2}\right)R(1\triangle) = (0, 0, K)$$

or

$$\left(\tfrac{1}{2}, \frac{1}{2\sqrt{3}}, \frac{K}{2}\right)L(1\triangle) + \left(\tfrac{1}{2}, -\frac{1}{2\sqrt{3}}, \frac{K}{2}\right)R(1\triangle) = (1, 0, K)$$

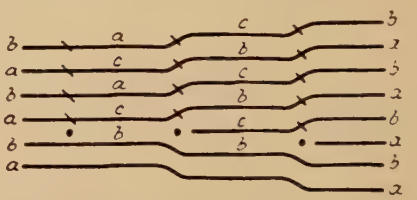

$$\left(0, -\frac{2}{\sqrt{3}}, 0\right)L(2\triangle) + \left(\tfrac{1}{2}, -\frac{1}{2\sqrt{3}}, \frac{K}{2}\right)R(1\triangle + \left(-\tfrac{1}{2}, -\frac{1}{2\sqrt{3}}, \frac{K}{2}\right)R(1\triangle) = (0, -\sqrt{3}, K)$$

Possible modes of extension of various perfect dislocations.

Other more complex stable or metastable arrays may be produced, provided only that the imperfect dislocations form the left and right boundaries for some kind of translation-twin and that the scalar products of the Burgers vectors of adjacent dislocations are positive, e.g. the combination

$$(0, -\tfrac{2}{3}\sqrt{3}, 0)L(2\triangle)+(\tfrac{1}{2}, -\tfrac{1}{6}\sqrt{3}, \tfrac{1}{2}K)R(1\triangle)+(-\tfrac{1}{2}, -\tfrac{1}{6}\sqrt{3}, \tfrac{1}{2}K)R(1\triangle) = (0, -\sqrt{3}, K)$$

which is shown in fig. 11.

§ 5. Body Centred Cubic Lattice

5.1. *Perfect Dislocations*

In the body-centred cubic lattice (e.g. sodium or α-iron), taking the customary unit cell to define a Cartesian reference system and a unit of length, a set of primitive vectors is $(-\frac{1}{2}, \frac{1}{2}, \frac{1}{2})$, $(\frac{1}{2}, -\frac{1}{2}, \frac{1}{2})$, and $(\frac{1}{2}, \frac{1}{2}, -\frac{1}{2})$. From these we can construct :

(*a*) 8 vectors : $(\frac{1}{2}, \frac{1}{2}, \frac{1}{2})$ etc., with $b^2=\frac{3}{4}$. These are the displacements from a lattice point to its nearest neighbours.

(*b*) 6 vectors : (1, 0, 0) etc., with $b^2=1$. These are the displacements to the second nearest neighbours.

Dislocations with Burgers vectors of types (*a*) and (*b*) are stable but all further combinations are unstable. This is the only case in the cubic system where we have found two different types of perfect dislocations with definite stability in the lattice.

5.2. *Imperfect Dislocations*

The body-centred cubic lattice can be described as a layer structure by taking layers perpendicular to a ⟨112⟩ direction. There are then six distinct layers (distinguished by their projections onto a {112} plane) and the perfect lattice is described by the continuing sequence . . . 12345612 . . . Since the twin of this structure is characterized by the sequence . . . 65432165 . . . , Cottrell and Bilby (1951) have proposed that translation-twins may be formed by sequences in which the stacking order is reversed at only one layer, e.g. . . . . 1234345612 . . . However, there is no convincing evidence that such a stacking fault has low energy and hence that such a translation-twin is a stable configuration. Experimentally, growth and recrystallization twins of this form are not observed. Theoretically, although the stacking fault does preserve the distances between atoms in neighbouring *layers*, it preserves neither the nearest neighbour distances, which are of importance if the binding of the lattice is due to central forces, nor the ' bond-angles ', which are important if directed valency bonds are involved. However, if we suppose such faults to exist, then the displacement necessary to form the translation-twin on (112) is $(-\frac{1}{6}, -\frac{1}{6}, \frac{1}{6})$ and from this we can derive the following Burgers vectors for stable imperfect dislocations :

(*a*) 2 vectors : $(-\frac{1}{6}, -\frac{1}{6}, \frac{1}{6})L$ and $(\frac{1}{6}, \frac{1}{6}, -\frac{1}{6})R$, having $b^2=1/12$. These are the twinning dislocations proposed by Cottrell and Bilby.

(*b*) 2 vectors : $(\frac{1}{3}, \frac{1}{3}, -\frac{1}{3})L$ and $(-\frac{1}{3}, -\frac{1}{3}, \frac{1}{3})R$, having $b^2=\frac{1}{3}$. The motion of dislocations with these vectors would cause twinning with twice as large a shear as motion of dislocations of type (*a*).

(*c*) 6 vectors : $(\frac{1}{3}, \frac{1}{3}, \frac{2}{3})L$, $(-\frac{2}{3}, \frac{1}{3}, -\frac{1}{3})L$, $(\frac{1}{3}, -\frac{2}{3}, -\frac{1}{3})L$, and their negatives R, having $b^2=2/3$.

(*d*) 6 vectors: $(-\frac{1}{6}, -\frac{1}{6}, -\frac{5}{6})L$, $(-\frac{1}{6}, \frac{5}{6}, \frac{1}{6})L$, $(\frac{5}{6}, -\frac{1}{6}, \frac{1}{6})L$, and their negatives R, having $b^2=\frac{3}{4}$.

The symbols L and R here refer to the left and right boundaries of a bounded translation-twin when [112] is taken as 'top'. Figure 12 shows the layer arrangement about dislocations with these Burgers vectors. Clearly, dislocations of types (*a*) and (*b*) are glissile but those of types (*c*) and (*d*) are sessile.

We should now consider all possible {112} planes and the possibilities of combinations of imperfect dislocations from different planes but this will not be done here since the evidence for the existence of a stacking fault at all is so inconclusive.

Fig. 12

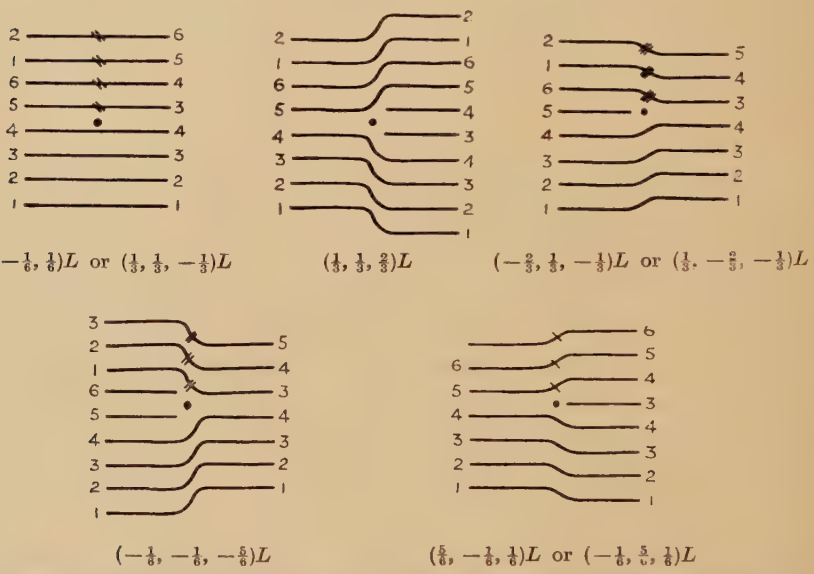

Layer structures about the stable L dislocations of the body-centred cubic lattice with [112] vertically upwards in the plane of the paper.

If these stacking faults do have a low energy, perfect dislocations having dislocation lines in a {112} plane may dissociate to form extended dislocations which have a lower total energy than the original perfect dislocation. If the dislocation line lies in (112), those dislocations of $(\frac{1}{2}, \frac{1}{2}, \frac{1}{2})$ type with Burgers vectors in (112) may extend in such a way as

$$(\tfrac{1}{2}, \tfrac{1}{2}, -\tfrac{1}{2}) \rightarrow (\tfrac{1}{3}, \tfrac{1}{3}, -\tfrac{1}{3})L + (\tfrac{1}{6}, \tfrac{1}{6}, -\tfrac{1}{6})R,$$

and the energy of the component dislocations is then less than that of the original perfect one. However, when the Burgers vector does not lie in (112) the dissociation would have to be of such a form as

$$(\tfrac{1}{2}, \tfrac{1}{2}, \tfrac{1}{2}) \rightarrow (\tfrac{1}{3}, \tfrac{1}{3}, \tfrac{2}{3})L + (\tfrac{1}{6}, \tfrac{1}{6}, -\tfrac{1}{6})R,$$

in which the total dislocation energy is not reduced. These extensions could only occur under an applied stress. However, all dislocations of (1, 0, 0) type can dissociate with a reduction in energy, e.g.

$$(1, 0, 0) \rightarrow (\tfrac{5}{6}, -\tfrac{1}{6}, \tfrac{1}{6})L + (\tfrac{1}{6}, \tfrac{1}{6}, -\tfrac{1}{6})R.$$

Acknowledgment

One of the authors (J.F.N.) would like to acknowledge the kindness of Professor N. F. Mott in allowing him to work at the H. H. Wills Physical Laboratory, University of Bristol, while this study was being carried out.

References

Cottrell, A. H., and Bilby, B. A., 1951, *Phil. Mag.*, **42,** 573.

Frank, F. C., 1949, *Proc. Phys. Soc.* A, **62,** 202 ; 1950, *Plastic Deformation of Crystalline Solids* (Pittsburgh : Carnegie Institute of Technology and U.S. Office of Naval Research), p. 101 ; 1951 a, *Phil. Mag.*, **42,** 809 ; 1951 b, *Ibid.*, **42,** 1014.

Heidenreich, R. D., and Shockley, W., 1948, *Report of the* 1947 *Bristol Conference on the Strength of Solids* (London : The Physical Society), p. 71.

Nabarro, F. R. N., 1952, *Advances in Physics*, **1,** 355 and 376 *et seq.*

Thompson, N., 1953, *Proc. Phys. Soc.* B, **66,** 481.

CXXIX. *The Surface Free Energy of a Metal—I: Normal State**

By R. Stratton†
University of Manchester‡

[Received July 1, 1953]

Abstract

The surface energy of a metal in the normal state is calculated using the model of a free electron gas in a finite potential well. A careful distinction is drawn between the ' lattice surface ' (i.e. the surface which just contains all the cells of the lattice) and the surface of the well. A previous calculation (Huntington 1951) for the terms due to electronic kinetic energy is repeated in a modified form ; it is shown how sums over wave number space can be replaced by integrations if a surface dependent density is used. Further a calculation by Huang and Wyllie (1949) is criticized in relation to the present results.

An estimate of the electrostatic energy of the double layer at the surface is given.

§ 1. Introduction

The total free energy of a piece of metal is the sum of two terms, one proportional to the volume, the other to the surface area. The former, or bulk energy term, will be given by considering a large specimen in which the distribution of electrons is uniform throughout. The latter, or surface energy term, requires a detailed picture of the non-uniform distribution of electrons near the surface of the metal. This in turn leads to a distribution of energy whose sum is in excess of that which would be expected if the density of electrons were uniform up to the surface and zero outside it. This excess is the surface energy of the electron gas which is the main contribution at the absolute zero of temperature. At a non-zero temperature there will be another contribution due to the surface term in the free energy of the lattice vibrations. This arises because the presence of a free surface changes the nature of the modes of vibration. In particular, modes confined to the surface (Rayleigh Waves) are introduced.

Our calculation will be based on the Sommerfeld model of a metal. Here it must be observed that when surface effects are calculated a clear distinction must be drawn between the barrier surface (i.e. position of the square cut potential barrier) and the lattice surface (i.e. the surface which just contains all the cells of the lattice). In fig. 1, the actual electronic

* This paper is part of a Manchester University Ph.D. thesis.
† Communicated by Prof. L. Rosenfeld.
‡ Now at Metropolitan-Vickers Electrical Co. Ltd., Trafford Park, Manchester.

potential, for the case of a flat plate, is plotted as a function of distance across the thickness of the plate. The free electron model implies some sort of averaging process applied to the periodic potential which determines the height of the potential step near the lattice surface. However, the actual position of the step, which must be outside the lattice surface, will be determined by internal properties. These require that the electronic charge density far from the surface must be equal to the positive ionic charge density and thus independent of the thickness of the plate.

The method used to determine the kinetic energy contribution consists in summing the kinetic energies of individual electrons over the occupied states in wave number space. It will, however, be shown that summations over wave number space can be replaced by integrations if the density of states is properly chosen. This density includes an additive surface term which is a function of position in wave number space. The derivation of this density is of importance since it can be used when the volume containing the occupied states is more complicated than the sphere which

Fig. 1

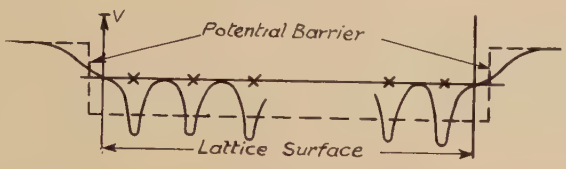

The electrostatic periodic potential (full line) which is replaced by the square cut potential well (broken line). The positions of the positive ions are indicated by crosses.

is used in Sommerfeld's model. In particular it will be used in a following paper for the calculation of the surface energy for a superconducting state.

Due to the fact that the electron distribution extends beyond the lattice surface, a double layer will be formed at the surface. An approximate value of the electrostatic energy of this double layer has also been found and gives a small contribution to the surface energy.

The first attempt to evaluate the surface energy due to an electron gas confined in a finite potential well is made in a paper by Huang and Wyllie (1949), where previous work is reviewed. These authors however, do not distinguish between the lattice and bounded surfaces and effectively take them as coincident. The result differs from the one we obtain.

Huntington (1951) has calculated the gain in energy when a large block is split along a surface. The model of the surface used is the same as ours and the same kinetic surface energy contributions are obtained. We have nevertheless briefly repeated his calculations for two reasons. Firstly, we want to derive the above mentioned relation between integrals and sums which will be used in our following paper. Secondly, we wish to comment on the discrepancy between Huang and Wyllie's calculation and the present one (cf. Appendix).

§ 2. Model

We consider the motion of free electrons in a cubic lattice (spacing a). The lattice is bounded by two parallel planes, a distance $2L_z$ apart, and perpendicular to one of the lattice axes (z axis). We shall calculate the total kinetic energy of the electrons in a rectangular block having dimensions $2L_x$, $2L_y$, $2L_z$ in the x, y, z directions respectively, where x and y are in the directions of the remaining lattice axes. The origin of coordinates is taken at the centre of the plate.

If L_x, $L_y \gg L_z$, the conditions on the surfaces $x=\pm L_x$, $y=\pm L_y$ will not affect the results and we shall take the usual periodic boundary conditions. For the surfaces parallel to the (x, y) plane the boundary condition will be determined by potential barriers, at $z=\pm \mathscr{L}_z (\mathscr{L}_z > L_z)$, where

$$\mathscr{L}_z = L_z(1+d/L_z) \quad . \quad . \quad . \quad . \quad . \quad . \quad . \quad . \quad . \quad (1)$$

and d is a small positive distance of order a, while $L_z \gg a$.

The number ($\mathscr{N}$) of free electrons in the plate is proportional to the number of atoms in the lattice, i.e. to the lattice volume ($V=8L_xL_yL_z$)

$$\mathscr{N} = NV = N\mathscr{V}[1-d/L_z+O(a^2/L_z^2)] \quad . \quad . \quad . \quad . \quad . \quad (2)$$

where $\mathscr{V}=8L_xL_yL_z$ is the volume of the potential well.

The wave functions for electrons fall into two classes, symmetric or antisymmetric with respect to the (x, y) plane namely:

(1) *Symmetric waves*

$$\psi_{\mathbf{k}} = \begin{cases} 2A_{\mathbf{k}} \cos k_z z \exp i(k_x x + k_y y), & |z| \leqslant \mathscr{L}_z \\ 2A_{\mathbf{k}}(-1)^{(n-1)/2} \dfrac{k_z}{\mu} \exp \gamma(\mathscr{L}_z \mp z) \exp i\,(k_x x + k_y y), & \begin{cases} z \geqslant \mathscr{L}_z \\ z \leqslant -\mathscr{L}_z \end{cases} \end{cases} \quad . \quad (3)$$

(2) *Antisymmetric waves*

$$\psi_{\mathbf{k}} = \begin{cases} 2A_{\mathbf{k}} \sin k_z z \exp i(k_x x + k_y y), & |z| \leqslant \mathscr{L}_z \\ \mp 2A_{\mathbf{k}}(-1)^{n/2} \dfrac{k_z}{\mu} \exp \gamma(\mathscr{L}_z \mp z) \exp i\,(k_x x + k_y y), & \begin{cases} z \geqslant \mathscr{L}_z \\ z \leqslant -\mathscr{L}_z \end{cases} \end{cases} \quad . \quad (4)$$

The wave number $\mathbf{k}$ is given by

$$(k_x, k_y, k_z) = \left(\frac{l\pi}{L_x}, \frac{m\pi}{L_y}, \frac{n\pi}{2\mathscr{L}_z} - \frac{\delta}{\mathscr{L}_z}\right) \quad . \quad . \quad . \quad . \quad . \quad (5)$$

where $\sin \delta = k_z/\mu$; $(0 \leqslant \delta < \pi/2)$ l and m are any integers, and n is a positive integer, odd for symmetric and even for antisymmetric waves. Finally, the wave number μ is defined in terms of the potential barrier height (m^* is the effective mass of the electron)

$$\phi = \hbar^2\mu^2/2m^* \quad . \quad . \quad . \quad . \quad . \quad . \quad . \quad . \quad . \quad (6)$$

and

$$\gamma^2 = \mu^2 - k_z^2. \quad . \quad . \quad . \quad . \quad . \quad . \quad . \quad . \quad . \quad (7)$$

§ 3. Summation over the Wave Number Space

The possible states can be represented by points in the k_x, k_y, k_z space according to (5). Since L_x, $L_y \gg L_z$, these points can be considered to lie on the planes $k_z=(n\pi/2\mathscr{L}_z)-\delta/\mathscr{L}_z$ distributed with the uniform density (L_xL_y/π^2). At the absolute zero of temperature, the occupied states will lie in a hemisphere of radius k_m, i.e. on circular sheets of radius $(k_m^2-k_z^2)^{1/2}$. Now k_m will be determined by the condition that the total number of electrons ($\mathscr{N}$) must equal twice the number of occupied states (2 electrons per state due to spin).

$$\mathscr{N}=\sum_{n=1}^{n_m} 2\,.\,\frac{L_xL_y}{\pi^2}[k_m^2-k_z^2]\pi \quad . \quad . \quad . \quad . \quad . \quad . \quad (8)$$

where n_m is the largest integer which satisfies

$$n_m\pi/2\ \mathscr{L}_z-\delta/\mathscr{L}_z\leqslant k_m, \quad . \quad . \quad . \quad . \quad . \quad . \quad (9)$$

so that in general we must put

$$k_m=n_m\pi/2L_z+\nu\pi/2L_z, \quad . \quad . \quad . \quad . \quad . \quad . \quad (10)$$

where ν is a small number of 0 (1).

Using the Euler–Maclaurin formula we can change the sum in (8) to an integral

$$\mathscr{N}=\frac{2L_xL_y}{\pi^2}\,.\,\pi\left\{\int_0^{n_m}(k_m^2-k_z^2)\,dn-\tfrac{1}{2}(k_m^2-k_z^2)_{n=0}+O\left(\frac{k_m}{L_z}\right)\right\} \quad . \quad (11)$$

where

$$dn=\left[1+\frac{1}{\gamma\mathscr{L}_z}\right]\cdot\frac{2\mathscr{L}_z}{\pi}\,dk_z \quad . \quad . \quad . \quad . \quad . \quad (12)$$

from eqn. (5). Carrying out the integration and substituting for $\mathscr{N}$ from (2) and n_m from (10) we find

$$\frac{k_m^3}{3\pi^2}=N\left[1-\frac{1}{L_z}(d-d_\infty+D)+O\left(\frac{1}{k_m^2L_z^2}\right)\right] \quad . \quad . \quad . \quad (13)$$

where

$$d_\infty=3\pi/8k_m \quad . \quad . \quad . \quad . \quad . \quad . \quad . \quad . \quad . \quad (14)$$

$$D=(3/4k_m)[(\lambda-1)^{1/2}+(2-\lambda)\sin^{-1}\lambda^{-1/2}] \quad . \quad . \quad (15)$$

and

$$\lambda=\mu^2/k_m^2>1. \quad . \quad . \quad . \quad . \quad . \quad . \quad . \quad . \quad . \quad (16)$$

Now a direct summation shows that near the centre of the plate the density of electrons has no term in $1/k_mL_z$ (surface term) but is given by

$$n(z=0)=(k_m^3/3\pi^2)[1+O(1/k_m^2L_z^2)]. \quad . \quad . \quad . \quad . \quad (17)$$

Since there cannot exist a free charge in the interior of the plate

$$-en(z=0)+Ne=0 \quad . \quad . \quad . \quad . \quad . \quad . \quad . \quad . \quad (17a)$$

so that

$$k_m^3/3\pi^2=N[1+O(1/k_m^2L_z^2)] \quad . \quad . \quad . \quad . \quad . \quad . \quad (18)$$

showing that k_m is surface independent. Thus from (13)

$$d=d_\infty-D\,; \quad . \quad . \quad . \quad . \quad . \quad . \quad . \quad . \quad . \quad (19)$$

d_∞ is the value of d when $\mu\to\infty$.

We can interpret the two main terms of the expression (11) for $\mathcal{N}$ as follows. The first is an integral over the hemisphere (radius k_m) with the wave number density

$$\rho(k_x, k_y, k_z)\, dk_x\, dk_y\, dk_z = \frac{\mathcal{V}}{2\pi^3}\left[1+\frac{1}{\gamma \mathscr{L}_z}\right] dk_x\, dk_y\, dk_z \quad . \quad . \quad (20)$$

i.e.
$$\rho = (V/2\pi^3)[1+(d+1/\gamma)/L_z] \quad . \quad . \quad . \quad . \quad . \quad . \quad (20a)$$

so that $V/2\pi^3$ is the density for a large specimen. The second term represents a correction due to states having $k_z=0$ which are included in the integral with weight $\frac{1}{2}$.

Similarly we can calculate the kinetic energy either by summing and using the Euler–Maclaurin formula or by using the above wave number density (eqn. 20) and correcting for zero wave number. This gives

$$\mathscr{T} = \mathcal{V}\frac{\hbar^2 k_m{}^5}{10\pi^2 m^*}\left[1-\frac{5\pi}{16 k_m L_z}+\frac{5}{k_m{}^5 L_z}\int_0^{k_m} k_z{}^3 \sin^{-1}\frac{k_z}{\mu}\, dk_z + O\left(\frac{1}{k_m{}^2 L_z{}^2}\right)\right] \quad (21)$$

and substituting for $\mathcal{V}$ from (2) and d from (19)

$$\mathscr{T} = VT + S(\sigma_1+\sigma_2) \quad . \quad . \quad . \quad . \quad . \quad . \quad . \quad . \quad . \quad . \quad . \quad . \quad (22)$$

where

$$T = \hbar^2 k_m{}^5/10\pi^2 m^* \quad . \quad . \quad . \quad . \quad . \quad . \quad . \quad . \quad . \quad . \quad . \quad . \quad (23)$$

is the bulk kinetic energy density,

$$S = 8 L_x L_y \quad . \quad . \quad . \quad . \quad . \quad . \quad . \quad . \quad . \quad . \quad . \quad . \quad . \quad . \quad (24)$$

the surface area, and

$$\sigma_1 = \hbar^2 k_m{}^4/160\pi m^* \quad . \quad . \quad . \quad . \quad . \quad . \quad . \quad . \quad . \quad . \quad . \quad . \quad (25)$$

$$\sigma_2 = -[\hbar^2 k_m{}^4/160\pi m^*][(\lambda-1)^{1/2}(14-15\lambda)+(8-24\lambda+15\lambda^2)\sin^{-1}\lambda^{-1/2}]. \quad . \quad . \quad . \quad . \quad . \quad . \quad (26)$$

The surface energy is made up of two terms, the former (σ_1) being its value for an infinite barrier ($\lambda\to\infty$) while the latter (σ_2) is the correction for a finite barrier (λ finite).

§ 4. The Electrostatic Energy of the Double Layer

Due to the penetration of electronic charge beyond the lattice surface an electrostatic double layer is formed at the surface of the metal. Thus there exists a non-uniform resultant charge distribution $p(Z)$ near the surface of the metal which is negative outside the lattice surface and predominantly positive inside. (We take $Z=z-\mathscr{L}_z$, so that $Z=0$ gives the position of the potential barrier.) The energy of the double layer is given by

$$\sigma_3 = -\pi\int_{-\infty}^{\infty}\int_{-\infty}^{\infty} p(Z_1)p(Z_2)\,|Z_2-Z_1|\,dZ_1\,dZ_2 \quad . \quad . \quad . \quad (27)$$

(Huang and Wyllie 1949).

The electrostatic charge density is given by

$$-en(Z)\, dx\, dy\, dZ = -e\, dx\, dy\, dZ \sum_{\mathbf{k}} |\psi_{\mathbf{k}}|^2. \quad . \quad . \quad . \quad . \quad (28)$$

We will use the free electron wave functions in this sum although the result will be used to calculate the electrostatic interaction energy σ_3. This is of course invalid, since some self-consistent solution should be used. However, we may expect to get the right order of magnitude even with the simple model and since this gives σ_3 only about 10% of σ_1, its exact value will not be so important.

Normalizing the electronic wave functions to obtain the amplitude $(A_{\mathbf{k}})$ we find that

$$\rho|A_{\mathbf{k}}|^2=\frac{1}{4\pi^3}\left[1+O\left(\frac{1}{k_m{}^2L_z{}^2}\right)\right] \quad . \quad . \quad . \quad . \quad . \quad (29)$$

so that the charge densities are independent of surface area as would be expected. Substituting for $\psi_{\mathbf{k}}$ into (28) and changing sums to integrals, gives

$$n(Z)=\frac{1}{\pi^2\mu^2}\int_0^{k_m}(k_m{}^2-k_z{}^2)\,k_z{}^2\,e^{-2\gamma Z}\,dk_z, \quad Z>0 \quad . \quad . \quad . \quad (30)$$

$$n(Z)=\frac{1}{\pi^2}\int_0^{k_m}(k_m{}^2-k_z{}^2)\left[\sin^2 k_zZ+\frac{k_z{}^2}{\mu^2}\cos 2k_zZ-\frac{k_z\gamma}{\mu^2}\sin 2k_zZ\right]dk_z, \quad Z<0.$$

$$. \quad . \quad . \quad . \quad . \quad . \quad . \quad (31)$$

Fig. 2

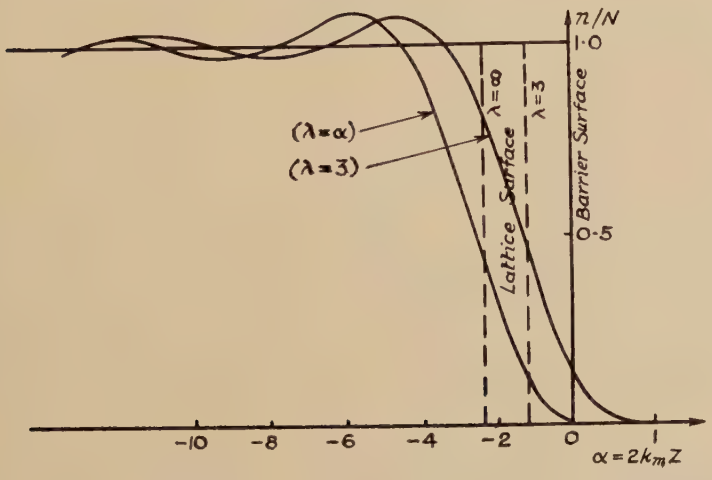

The variation of electron density with distance from the surface.

For an infinite barrier $n(Z)=0$ for $Z>0$ while for $Z<0$

$$n(Z)=\frac{k_m{}^3}{3\pi^2}\left[1+\frac{3}{4}\frac{\cos 2\,k_mZ}{k_m{}^2Z^2}-\frac{3}{8}\frac{\sin 2\,k_mZ}{k_m{}^3Z^3}\right]. \quad . \quad . \quad (32)$$

The function is exhibited in fig. 2, where the positions of the potential barrier $(Z=0)$ and lattice surface are indicated.

When λ is finite, we evaluate the integrals approximately by taking γ as a constant, different for the two integrals, and determining the two appropriate values to give conservation of charge and the correct total

number of electrons outside the potential barrier ($\mathcal{N}_0$ per unit area) which can be determined. Thus

$$\int_{-L}^{\infty} n(z)\,dz = \int_{-L}^{-d} N dZ \quad \ldots\ldots (33)$$

where $L \gg k_m^{-1}$, i.e. a point far removed from the surface, and the positive charge density of the ions is taken to be uniform. We can rewrite (33) as

$$\int_{-\infty}^{0} [N - n(Z)]dZ = \int_{0}^{\infty} n(Z)\,dZ + Nd = \mathcal{N}_0 + Nd \quad \ldots (34)$$

where

$$\mathcal{N}_0 = \int_0^{\infty} n(Z)\,dZ = \frac{3N}{16k_m}[(3\lambda-2)(\lambda-1)^{1/2} + (4-3\lambda)\,\lambda \sin^{-1}\lambda^{-1/2}]. \quad \ldots\ldots (35)$$

Thus

$$n(Z) = N(2/5\lambda)\exp(-\alpha/f) \qquad Z>0 \quad \ldots\ldots (36)$$

$$= N\left[1 - 3\sin\alpha\left\{-\frac{2}{g\lambda}\cdot\frac{1}{\alpha^2} + \left(1-\frac{10}{\lambda}\right)\frac{1}{\alpha^3} + \frac{6}{g\lambda}\frac{1}{\alpha^4} + \frac{24}{\alpha^5}\right\}\right.$$

$$\left. + 3\cos\alpha\left\{\left(1-\frac{2}{\lambda}\right)\frac{1}{\alpha^2} + \frac{6}{g\lambda}\frac{1}{\alpha^3} + \frac{24}{\lambda}\frac{1}{\alpha^4}\right\}\right] \quad \ldots\ldots (37)$$

where $\alpha = 2k_m Z$, $f = k_m/\gamma_0$, $g = k_m/\gamma_i$, and γ_0, γ_i are the two constants to be determined by substituting (36) into (35) and (37) into (34) respectively. This gives

$$f = (15/16)[(3\lambda-2)(\lambda-1)^{1/2} + \lambda(4-3\lambda)\sin^{-1}\lambda^{-1/2}] \quad \ldots (38)$$

$$1/g = (3/16)[(2+\lambda)(\lambda-1)^{1/2} + \lambda(4-\lambda)\sin^{-1}\lambda^{-1/2}]. \quad \ldots (39)$$

The approximation is good for large λ. Since $n(0)$ which is equal to $2N/5\lambda$ does not involve γ in the integrands of (30) and (31), the approximate solutions will be continuous at $Z=0$. The gradient is, however, discontinuous at $Z=0$, the ratio of the two values being γ_i/γ_0. In fig. 2 we also show the approximate solution corresponding to $\lambda=3$, where the approximation is still good.

Now the charge density to be used in the integral for σ_3 is

$$\left.\begin{aligned} p(Z) &= -en(Z) && -d<Z \\ &= [N-n(Z)]e && -d>Z \end{aligned}\right\} \quad \ldots\ldots (40)$$

We have evaluated σ_3 for the particular case $\lambda=3$ by a series of approximations and find

$$\sigma_3 = \nu N e^2\,;\ \nu \approx 5{\cdot}2\,.\,10^{-3}$$

$$\therefore \frac{\sigma_3}{\sigma_1} = \frac{160}{3\pi}\left(\frac{e^2 m}{\hbar^2}\right)\frac{\nu}{k_m} \approx 1{\cdot}0\ 10^9\,\nu/N^{1/3}. \quad \ldots\ldots (41)$$

In the case of Au ($\lambda=2{\cdot}97$, $N=5{\cdot}93\ 10^{22}$), $\sigma_3/\sigma_1 \approx 0{\cdot}13$.

The calculation showed that ν was not very dependent on λ so that (41) with $\nu \approx 5\,.\,10^{-3}$ will be used as an approximate result for all the metals.

§ 5. The Total Surface Free Energy

To estimate the numerical value of σ we require the value of ϕ. This is a bulk property of the metal and can be obtained from the binding energy (W). The free electron wave functions satisfy the equation

$$-\frac{\hbar^2}{2m}\nabla^2\psi_{\mathbf{k}}+\Phi(\mathbf{r})\,\psi_{\mathbf{k}}=\epsilon_{\mathbf{k}}\,\psi_{\mathbf{k}} \quad . \quad . \quad . \quad . \quad . \quad (42)$$

where we have taken the potential funtion $\Phi(\mathbf{r})$ to be zero outside the metal and $-\phi$ inside it. Thus the total electronic energy is

$$\left.\begin{aligned}\mathscr{E}&=\sum_{\mathbf{k}}\epsilon_{\mathbf{k}}=\sum_{\mathbf{k}}\left(\frac{\hbar^2k^2}{2m}-\phi\right)=\sum_{\mathbf{k}}\frac{\hbar^2k^2}{2m}-\mathscr{N}\phi\\&=VT+S\,(\sigma_1+\sigma_2)-VN\phi.\end{aligned}\right\} \quad . \quad . \quad . \quad (43)$$

(The surface term σ_3 is omitted, since the Coulomb interaction is not taken into account in eqn. (42).)

Fig. 3

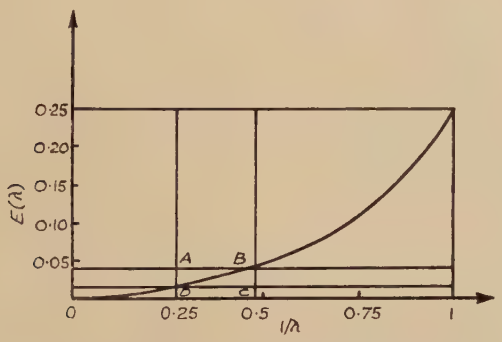

The correction term for finite barriers. The experimental points for monovalent metals are inside the rectangle ABCD.

The value of ϕ is now obtained by equating the bulk energy to the binding energy

$$-W=V(T-N\phi). \quad . \quad . \quad . \quad . \quad . \quad . \quad (44)$$

Table 1 contains values of λ based on values of ϕ as obtained from eqn. (44) by Huang and Wyllie.

Collecting our results, the surface free energy at the absolute zero of temperature is

$$\begin{aligned}\sigma(O)&=\sigma_1+\sigma_2+\sigma_3\\&=2{\cdot}22\,(N\,.\,10^{-21})^{4/3}[1+\epsilon(\lambda)]+1{\cdot}1\,N\,10^{-21}\,\text{erg. cm}^{-2} \quad . \quad . \quad (45)\end{aligned}$$

where $\epsilon(\lambda)=\sigma_2/\sigma_1$, and is plotted in fig. 3. (The normal mass of the electron has been used.)

The change in σ due to a finite temperature T will in the main be due to the thermal excitation of the lattice waves. This contribution has been

recalculated by the author (Stratton 1953) and is

$$\sigma_L = -9A(K)\, k\theta_D N^{2/3} Z(x) \quad . \quad . \quad . \quad . \quad . \quad . \quad . \quad (46)$$

where

$$Z(x) = \frac{1}{x^3}\int_0^x \frac{u^2 du}{e^u - 1}\ ; \quad x = \theta_D/T \quad . \quad . \quad . \quad . \quad . \quad . \quad . \quad (47)$$

and θ_D is the Debye temperature. The function $Z(x)$ is tabulated in Huang and Wyllie's paper while the constant $A(K)$ has been evaluated for three values of the elastic constant K ($K = 1/2s - 1$ where s is Poissons' ratio) by the author.

Except for an experiment on copper (Udin *et al.* 1949) all the experimental values of surface energy refer to liquid metals. We thus evaluate σ_L at the melting point and compare the theoretical and experimental values of surface energy (table 1). Since σ_L is in any case negative we

Table 1

Metal	$N \times 10^{-22}$	λ	σ_1 (erg cm^{-2})	$\epsilon(\lambda)$	σ_2 (erg cm^{-2})	σ_3 (erg cm^{-2})	$\sigma(0)$ (erg cm^{-2})	$-\sigma_L(T_m)$ (erg cm^{-2})	$\sigma(T_m)$ (erg cm^{-2})	σ exp (T_m) (erg cm^{-2})
Cu	8·5	2·18	830	0·040	30	90	950	260	740	1100 (1400)
Au	5·93	2·97	510	0·025	10	70	590	140	450	600–1000
Ag	5·90	2·49	510	0·033	20	70	600	150	450	800
Li	4·63	2·09	370	0·044	20	50	440	40	400	—
Na	2·56	2·58	170	0·030	5	30	210	20	190	290
K	1·33	3·18	70	0·022	2	10	80	10	70	200–400
Rb	1·08	3·43	53	0·020	1	10	60	10	50	—
Cs	0·87	3·70	40	0·019	1	10	50	10	40	—
Hg	4·40	3	350	0·025	9	50	410	20	390	460

(The values of σ_{exp} are taken from Huang and Wyllie's paper while the second experimental value for Cu quoted is that for solid Cu near the melting point.)

cannot expect a very close agreement as $\sigma(O)$ is already less than the experimental result in all cases. Thus to get some idea of the order of magnitude involved we take $K = 1$, corresponding to metals obeying Couchy's relation. Thus

$$\sigma(T) = 2{\cdot}22\ (N\ .\ 10^{-21})^{4/3}[1 + \epsilon(\lambda)] + 1{\cdot}1\ N\ 10^{-21} - 0{\cdot}016\, \theta_D Z(x)\ N\ 10^{-21}$$

$$\text{erg cm}^{-2}. \quad . \quad . \quad . \quad . \quad . \quad . \quad (48)$$

The various quantities are given in table 1 for monovalent metals and mercury taking one free electron per atom in each case. Although the results are probably only applicable to monovalent metals, mercury is included since we will deal with its surface energy in the superconducting state.

§ 6. Further Remarks

We can find the kinetic energy density $t(Z)$ in exactly the same way as $n(Z)$. This shows that $t(Z)\to T$ as $Z\to-\infty$, i.e. far from the surface. The behaviour of $t(Z)$ which is similar to that of $n(Z)$, shows that the surface energy contributions are really confined to the surface region.

The calculated values of the surface energy are about two thirds of the measured values. This is probably all that can be expected from the use of the free electron model, to calculate the predominant term σ_1.

It can easily be seen from the results of § 3 that the total kinetic energy can be written as a series

$$\mathscr{T}=VT[1+c_1a/L_z+c_2a^2/L_z^2+\dots] \quad . \quad . \quad . \quad . \quad . \quad (49)$$

where the second term corresponds to the surface energy. Thus when L_z becomes comparable with a more terms must be evaluated to give the total energy. However, in this case it would be better to treat the problem as two-dimensional.

Acknowledgments

The author wishes to thank Professor L. Rosenfeld and Dr. A. Papapetrou for the interest they have taken in the work at all stages. It was done during the tenure of a grant from the Department of Scientific and Industrial Research.

APPENDIX

On Huang and Wyllie's Calculation

The authors effectively assume $d=O$ at the outset. Thus their value of k_m, as given by eqn. (13) is

$$k_m^3/3\pi^2=N[1+(d_\infty+D)/L_z]. \quad . \quad . \quad . \quad . \quad . \quad (50)$$

Using this value of k_m as the upper limit in the integrals over wave number space and putting $d=O$ in the density ρ (eqn. (20)) gives their result. A surface dependent k_m, however, incompatible with charge conservation as may be seen from eqn. (18).

The authors do not notice this inconsistency because in their calculation of the σ_3-term they effectively use the surface independent value ($k_m^3=3\pi^2N$). This is the origin of the misleading remark that (in the interior of the metal) " charge is conserved by their method within the Fermi–Thomas approximation " (c.f. part of a letter by Wyllie quoted by Huntington (1951)). In actual fact, the discrepancy cannot be removed whatever method is used ; the question raised by Huntington about the adequacy of the Fermi Thomas method, used to obtain a self-consistent solution, is irrelevant in this connection.

The consistent way of using the Fermi–Thomas method is as follows. If $-eV$ is the potential energy of the electron, we have

$$\frac{d^2V}{dZ^2} = 4\pi e\,[N - n(Z)]\,; \quad n(Z) = \sum_{\mathbf{k}} |\psi_{\mathbf{k}}|^2. \quad . \quad . \quad . \quad . \quad (51)$$

Now if we rewrite eqns. (36) and (37) as $n(Z) = NQ(k_m Z)$ then, including the space dependence of k_m introduced in the Fermi–Thomas approximation, we have

$$n(Z) = \frac{[\{E_m + eV(Z)\}2m]^{3/2}}{3\pi^2\hbar} Q[(3\pi^2 N)^{1/3} Z] \quad . \quad . \quad . \quad (52)$$

where $E_m = \hbar^2 k_m{}^2/2m$ is the Fermi energy in the interior. The additional factor Q makes the solution of (51) very difficult. In view of the smallness of σ_3 as estimated in § 4 no attempt has been made in this direction.

References

Huang, K., and Wyllie, G., 1949, *Proc. Phys. Soc.* A, **62,** 180.
Huntington, H. B., 1951, *Phys. Rev.*, **81,** 1035.
Stratton, R., 1953, *Phil. Mag.*, **44,** 519.
Udin, H., Shaler, A. J., and Wulff, J., 1949, *J. of Metals* (*Trans.*), **1,** 186.

CXXX. *The Surface Free Energy of a Metal II : Superconducting State**

By R. Stratton†
University of Manchester‡

[Received July 1, 1953]

Abstract

The matrix elements of the electron-lattice interaction, for a plate of finite thickness, are calculated using Bethe's (1933) method. These are then used to calculate the energy of the superconducting state as described by Fröhlich (1950). Previous calculations are extended by including terms proportional to the surface area. The technique of replacing sums by integrals with surface dependent densities has been used throughout.

§ 1. Introduction

It has long been recognized that the critical magnetic field H_c which can destroy superconductivity in a metal cooled below the transition temperature, depends on the dimensions of the specimen. (Longitudinal magnetic field, cylindrical specimen or flat plate.) This dependence is, however, very slight, a notable increase in H_c occurring only when one of the dimensions is of the order of the penetration depth ($\lambda \simeq 10^{-5}-10^{-6}$ cm). The increase is due to two surface effects, entering into the free energy balance at the transition, which have been discussed by Ginsburg (1945). London's theory gives an electromagnetic energy which is confined to a layer at the surface whose thickness is of order λ, while we may also expect a change in the surface energy of the metal. It should be pointed out that the origin of these energies is quite different ; the former is due to the penetration of the magnetic field and is a macroscopic effect, the latter is due to the finite size of the lattice and is a microscopic effect confined to a surface layer whose thickness is of the order of 10^{-8} cm.

The following investigation was undertaken in order to get some idea of the origin and order of magnitude of the surface energy difference. It is based on Fröhlich's (1950, referred to as F_1) theory of the superconducting state. Fröhlich shows that when electron-lattice interactions are considered, the normal or Fermi distribution does not lead to a stable state. A new distribution is derived leading to a stable state (for sufficiently strong electron-lattice coupling) which is identified with the superconducting state. We have recalculated the energy of this new state for the particular

* This paper is part of a Manchester University Ph.D. thesis.
† Communicated by Prof. L. Rosenfeld.
‡ Now at Metropolitan-Vickers Electrical Co. Ltd., Trafford Park, Manchester.

case of a flat plate (using the model of I) including terms proportional to the surface area. In § 2 we give the electronic wave functions and lattice waves for a finite lattice which are then used to derive the matrix elements of the interaction (§ 3). These can finally be used to calculate the energy of the new state by means of a second order perturbation calculation (§ 4). The method consists essentially in the replacement of sums over wave number space by integrals with proper densities which have been previously used by the author.

§ 2. Model

We will assume that the periodic potential energy of an electron has the form

$$V(x, y, z)=V_1(z)+V_2(x, y). \quad . \quad . \quad . \quad . \quad . \quad . \quad (1)$$

Here V_2 will have the periodicity of the lattice in the x, y directions while V_1 has the form indicated by fig. 1 in I. (Note that $V_1=-eV$ here.) The wave functions then have the simple form (inside the lattice surface)

$$\phi_{\mathbf{k}}(x, y, z)=(A_{k_z}u_{k_z}(z)\exp ik_z z+A_{-k_z}u_{-k_z}(z)\exp(-ik_z z))v_{\hat{\mathbf{k}}}(x, y)\exp i\hat{\mathbf{k}}\,.\,\hat{\mathbf{r}}. \quad . \quad . \quad . \quad . \quad . \quad . \quad (2)$$

The first factor, which corresponds to the solution of the separated wave equation containing V_1, has been discussed by Shockley (1939). Here u_{k_z} is a function of z having the lattice periodicity while A_{k_z} is a constant. The permitted values of k_z can be determined from the boundary conditions. The second factor is the two-dimensional analogue of the usual Bloch wave corresponding to V_2 so that

$$\hat{\mathbf{k}}=(k_x, k_y)=(n_x\pi/L_x, n_y\pi/L_y) \text{ and } \hat{r}=(x, y) \quad . \quad . \quad . \quad . \quad . \quad (3)$$

where n_x and n_y are any integers. The constants are chosen so that the uv are normalized per unit cell, i.e.

$$\int u_{k_z}{}^{*}\, v_{\hat{\mathbf{k}}}{}^{*}\, u_{k_z}\, v_{\hat{\mathbf{k}}}\, d\tau_0=1 \quad . \quad . \quad . \quad . \quad . \quad . \quad . \quad (4)$$

where $d\tau_0$ is the volume element of a unit cell.

As a rough approximation we will take the values of k_z and A_{k_z} obtained in I for a constant electrostatic potential. Thus

$$|A_{k_z}|^2=|A_{-k_z}|^2=\frac{a^2}{2V}\left[1-\frac{1}{L_z}\left(\frac{1}{y}+d\right)\right] \quad . \quad . \quad . \quad . \quad (5)$$

since (4) reduces to $|u_{k_z}u_{\hat{\mathbf{k}}}|^2=1/a^3$.

The lattice waves will be replaced by the corresponding elastic waves obtained when the discrete lattice is identified with an isotropic elastic medium (Stratton 1953, referred to as ξ). The analysis shows that the normal modes fall into four classes, three of which consist of mixtures of a longitudinal (wave number q_l) and a transverse (wave number q_t) compon-

ent while one consists of purely transverse waves. The most general displacement can then be written in the form

$$\mathbf{u}(r)=\sum_{\mathbf{q}}[\underline{Z_{\mathbf{q}}}(z)\exp(i\hat{\mathbf{q}}\cdot\hat{\mathbf{r}})\ \theta_{\mathbf{q}}+\underline{Z_{\mathbf{q}}}^{*}(z)\exp(-i\hat{\mathbf{q}}\cdot\mathbf{r})\,\theta_{\mathbf{q}}^{*}] \quad . \quad . \quad . \quad (6)$$

where ($\hat{\mathbf{q}}=(q_x, q_y)$, $\boldsymbol{\zeta}$=unit vector in z direction)

$$\overset{S}{A}\underline{Z_{\mathbf{q}}}=\hat{\mathbf{q}}\,[\overset{S}{A}\mathscr{P}_l\{\exp(iq_{lz}z)\pm\exp(-iq_{lz}z)\}+\overset{S}{A}\mathscr{P}_t\{\exp(iq_{tz}z)\pm\exp(-iq_{tz}z)\}\,q_{tz}/q]$$
$$+\boldsymbol{\zeta}[\overset{S}{A}\mathscr{P}_l\{\exp(iq_{lz}z)\mp\exp(-iq_{lz}z)\}q_{lz}-\overset{S}{A}\mathscr{P}_t\{\exp(iq_{tz}z)\mp\exp(-iq_{lz}z)\}\hat{q}] \quad . \quad . \quad . \quad . \quad (7)$$

for the three mixed types, and the θ_q are time dependent normal coordinates if the Z are normalized, i.e.

$$2\rho_0\int \underline{Z_{\mathbf{q}}}^{*}\cdot\underline{Z_{\mathbf{q}}}\,d\tau=8L_xL_y\rho_0\int_{-L_z}^{L_z}\underline{Z_{\mathbf{q}}}^{*}\,\underline{Z_{\mathbf{q}}}\,dz=1 \quad . \quad . \quad . \quad . \quad . \quad . \quad (8)$$

(ρ_0 is the density of the medium). The sum is to include terms for the four types of vibration, both symmetrical (S) and antisymmetrical (A) and all the permitted wave numbers $\mathbf{q}_t$ (or $\mathbf{q}_l$) discussed in S. Quantization of the Hamiltonian gives the matrix elements of the normal coordinates :

$$(\theta_q)_{N_{\mathbf{q}}-1,\,N_{\mathbf{q}}}=\sqrt{\left(\frac{\hbar N_{\mathbf{q}}}{\omega_{\mathbf{q}}}\right)};\ (\theta^{*})_{N_{\mathbf{q}}+1,\,N_{\mathbf{q}}}=\sqrt{\left(\frac{\hbar(N_{\mathbf{q}}+1)}{\omega_{\mathbf{q}}}\right)} \quad . \quad . \quad . \quad . \quad (9)$$

all other elements begin zero. ($N_{\mathbf{q}}$ is the quantum number of the vibration with wave number $\mathbf{q}$ and angular frequency ω_q.)

The normalization condition and the known relation between the amplitudes $\mathscr{P}_l$ and $\mathscr{P}_t$ (S eqn. (13)) enables us to calculate these constants in terms of the wave number of the mode. We shall only be interested in the results for waves of type 3 which consist of the superposition of a longitudinal and a transverse bulk wave, whose amplitude is constant over the volume of the plate. Here the results show that if we neglect surface terms

$$\left(\overset{S}{A}\mathscr{P}_l\right)^2=\pm\frac{1}{4\rho_0 V q_l^{\,2}}\left[1+\frac{2K+1}{K}\frac{q_{lz}}{q_{tz}}\right]^{-1} \quad . \quad . \quad . \quad . \quad . \quad . \quad (10)$$

while even if we conclude surface terms

$$\left|\overset{S}{A}\mathscr{P}_l\right|^2\rho\overset{S}{A}(q_{lz})=\frac{1}{4\rho_0 V}\frac{L_z}{\pi} \quad . \quad . \quad . \quad . \quad . \quad . \quad . \quad . \quad (11)$$

In this formulae $\rho(q_{lz})dq_{lz}$ is the number of permitted values of q_{lz} in the range q_{lz}, $q_{lz}+dq_{lz}$ for given q. This result is analogous to the one we obtained for electron waves (I, eqn. (29)) in that the surface terms in the amplitude and the density just cancel out. (K is an elastic constant equal to $(1/2\sigma)-1$ where σ is Poisson's ratio.)

§ 3. The Matrix Elements for the Electron Lattice Interaction

With Bloch (c.f. Bethe 1933) we assume a perturbing potential

$$U(\mathbf{r})=-\underline{u(\mathbf{r})}\cdot\operatorname{grad} V \quad . \quad . \quad . \quad . \quad . \quad . \quad . \quad (12)$$

acting on an electron at $\mathbf{r}$ due to the lattice vibrations. The wave function for the system of one electron, in the vibrational field of the lattice may be expressed as

$$\Psi(N_{\mathbf{q}}, \mathbf{k}) = \phi_{\mathbf{k}}(\mathbf{r}) \prod_{\mathbf{q}} \Psi_{N_{\mathbf{q}}}(\theta_{\mathbf{q}}) \quad . . . . . (13)$$

the product extending over all the wave functions of the lattice waves. We require the matrix elements of $U(\mathbf{r})$ with respect to these functions

$$J = \int \Psi^*(\mathbf{k}', N'_{\mathbf{q}})\, U(\mathbf{r})\, \Psi(\mathbf{k}, N_{\mathbf{q}})\, dx\, dy\, dz\, d\theta \quad . . . (14)$$

$$= \sum_{\mathbf{q}} (J_{\mathbf{q}}^{+} + J_{\mathbf{q}}^{-}) \ldots \quad . . . . . (15)$$

where

$$J_q^{+} = \int \phi^*_{\mathbf{k}'} (Z \,.\, \mathrm{grad}\, V) \exp(i\hat{\mathbf{q}} \,.\, \hat{\mathbf{r}})\, \phi_{\mathbf{k}}\, dr \times \int \psi^*_{N'_{\mathbf{q}}} \theta_{\mathbf{q}}\, \psi_{N_{\mathbf{q}}}\, d\theta_{\mathbf{q}} \prod_{\mathbf{p} \neq \mathbf{q}} \int \psi^*_{N'_p} \psi_{N_p}\, d\theta_p, \quad . . . (16)$$

$$J_q^{-} = \int \phi^*_{\mathbf{k}'} (Z^* \,.\, \mathrm{grad}\, V) \exp(-i\hat{\mathbf{q}} \,.\, \hat{\mathbf{r}})\, \phi_{\mathbf{k}}\, dr \times \int \psi^*_{N'_{\mathbf{q}}} \theta_{\mathbf{q}}{}^* \psi_{N_{\mathbf{q}}}\, d\theta_q \prod_{\mathbf{p}=\mathbf{q}} \int \psi^*_{N'_{\mathbf{p}}} \psi_{N\mathbf{p}}\, d\theta_p. \quad . . . (17)$$

A somewhat lengthy calculation along the lines of Bethe's article shows that the perturbing potential leads to two kinds of changes in the system which involve only the longitudinal component of type 3.

3.1. *Absorption*

An electron with wave number $\mathbf{k}$ (energy $\epsilon_{\mathbf{k}}$) absorbs a quantum of energy from the elastic wave with wave number $\mathbf{q}$ and changes to a state with wave number $\mathbf{k}'$ (energy $\epsilon_{\mathbf{k}'}$). The probability for the process is given by

$$P_A(\mathbf{k}', N'_{\mathbf{q}}, \mathbf{k}, N_{\mathbf{q}}) = |J_{\mathbf{q}}^{+}|^2 \Omega(X) = \frac{16}{9} \cdot \frac{\hbar N_{\mathbf{q}}}{\omega_{\mathbf{q}}} \frac{V^2}{a^6} |A_{k'_z} A_{k_z}|^2 \overset{S}{A} \mathscr{P}_l |^2 q_l^4 \, |\sum_{\alpha} C(\alpha) S(\alpha)|^2 \Omega(X) \quad . . . (18)$$

where

$$\Omega(X) = 2(1 - \cos Xt/\hbar)/(X/\hbar)^2\,; \quad X = \epsilon_{\mathbf{k}'} - \epsilon_{\mathbf{k}} - \hbar\omega_{\mathbf{q}} \quad . . . . . (19)$$

$$C(\alpha) = \frac{3}{2iq_l{}^2} \mathbf{q}_l \cdot \int u^*_{k'_z} v^{\hat{}}_{\mathbf{k}'}{}^* \,\mathrm{grad}\, V u_{k_z} v^{\hat{}}_{\mathbf{k}} \exp(i\alpha z_0)\, d\tau_0 \quad . . . . (20)$$

$$S(\alpha) = \frac{a}{2L_z} \frac{\sin \alpha L_z}{\sin \alpha a/2}. \quad . . . . . (21)$$

The sum in (18) extends over the four arguments

$$\alpha = k_z \pm q_{lz} \mp k'_z \quad . . . . . (22)$$

where the initial and the final state are connected by the relations

$$N'_q = N_q - 1\,; \quad \hat{\mathbf{k}}' = \hat{\mathbf{k}} + \hat{\mathbf{q}} \quad . . . . . (23)$$

and the condition that symmetrical lattice waves lead to transitions between electron states of like symmetry while antisymmetrical lattice waves involves states of opposite symmetry.

$C(\alpha)$ has been chosen so that $C(O)$ reduces to the constant C introduced by Bethe to give the strength of the interaction. The function $S(\alpha)$ can be written

$$S(\alpha) \approx \frac{\sin \alpha L_z}{\alpha L_z} \text{ when } \frac{\alpha a}{2} \ll 1 \quad . . . . . (24)$$

which has a large maximum at $\alpha=0$. (We will neglect the maxima occurring when α is equal to an integral number of π. They correspond to Peierls' " Umklappprozesse ".) Now the range of $\alpha a/2$ is $q_{mt}a/2$, which is about $\pi/2$. Thus near the extremes of the range the approximation $\sin\alpha\ \alpha a/2 \gtrsim \alpha a/2$ is bad, but then $S(\alpha)$ is in any case small. We will thus use (24) for all α.

The transition probability is small unless one of the α vanishes, when for example (eqns. (5) and (10))

$$P_A \gtrsim \frac{2}{9}\frac{\hbar N_{\mathbf{q}}\, C^2 {q_l}^2}{N_a M \omega_{\mathbf{q}} V}\, \Omega(X)\, .\, \frac{1}{2}\left[1+\frac{(2K+1)}{K}\frac{q_{lz}}{q_{tz}}\right]^{-1}, \quad . \quad . \quad (25)$$

where surface effects have been neglected and $\rho_0 = N_a M$ (N_a=number of atoms per unit volume, M=isotopic mass).

This agrees with Bethe's result (cf. eqn. (34) of Bethe's article) for large specimens except for the factor $\{2[1+(2K+1)q_{lz}/Kq_{tz}]\}^{-1}$ which occurs due to the different amplitudes of the electron and lattice waves used in our problem.

The finite thickness ($2L_z$) of the lattice thus results in an ' uncertainty ' in the condition for the conservation of wave numbers. Thus for q_{lz} such that one of the equations $\alpha=0$ is nearly satisfied

$$P \propto C^2 S^2(\alpha)\Omega(X).$$

Now the ' effective width ' of the function $S^2(\alpha)$ is of the order $\Delta\alpha \gtrsim \pi/L_z$ (cf. eqn. (24))

$$\therefore \Delta(\alpha)\, .\, 2L_z \gtrsim 1.$$

In a similar manner the function $\Omega(X)$ is small unless $X \gtrsim 0$ leading to an ' uncertainty ' in the distribution of frequency $\Delta(X/\hbar)\, .\, t \gtrsim 1$.

3.2. *Emission*

An electron in the state $\mathbf{k}$ emits a quantum of energy which is absorbed by the elastic wave with wave number $\mathbf{q}$ and changes to a state $\mathbf{k}'$. The probability for the process is given by

$$\begin{aligned} P_E(\mathbf{k}', N_{\mathbf{q}}', \mathbf{k}, N_{\mathbf{q}}) &= |\, J_{\mathbf{q}}^{-}\, |^2 \Omega(X) \\ &= \frac{16}{9}\frac{\hbar(N_{\mathbf{q}}+1)}{\omega_{\mathbf{q}}}\frac{V^2}{a^6}\, |\, A_{k'_z} A_{k_z}\, \overset{S}{\underset{A}{}}\mathscr{P}_l\, |^2 {q_l}^4\, |\, \sum_{\alpha} S(\alpha)C(\alpha)\, |^2 \Omega(X). \quad . \quad (26) \end{aligned}$$

All the quantities have the meaning assigned to them for the previous process.

The calculations further show that all the transverse components give zero contributions while the longitudinal surface waves give probabilities which are smaller by a factor of $O(1/q^2L^2_z)$ than the ones discussed above.

§ 4. The Surface Energy of a Metal in the Superconducting State of the Absolute Zero

With Fröhlich (F_1) we now treat the electron lattice interaction as a small quantity so that perturbation theory leads to a second order change

in energy (E). From a formal point of view this energy can be attributed to the virtual emission and re-absorption of vibrational quanta by the electrons. Thus an electron in state $\mathbf{k}$ emits a quantum $\hbar q_l c_l$ and is transferred to an intermediate state $\mathbf{k}'$, where

$$\hat{\mathbf{k}}' = \hat{\mathbf{k}} - \hat{\mathbf{q}}_l \quad . \quad . \quad . \quad . \quad . \quad . \quad . \quad . \quad . \quad (27)$$

and k_z' can have any value. The probability for the transition is however small unless k_z' takes one of the two positive values.

$$\pm k_z' = k_z \pm q_{lz}. \quad . \quad . \quad . \quad . \quad . \quad . \quad . \quad . \quad . \quad (28)$$

In the intermediate state the energy of the system consisting of the electron in the vibrational field of the lattice is

$$\epsilon_{\mathbf{k}'} + \hbar q_l c_l.$$

The electron can then re-absorb the quanta and return to its original state. Thus

$$E = -8 \Sigma\Sigma \sum_{q_{lz}=0}^{q_{ml}} \frac{|J_{\mathbf{q}}^{-}|^2 f_{\mathbf{k}}(1-f_{\mathbf{k}'})}{\epsilon_{\mathbf{k}'} - \epsilon_{\mathbf{k}} + \hbar q_l c_l} \quad . \quad . \quad . \quad . \quad . \quad (29)$$

(q_{ml}=value of q_l corresponding to the Debye frequency) where the intermediate state is defined by $\mathbf{k}'$ and q_{lz} and $f_{\mathbf{k}}$ is the probability that the state $\mathbf{k}$ is occupied. The sums go over all the possible wave numbers corresponding to one symmetry with the proviso that symmetrical lattice waves connect states of like symmetry and vice versa. This, together with the two spin systems which may be treated independently, gives the factor 8. Substituting for $|J_q^-|^2$ (eqn. (26) with $N_{\mathbf{q}}=0$) and changing sums to integrals leads to the result

$$E = -2\left(\frac{2C^2\hbar}{9N_a V M c_l}\right)\left(\frac{V}{(2\pi)^3}\right)^2 \left[\int_{-\infty}^{\infty} d\mathbf{k} \int_{-\infty}^{\infty} d\mathbf{k}' \frac{f_{\mathbf{k}}(1-f_{\mathbf{k}'})q_l}{\epsilon_{\mathbf{k}'} - \epsilon_{\mathbf{k}} + \hbar c_l q_l}\right.$$

$$\left. + \frac{\pi}{2L_z} \int_{-\infty}^{\infty} d\mathbf{k}' \int_{-\infty}^{\infty} d\hat{\mathbf{k}} \left(\frac{f_{\mathbf{k}}(1-f_{\mathbf{k}'})\hat{q}_l}{\epsilon_{\mathbf{k}'} - \epsilon_{\mathbf{k}} + \hbar c_l \hat{q}_l} \right)_{k_z = k'_z} \right] \quad . \quad . \quad . \quad . \quad . \quad . \quad (30)$$

(where $\mathbf{q}_l = \mathbf{k} - \mathbf{k}'$) correct down to terms of $O(1/k_m L_z)$. It should be observed that in this result it is convenient to integrate over negative values of k_z. This is purely formal (only positive values of k_z give real states) and depends on the fact that we may define all the functions of $\mathbf{k}$ as even functions in k_z. The integration over q_{lz} can be carried out but great care must be taken to include all the surface terms that arise. A correction for zero wave number states (cf. I, § 3, eqn. (11)) is included n (30).

Neglecting the surface term, the result agrees with the value of E given n F_1 (eqns. (2.11) and (3.1) in F_1) except that the value of the matrix elements used in F_1 should be multiplied by a factor 2 (cf. Bethe 1933). Following Fröhlich, we can split E into the sum of two terms one of

which (E_1) leads to a simple small shift in the energy levels while the other (E_2) can be written as

$$E_2=-\frac{4F\epsilon_m\sigma_0^2}{3N_aV}\left(\frac{V}{(2\pi)^3}\right)^2\left[\int d\mathbf{k}'\int d\mathbf{k}\,\frac{f_{\mathbf{k}}f_{\mathbf{k}'}q_l^2}{(k'^2-k^2)^2-\sigma_0^2q_l^2}\right.$$
$$\left.+\frac{\pi}{2L_z}\int d\mathbf{k}'\int d\hat{\mathbf{k}}\left(\frac{f_{\mathbf{k}}f_{\mathbf{k}'}\hat{q}_l^2}{(\hat{k}'^2-\hat{k}^2)^2-\sigma_0^2q_l^2}\right)_{k_z=k'_z}\right], \quad . \quad . \quad . \quad (31)$$

where

$$F=C^2/(3\epsilon_mMc_l^2)\,; \qquad \sigma_0=2mc_l/\hbar, \quad . \quad . \quad . \quad . \quad . \quad (32)$$

and we have used the free electron value of ϵ_k equal to $\hbar^2k^2/2m$ ($\epsilon_m=\hbar^2k_m^2/2m$, the Fermi energy). The dimensionless constant F, introduced by Fröhlich, is used in the criterion for superconductivity (cf. eqn. (59) below), and $(\sigma_0/2)$ is the wave number of an electron moving with velocity c_l.

We now consider the change in the energy when the normal Fermi distribution is altered by moving the states in a shell of thickness a near the surface of the distribution a distance a outwards. Thus if

Fig. 1

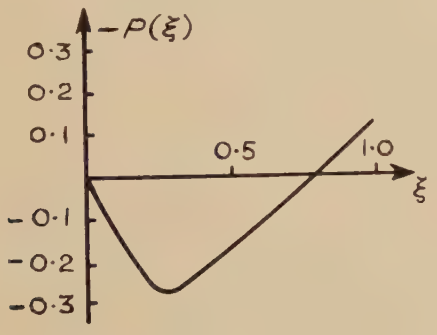

Taken from F_1.

$$x=k-k_m\,; \qquad y=k'-k_m, \quad . \quad . \quad . \quad . \quad . \quad . \quad . \quad (33)$$

$$f_{\mathbf{k}}=f_0(x)+f(x), \quad . \quad . \quad . \quad . \quad . \quad . \quad . \quad . \quad . \quad . \quad (34)$$

where

$$f_0(x)=1, \qquad -k_m\leqslant x\leqslant 0, \qquad f_0(x)=0, \qquad x>0, \quad . \quad . \quad (35)$$

$$f(x)=-1, \quad -a\leqslant x<0, \quad f(x)=1, \quad 0<x\leqslant a\,.f(x)=0, \quad |x|>a, \quad (36)$$

and we take x/k_m as a small quantity of order σ_0/k_m i.e. 10^{-3}. Thus

$$(k'^2-k^2)\simeq 2k_m(y-x), \qquad q_l^2\simeq 4k_m^2\sin^2\theta/2, \quad . \quad . \quad . \quad (37)$$

where θ is the angle between $\mathbf{k}$ and $\mathbf{k}'$. Substituting into the first term of (31), the energy change will be given by

$$\mathscr{S}_1=-\frac{4F\epsilon_m}{3N_a}\left(\frac{1}{8\pi^3}\right)^2V\left[\int d\mathbf{k}\int d\mathbf{k}'[f_0(x)+f(x)]f(y)\psi(x,y), \qquad (38)\right.$$

where

$$\psi(x,y)=2\sigma_0^2\sin^2\tfrac{\theta}{2}/[(y-x)^2-\sigma_0^2\sin^2\theta/2]. \quad . \quad . \quad . \quad (39)$$

The integration has been carried out by Fröhlich in terms of a function $P(\xi)$, (cf. fig. 1) where $\xi=a^2/\sigma^2$ and σ is the largest value of $\sigma_0\sin(\theta/2)$.

Thus

$$\mathscr{S}_1 = -V\frac{4F\epsilon_m}{3N_a}2\left(\frac{2k_m{}^2}{(2\pi)^2}\right)\frac{\sigma^4}{\sigma_0{}^2}\,P(\xi), \quad . \quad . \quad . \quad . \quad (40)$$

where

$$\frac{\sigma}{\sigma_0}=\frac{q_{ml}}{2k_m} \quad \text{if} \quad q_{ml}<2k_m\,; \qquad \frac{\sigma}{\sigma_0}=1 \quad \text{if} \quad q_{ml}>2k_m. \quad . \quad (41)$$

For the Born modification of the Debye theory, i.e. $q_{mt}=q_{ml}=q_m$, say, and neglecting surface effects, these two values are

$$\sigma^3/\sigma_0{}^3=1/4\nu, \quad 4\nu>1\,. \quad \sigma/\sigma_0{}^3=1, \quad 4\nu<1, \quad . \quad . \quad . \quad (41a)$$

where $\nu=N/N_a$ and N is the number of electrons per unit volume.

However, the theory in S requires a Debye maximum frequency $(\omega_m/2\pi)$ to cut off the infinite spectrum (i.e. $q_{mt}>q_{ml}$). Now we can rewrite the formulae for $M(\omega_m)$, the total number of excited modes (S, eqn. (68)) as

$$M(\omega_m)=V\left[2\,\frac{q_{mt}{}^3}{6\pi^2}\left(1+\frac{3b}{q_{mt}L_z}\right)+\frac{q_{ml}{}^3}{6\pi^2}\left(1+\frac{3b}{q_{ml}L_z}\right)\right], \quad . \quad (42)$$

where

$$b(K)=A(K)(18\pi^2)^{1/3}[2+(K/[1+2K])^{3/2}]/[2+(K/[1+2K])], \quad (43)$$

and $A(K)$ is a constant given in S for $K=0,\ 1,\ \infty$.

In analogy to the Born modification we now assume formally that

$$q_{mt}=q_{ml}=q_m \quad . \quad . \quad . \quad . \quad . \quad . \quad . \quad . \quad (44)$$

in eqn. (42). Thus

$$M(q_m)=3N_a=\frac{q_m{}^3}{2\pi^2}\left(1+\frac{3b}{q_mL_z}\right), \quad . \quad . \quad . \quad . \quad (45)$$

$$\therefore q_m=\bar{q}_m(1-b/q_mL_z) \quad \text{where} \quad \bar{q}_m{}^3=6\pi^2Na, \quad . \quad . \quad . \quad . \quad (46)$$

giving the dependence of the maximum wave number on the surface area.

Using (46) we can express the surface dependence of σ for the case $4\nu>1$ (to which we confine ourselves in what follows) as

$$\frac{\sigma^3}{\sigma_0{}^3}=\frac{1}{4\nu}\left(1-\frac{3b}{q_mL_z}\right)=\frac{\bar{\sigma}^3}{\sigma_0{}^3}\left(1-\frac{3b}{q_mL_z}\right)$$

$$\therefore \sigma=\bar{\sigma}(1-b/q_mL_z), \quad . \quad . \quad . \quad . \quad . \quad . \quad . \quad . \quad (47)$$

where $\sigma\to\bar{\sigma}$ as $L_z\to\infty$. Similarly

$$\xi=a^2/\sigma^2=\bar{\xi}(1+2b/q_mL_z) \quad \text{where} \quad \bar{\xi}=a^2/\bar{\sigma}^2. \quad . \quad . \quad . \quad (48)$$

It should be observed that $\bar{\xi}$ itself may still be surface dependent if the equilibrium value of a is. However we will show that this latter dependence does not affect the surface energies. Substituting into (40) for ξ from (48) gives

$$\mathscr{S}_1=-V\frac{3mc_l{}^2N}{2^{1/3}\nu^{2/3}}\left[-\frac{F}{2}(4\nu)^{1/3}P(\bar{\xi})\right.$$

$$\left.+\frac{F}{2}(4\nu)^{1/3}\frac{2b}{q_mL_z}\{2P(\bar{\xi})-\bar{\xi}P'(\bar{\xi})\}\right], \quad . \quad . \quad . \quad . \quad . \quad (49)$$

say, $\mathscr{S}_1=V(S_1+s_1/L_z)$.

We now consider the change in the second term of eqn. (31). Let

$$\hat{k}_m{}^2=k_m{}^2-k_z{}^2\,; \qquad \hat{x}=\hat{k}-\hat{k}_m\,; \qquad \hat{y}=\hat{k}'-\hat{k}_m, \quad . \; . \; (50)$$

and $\hat{\theta}$ be the angle between $\hat{\mathbf{k}}$ and $\hat{\mathbf{k}}'$.

The contribution to the change from the second term is thus given by

$$-s_2V/L_z=\frac{V}{L_z}\frac{4F\epsilon_m}{3N_a}\left(\frac{1}{8\pi^3}\right)^2\cdot\frac{\pi}{2}\int\int[f_0(x)+f(x)]f(y)\psi(\hat{x},\hat{y})\,d\mathbf{k}'\,d\hat{\mathbf{k}}. \quad (51)$$

The multiple integral can only be partly evaluated in terms of known functions. The remaining numerical integration becomes rather tedious because the limits of integration become functions of the next variable over which integration is to take place. Writing the result as

$$s_2=-\frac{4F\epsilon_m}{3N_a}2\left(\frac{2k_m{}^2}{(2\pi)^2}\right)\frac{\sigma^4}{\sigma_0{}^2}\frac{R(\nu,\bar{\bar{\xi}})}{k_m}, \quad . \; . \; . \; . \; . \; (52)$$

we have computed the one value

$$R(1,\,0{\cdot}3)\approx 1{\cdot}4. \quad . \; . \; . \; . \; . \; . \; . \; . \; . \; (53)$$

The value of $\bar{\bar{\xi}}$ chosen corresponds to the minimum of $-P(\xi)$.

Finally we must consider the change in the zero order (kinetic energy). This is

$$\mathscr{S}_3=\sum_{\mathbf{k}}\frac{\hbar^2k^2}{2m}f(x)=\frac{2\epsilon_m}{k_m}\Sigma xf(x)=\frac{2\epsilon_m}{k_m}\left[\int_0^a+\int_0^{-a}\right]\rho(k_m+x)x\,dx, \quad . \quad (54)$$

where $\rho(k)$ is the number of states in the range k, $k+dk$ and can be deduced from the formula giving the total number of states having k less than a given value (cf. I, eqn. (11)).

$$\rho(k)\,dk=\frac{d}{dk}\left[\mathscr{V}\frac{k^3}{3\pi^2}\left(1-\frac{3}{8}\frac{\pi}{kL_z}+\frac{3}{k^3L_z}\int_0^k k_z\sin^{-1}\frac{k_z}{\mu}dk\right)\right]dk-\frac{Vk^2}{\pi^2}\cdot\frac{\pi}{4kL_z}.$$

The second term is the zero wave number correction

$$\therefore\rho(k)=\frac{\mathscr{V}}{\pi^2}\left[1-\frac{\pi}{8kL_z}+\frac{1}{kL_z}\sin^{-1}\frac{k}{\mu}\right] \; . \; . \; . \; . \; . \quad (55)$$

Substituting into (54), taking $\rho(k_m+x)=\rho(k_m)$ and the value of $\mathscr{V}$ from I, eqns. (2), (14), (15) and (19), we have

$$\begin{aligned}\mathscr{S}_3&=V\frac{4\epsilon_m}{k_m}\left(\frac{2k_m{}^2}{(2\pi)^2}\right)^2\bar{\sigma}^2\bar{\bar{\xi}}\left[1+\frac{1}{k_mL_z}\left\{\frac{\pi}{4}+\frac{3\lambda-2}{4}\sin^{-1}\lambda^{-1/2}-\frac{3}{4}(\lambda-1)^{1/2}\right\}\right]\\&=V(S_3+s_3/L_z). \qquad . \; . \; . \; . \; . \; . \; . \; . \; . \; . \; . \; . \; . \; . \; . \; . \quad (56)\end{aligned}$$

Collecting our results the change in the total energy is given by (eqns. (49), (52) and (56))

$$\begin{aligned}\mathscr{S}&=V[(S_1+S_3)+(s_1+s_2+s_3)/L_z]=V[S(a)+s(a)/L_z]\\&=V\frac{3mc_l{}^2N}{2^{1/3}\nu^{2/3}}\left[-\frac{F}{2}(4\nu)^{1/3}P(\bar{\bar{\xi}})+2\bar{\bar{\xi}}\right.\\&\quad+\frac{1}{2k_mL_z}\{-F(4\nu)^{1/3}[R(\nu,\bar{\bar{\xi}})-2b\{2P(\bar{\bar{\xi}})-\bar{\bar{\xi}}P'(\bar{\bar{\xi}})\}]\\&\quad\left.+\bar{\bar{\xi}}(\pi+(3\lambda-2)\sin^{-1}\lambda^{-1/2}-3(\lambda-1)^{1/2})\}\right]. \qquad . \; . \; . \; . \; . \quad (57)\end{aligned}$$

The minimum of $\mathscr{S}(a)$ with respect to variation of a is given by

$$\mathscr{S}'(a)=V(S'(a)+s'(a)/L_z)=0. \quad . \quad . \quad . \quad . \quad . \quad (58)$$

Thus for large L_z, $S'=0$, which corresponds to the minimum found by Fröhlich occurring for a value of $\bar{\xi} \equiv \bar{a}^2/\bar{\sigma}^2 \lesssim 0{\cdot}3$. The condition for the minimum to occur is

$$(F/2)(4\nu)^{1/3}>2\,; \qquad (4\nu>1) \quad . \quad . \quad . \quad . \quad . \quad . \quad (59)$$

and should be satisfied by the superconducting metals (cf. table of values in F_1).

For finite L_z we write a in the form

$$a=\bar{a}(1+\alpha/L_z).$$

Substituting into (58) gives

$$\alpha=-s'(\bar{a})/S''(\bar{a}). \quad . \quad . \quad . \quad . \quad . \quad . \quad . \quad (60)$$

However, we can use the asymptotic value $\bar{a}$ for a even in the bulk term since

$$\mathscr{S}(a)=V\left[S(\bar{a})+\frac{\alpha}{L_z}S'(\bar{a})+\frac{s(\bar{a})}{L_z}\right]$$

$$=V[S(\bar{a})+s(\bar{a})/L_z]. \quad . \quad . \quad . \quad . \quad . \quad . \quad . \quad (61)$$

If we identify the new state with the superconducting state, then

$$-\mathscr{S}_{\min}=V[\Delta F+\Delta f/L_z]=V\left[\frac{H_{CM}^2}{2}\left(1+\frac{\mu}{L_z}\right)\right], \quad . \quad (62)$$

where ΔF=difference in free energy per unit volume between the normal and superconducting phases ; Δf=difference in surface free energy per unit area ; H_{CM}=critical magnetic field for a large specimen ($L_z \to \infty$) and

$$\mu=\Delta f/\Delta F=2\Delta f/H_{CM}^2. \quad . \quad . \quad . \quad . \quad (63)$$

For the purposes of calculating numerical values we take $P(\xi)\lesssim\xi$ when $\xi<\bar{\xi}\lesssim 0{\cdot}3$ and $\nu=1$ in (57). Further we use the value of $b(K)$ corresponding to $K=1(b(1)=0{\cdot}56)$ and neglect the small terms in λ.

$$\frac{H_{CM}^2}{2}=\frac{3mc_i^2N}{2^{1/3}}\left[(4)^{1/3}\frac{F}{2}-2\right]0{\cdot}3, \quad . \quad . \quad . \quad . \quad (64)$$

$$f\Delta=\frac{3mc_i^2N}{2^{1/3}}\left[(4)^{1/3}\frac{F}{2}\,.\,1{\cdot}1-1{\cdot}9\right], \quad . \quad . \quad . \quad . \quad (65)$$

$$\mu=\frac{1}{k_m}\frac{(4)^{1/3}(F/2)1{\cdot}1-1{\cdot}9}{[(4)^{1/3}(F/2)-2]0{\cdot}3} \quad . \quad . \quad . \quad . \quad . \quad . \quad (66)$$

For mercury the values found are

$$H_{CM}^2/2=6{\cdot}95\times10^5 \text{ erg cm}^{-3}, \qquad H_{CM}=1600 \text{ gauss.}$$

$$\Delta f=0{\cdot}03 \text{ erg cm}^{-2}, \qquad \mu=5\times10^{-8} \text{ cm.}$$

$$. \quad . \quad . \quad . \quad (67)$$

§ 5. Experimental Results and Discussion

We have neglected the change in the double layer energy discussed in I. There it was shown that in the normal state this energy

$$\sigma_3 \propto N \propto 1/k_m{}^3. \quad . \quad . \quad . \quad . \quad . \quad . \quad . \quad (68)$$

Thus for the superconducting state the energy will be

$$\left[\sigma_3+\sigma_3{}'a+\sigma_3{}''\frac{a^2}{2!}\ldots\right]+\left[\sigma_3-\sigma_3{}'a+\frac{\sigma_3{}''}{2!}a^2\ldots\right]-\sigma_3,$$

where dashes denote differentiation with respect to k (writing $\sigma_3 \propto 1/k^3$ in general) and the derivatives are evaluated at $k=k_m$. Thus the difference ($\Delta\sigma_3$) between the two energies is roughly

$$\frac{\Delta\sigma_3}{\sigma_3} \approx 3\left(\frac{a}{k_m}\right)^2 = 3\bar{\xi}(\sigma^2/k_m{}^2) \approx 10^{-3}\bar{\xi}. \quad . \quad . \quad . \quad . \quad (69)$$

This is negligible as may be seen by examining the tabulated values of σ_3.

The integrations over the shell will only be valid if the k spacing between the wave number sheets in **k** space is much smaller than the thickness of the shell, i.e.

$$a \gg 1/L_z \quad \text{or} \quad L \gg 1/\sigma_0 \approx 10^{-5}\text{ cm}. \quad . \quad . \quad . \quad . \quad . \quad (70)$$

[This a which is the thickness of the shell in wave number space must not be confused with the lattice spacing which has a similar symbol but reciprocal dimension.]

We may thus expect changed values of the surface energy when $L_z \lesssim 10^{-5}$ cm, i.e. when it becomes of the order of the penetration depth (λ). It seems probable that if we included non-symmetrical distributions in our variational problem a lower minimum energy could be found for these small thicknesses. Thus our calculation shows that as regards the surface term electrons on the surface of the normal distribution with large k_z values tend to be expelled from the surface while those with small k_z do not. The bulk term however shows that all electrons on the surface tend to be expelled (cf. the discussion in F_1 with regard to the function $L(y)$). Thus a shell, thicker for large k_z values and thinner for small k_z values, may lead to a better approximation for very thin films.

Unfortunately, the increase in critical magnetic field (H_c) only becomes measurable when the thickness is of the order of the penetration depth. In fact Ginsburg (1945) shows that

$$\left(\frac{H_c}{H_{\text{CM}}}\right)^2 = \frac{1+\mu/L_z}{1-(\lambda/L_z)\tanh(L_z/\lambda)}, \quad . \quad . \quad . \quad . \quad . \quad (71)$$

where H_{CM} is the value of H_c as $L_z \to \infty$ i.e. for a massive specimen. Further, when $L_z \gg \lambda, \mu$

$$H_c/H_{\text{CM}} \sim 1+(\mu+\lambda)/2L_z = 1+\lambda'/2L_z. \quad . \quad . \quad . \quad (72)$$

This analysis has been applied to the extensive experiments of Appleyard *et al.* (1939), on thin films of mercury. Extrapolating to the zero of temperature and using (72) gives $\lambda' \approx 1{\cdot}2 \,.\, 10^{-5}$ cm for the thickest film ($L_z = 5{\cdot}44 \,.\, 10^{-5}$ cm). Using the value $\lambda \approx 4{\cdot}3.10^{-6}$ cm given by

Lauerman and Shoenberg (1949) leaves $\mu \simeq 7{\cdot}9 \,.\, 10^{-6}$. (Using the exact expression for H_c and the above value of λ gives $\mu \simeq 6{\cdot}5 \,.\, 10^{-6}$ cm.) We calculated μ at various temperatures and thicknesses, finding similar curves of μ against L_z at constant T and μ against T at constant L_z. The range of μ is from 5.10^{-6} to 3.10^{-5} cm, but the variation with L_z is not monotone. Unsuccessful attempts were made to reproduce the experimental H_c/L_z curves with constant μ and a different (constant) λ.

These experimental values of μ are larger than the theoretical values by a factor 100. However it must be remembered that the theoretical values refer to thicker plates only.

Further the theoretical value of the bulk term $H_{\mathrm{CM}}{}^2/2$ is too large by a factor of about 16, so that Δf is ony about $\frac{1}{6}$ of the experimental value. In any case it is unlikely that λ itself will remain constant as L_z becomes of the order of 10^{-5} cm.

While we have not been able to give a very definite answer about the importance of the surface free energy in thin film experiments, we have been able to show on what factors it depends. This should help to give a more definite quantitative value when the theory reaches a greater degree of refinement in regard to both bulk and thin specimen.

Acknowledgments

The author would like to thank Professor L. Rosenfeld for suggesting this problem, and for the interest he has taken in the work at all stages. It was done during the tenure of a research grant from the Department of Scientific and Industrial Research. The author must also thank Professor A. Papapetrou for many valuable discussions.

References

Appleyard, E. P. S., *et al.*, 1939, *Proc. Roy. Soc.* A, **172,** 540.
Bethe, H., 1939, *Handb. d. Physik*, **24/2,** 509.
Fröhlich, H., 1950, *Phys. Rev.*, **79,** 845.
Ginsburg, V., 1945, *J. Phys. U.S.S.R.*, **9,** 305.
Lauerman, E., and Shoenberg, D., 1949, *Proc. Roy. Soc.* A, **198,** 560.
Shockley, W., 1939, *Phys. Rev.*, **56,** 317.
Stratton, R., 1953, *Phil. Mag.*, **44,** 519.

Note added in Proof.—Recently, Pippard (1951) analysed some earlier measurements of Shoenberg (1940) on mercury colloids and found values of μ ten times less than λ. He also points out that Ginsburg's theory is only valid if the magnetic moment is proportional to the magnetic field up to a certain critical value and then drops discontinuously to zero. Some experiments by Lock (1951) on tin and indium thin films show that the magnetization curve is actually continuous and when analysed by Pippard's method the results yield values of μ which are again somewhat smaller than previous estimates. These new experimental values of μ are in better agreement with the calculated values.

References

Lock, J. M., 1951, *Proc. Roy. Soc.* A, **208,** 391.
Pippard, A. B., 1951, *Proc. Camb. Phil. Soc.*, **47,** 617.
Shoenberg, D., 1940, *Proc. Roy. Soc.* A, **175,** 49.

CXXXI. *The Angular Distribution of Long-Range Alpha Particles from the Proton Bombardment of* ^{15}N

By A. V. Cohen and A. P. French
Cavendish Laboratory, Cambridge*

[Received June 26, 1953]

Summary

The angular distribution of long-range alpha particles from the reaction $^{15}N(p, \alpha)$ has been investigated over the range 230 kev–960 kev proton energy. It is found that the levels in ^{16}O formed by resonant capture of protons of energy 340 kev and 1050 kev have spin and parity $(0, +)$ and $(1, -)$ respectively. Interference effects in the angular distribution caused by these two levels have been observed, but the phase differences necessary to account for these effects are not in full agreement with those predicted from modern dispersion theory.

§ 1. Introduction

The reaction $^{15}N(p, \alpha)$ was first observed by Burcham and Smith (1939). Freeman (1950) measured the Q of the reaction as $4{\cdot}96 \pm 0{\cdot}05$ Mev. Cochrane and Hester (1949) studied the excitation curve by a photographic plate technique and reported a resonance at about 400 kev. A study by these workers of angular distributions at 445 and 380 kev did not reveal any anisotropy greater than about 10%. Mileikowsky and Pauli (1952) studied the excitation curve at 90° with protons ranging in energy from 200 kev to 940 kev and observed a resonance about 140 kev wide at 340 kev.

Schardt *et al.* (1952) studied the excitation curve of the reaction $^{15}N(p, \alpha)$ for proton energies up to 1600 kev. In two overlapping sets of measurements the alpha particles were observed (*a*) at 90° for proton energies between 273 and 830 kev, (*b*) at 138° for proton energies from 650 kev upwards. Resonances for long-range alpha particle production were found to occur at 360 kev, 1020 kev and 1210 kev, of width 94, 150 and 22·5 kev respectively. (Because of penetrability effects the resonance at 360 kev corresponds to a level at 340 kev.) In the work of Schardt *et al.* the $^{15}N(p, \alpha\gamma)$ and $^{15}N(p, \gamma)$ processes were also studied and appeared to have certain resonances in common with $^{15}N(p, \alpha)$; these observations are relevant to the interpretation of the present experiments and will be discussed in detail later. Absolute cross sections for all three reactions were determined by Schardt *et al.* and an accuracy of $\pm 15\%$ was claimed; their figures have been used in our work.

* Communicated by the Authors.

The present paper describes an investigation of the angular distribution of long-range alpha particles for incident proton energies between 230 kev and 960 kev with particular attention to interference effects taking place between the levels formed at 340 and 1050 kev.

§2. Experimental Technique and Procedure

Nitrogen-15 targets were deposited on a tantalum sheet in the electromagnetic separator of the Atomic Energy Research Establishment, Harwell. Proportional counters were used to detect the long-range alpha particles produced when the targets were bombarded with protons. The experimental technique is fully described in an earlier paper (Cohen 1953).

The range of angles permitted by the geometry of the apparatus was from 30° to 160° and this complete range could be explored up to 930 kev. Above this energy the range of angles was progressively restricted by scattered protons and useful observations became impossible above 960 kev.

Angular distributions were taken at a series of proton energies (mostly at 50 kev intervals) and a study was also made of the energy-dependence of $I(150°)/I(90°)$ (the ratio of the intensity at 150° to that at 90°). The variation with energy of the angular distribution was thus related to the observed excitation curve.

§3. Results

In fig. 1 we show typical angular distributions (reduced to the centre of mass system) at 380 kev and 930 kev. The former, taken about 20 kev above the lower resonance, should correspond roughly to the angular distribution obtained by Cochrane and Hester at 412 kev, which does not depart very significantly from isotropy. The 930 kev curve implies a very strong interference effect in the angular distribution at this energy. The results at all intermediate energies exhibit this interference to a lesser extent.

Each angular distribution was fitted twice assuming it to be alternatively linear or parabolic in $\cos\theta$. The variance ratio test was then applied to find if the improvement in fit by taking the parabolic term was at all significant. The variance of the experimental points from the curves fitted to them was compared, using the χ^2 test, with the variance expected from the finite numbers of counts, and in no case was there evidence that other random errors were significant.

Below 380 kev, angular distributions were isotropic or contained only a few per cent of $\cos\theta$ term. Above this energy strong negative $\cos\theta$ terms were found, up to about 0·70 of the isotropic component. Above 730 kev, strongly significant negative $\cos^2\theta$ terms were observed, rising to about −0·30 at the highest energies, for which the level of significance of the $\cos^2\theta$ terms is better than 0·1%. The χ^2 test indicated in each case that there was no reason to invoke higher powers of $\cos\theta$.

In figs. 2 (*a*), (*b*) and (*c*), we show respectively $I(150°)/I(90°)$, the yield at 90°, and the observed coefficient of $\cos^2\theta$, as functions of proton energy. The beam energy definition was ± 5 kev at 400 kev and ± 11 kev at 900 kev. The excitation curve does not differ significantly from that of Schardt *et al.*, though unfortunately our technique did not permit us to go as high as the resonant energy near 1050 kev. The

Fig. 1

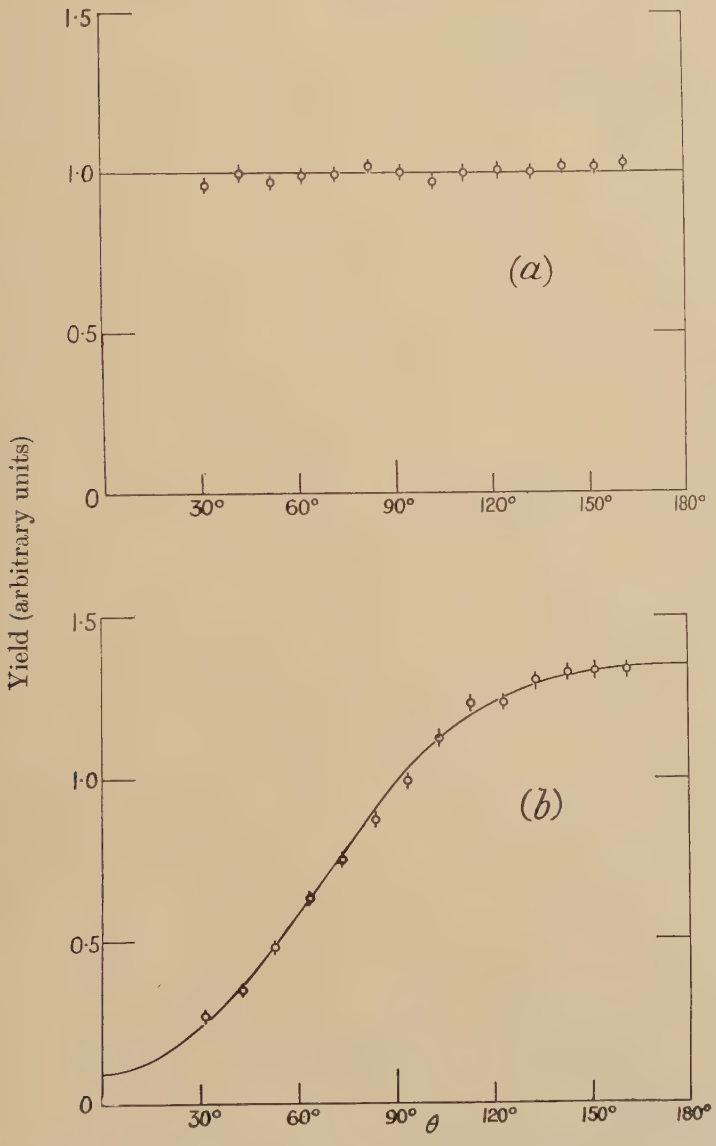

Some observed angular distributions.

(*a*) 380 kev : no anisotropy above the 5% level of significance.
(*b*) 930 kev : $(1 \pm 0{\cdot}01) - (0{\cdot}64 \pm 0{\cdot}025) \cos\theta - (0{\cdot}26 \pm 0{\cdot}04) \cos^2\theta$.

Fig. 2

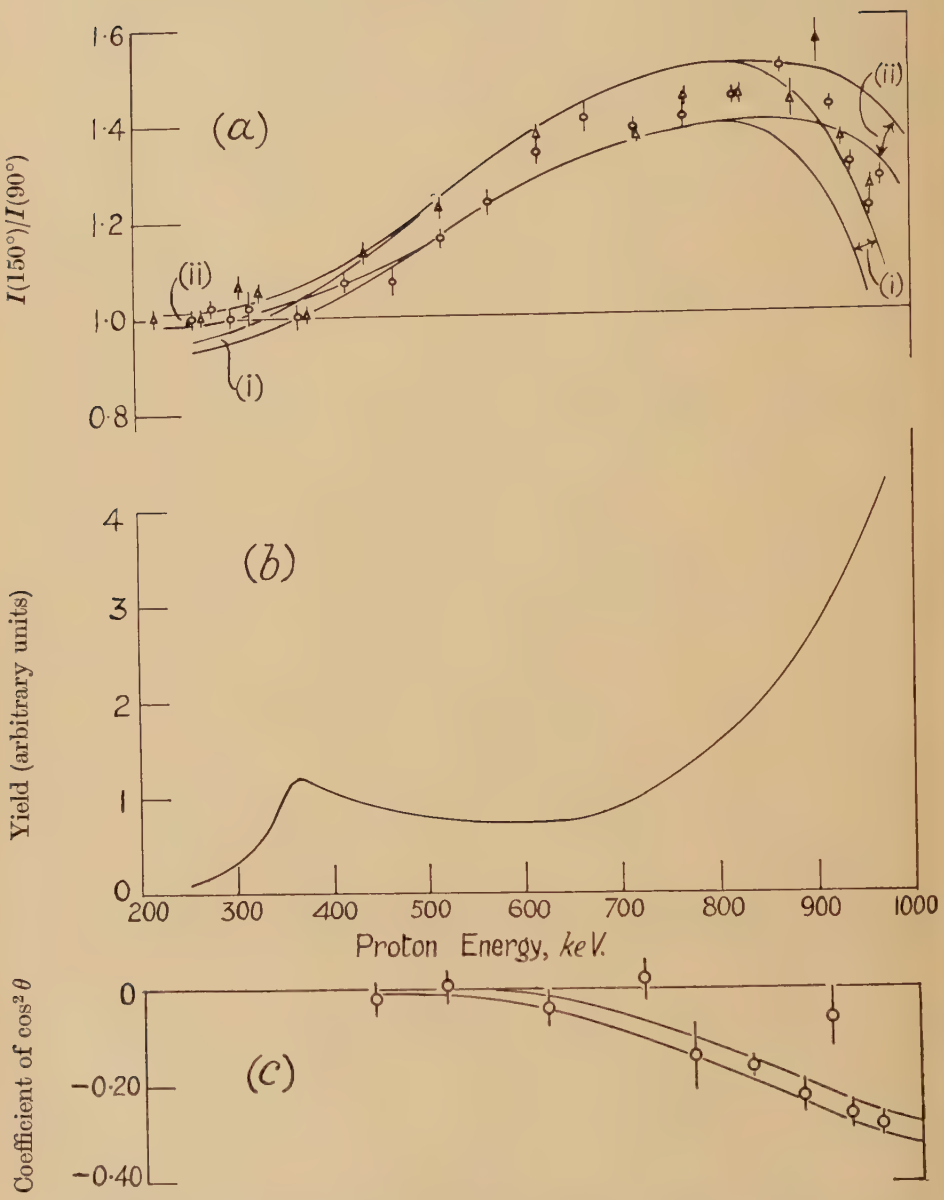

(*a*) Variation of $I(150°)/I(90°)$ with proton energy. Triangles represent points obtained from complete angular distributions. The curves, fitted as explained in § 5.2, enclose a band showing the standard deviation in the fit. That branch marked (i) is obtained with $\phi=15°$; that marked (ii) with $\phi=121°$.

(*b*) Excitation curve at 90°.

(*c*) The coefficient of $\cos^2\theta$ in the angular distributions plotted as a function of proton energy. The curves are fitted as explained in § 5.2 and show the standard deviation in the fit.

growth of the $\cos^2\theta$ term with increasing energy is clearly shown, and its association in some way with the 1050 kev resonance is strongly indicated. The $I(150°)/I(90°)$ curve shows the change in the character of the angular distribution with energy. The full curves in figs. 2 (*a*) and 2 (*c*) are theoretical fits which will be discussed later.

It is evident without any formal analysis that in this reaction there is strong interference between two states of opposite parity. In the following sections we discuss the situation in detail, with the principal aim of establishing the spins and parities of these states.

§ 4. Theoretical Angular Distributions

4.1. *Single Levels*

The reaction we are considering is :

$$p+{}^{15}N \longrightarrow {}^{16}O^* \longrightarrow {}^{12}C+\alpha.$$

The ground state of ^{15}N has spin $\frac{1}{2}$ (Krüger 1938, and Wood and Dieche 1938) and the shell-model predicts odd parity (Hornyak *et al.* 1950). The ground state of ^{12}C has spin O and any reasonable model predicts even parity; the proton and the alpha particle are $(\frac{1}{2}, +)$ and $(0, +)$ respectively. Thus the spin state of the initial system can be $(0, -)$ or $(1, -)$, and that of the final system is $(0, +)$.

The selection rules for angular momentum and parity demand that those states in the compound nucleus ^{16}O which emit long-range alpha particles (leaving ^{12}C in its ground state) must be $(0, +)$, $(1, -)$, $(2, +)$, etc. Moreover, none of these states can be formed from an initial spin configuration $(0, -)$; the ^{16}O states that concern us must therefore be formed from the initial configuration $(1, -)$. The state $(0, +)$ is formed by p-protons, the state $(1, -)$ by s- and d-protons $(2, +)$ by p- and f-protons, and so on.

The emission of alpha particles from a compound state $(0, +)$ is of course isotropic; the angular distribution expected from a $(1, -)$ state in ^{16}O is

$$I(\theta)\sim 1+2c(p_2/p_0)^{1/2}(1-3\cos^2\theta)\cos\gamma+c^2(p_2/p_0)(1+3\cos^2\theta), \quad (1)$$

where the isotropic term arises from formation of the compound nucleus by s-protons, the term in $(1+3\cos^2\theta)$ from d-protons, and the term in $(1-3\cos^2\theta)$ from an interference between s- and d-protons. c^2 represents the probability of formation of ^{16}O through d-protons relative to that through s-protons, γ is the phase difference between the s- and d-proton wave functions at the nuclear surface, and p_l the barrier penetrability for protons of orbital momentum l. As p_2 is much less than p_0 at the energies considered, we might expect the first term to be predominant, and the third term probably negligible.

Alpha particles from states $(2, +)$ and $(3, -)$ would be expected to have angular distributions predominantly of the forms $(1+3\cos^2\theta)$ and $(1-2\cos^2\theta+5\cos^4\theta)$ respectively, if one makes the plausible assumption that their formation is mainly due to protons of the lowest possible orbital momentum.

The angular distribution near the lower resonance is isotropic ; this level is therefore either $(0, +)$ or $(1, -)$. One may argue that the 1050 kev level is also either $(0, +)$ or $(1, -)$, since even at energies where the yield might be expected to be predominantly due to it, no positive terms in $\cos^2\theta$ or $\cos^4\theta$ were found in the angular distributions, although there are negative $\cos^2\theta$ terms of about $-0{\cdot}30$. This makes it very unlikely that the level at 1050 kev is $(2, +)$ or $(3, -)$, and considerations of yield and width exclude spins higher than 3. Since the appearance of a strong $\cos\theta$ term at intermediate energies makes it quite certain that the levels are of opposite parity, it is very probable that one of the levels is $(0, +)$ and the other $(1, -)$, and we shall next consider the angular distributions arising from the interaction of two states with these values of spin and parity.

4.2. *Interference Effects*

The angular distributions expected from overlapping levels have been discussed more fully elsewhere (Devons and Hine 1949, Thomson *et al.* 1952, Cohen 1953) and we shall merely quote the relevant result. Let r_1, δ_1, refer to the amplitude and phase of the complex Breit–Wigner denominator of the level $(0, +)$ and let $Ae^{i\alpha}$ represent the complex amplitude of its inherent probability of formation. Let the quantities r_2, δ_2, $Be^{i\beta}$ be the corresponding quantities for the level $(1, -)$ as formed by s-protons. Then if we put $(B/A)=x$, $(r_1/r_2)=r$, $(\beta-\alpha)=\phi$, and $(\delta_2-\delta_1)=\delta$, the expected (energy-dependent) angular distribution is

$$I(\theta)\sim 1+(p_0/p_1)x^2r^2\{1+2(p_2/p_0)^{1/2}c(1-3\cos^2\theta)\cos\gamma + (p_2/p_0)c^2(1+3\cos^2\theta)\} - 2(p_0/p_1)^{1/2}xr\{\cos(\phi-\delta)-2(p_2/p_0)^{1/2}c\cos(\phi-\delta+\gamma)\}\cos\theta. \quad (2)$$

Here p, c, and γ have the same meaning as in eqn. (1). c, γ, x and ϕ are expected to be nearly independent of energy.

In the next section we shall make use of eqn. (2) to interpret the experimental results.

§ 5. Comparison of Theory with Experiment

5.1. *Identification of the Levels*

The appearance of negative $\cos^2\theta$ terms at the higher energies makes it very likely that the $(1, -)$ spin assignment should be made to the 1050 kev level. The only other plausible explanation would be that the $\cos^2\theta$ term arises from interference between the 1050 kev level (assumed to be $(0, +)$) and the 1210 kev level (assumed to be of even parity and non-zero spin). The relative intensities of the levels as found by Schardt *et al.* (*loc. cit.*) would give rise to a $\cos^2\theta$ term of about $0{\cdot}20$ if the 1210 kev level had spin 2. However, the work of Kraus *et al.* (1953) on the reaction $^{15}\mathrm{N}(\mathrm{p}, \alpha\gamma)$, which also is resonant at this energy, makes it almost certain that the spin of the 1210 kev level is $(4, +)$. Calculation shows that if this is so, interference terms from this level cannot be greater than 10% in the energy range considered ; thus one cannot account for our results in this way.

5.2. *The Fitting of the Angular Distributions*

If we accept the assignment (1, −) to the upper level, the level at 340 kev must be (0, +) formed by p-protons. With these assumptions, the variation with energy of the coefficient of $\cos^2\theta$ was fitted by least squares and gave

$$2c\cos\gamma=(0{\cdot}80\pm0{\cdot}06),\ x^2=(0{\cdot}06_8\pm0{\cdot}03).$$

The fit is shown in fig. 2 (*c*). The negative $\cos^2\theta$ term is at some energies certainly more than 0·25, and because of this it follows from eqn. (2) that $\cos\gamma$ must be more than 0·34.

To explain the observed $\cos\theta$ term, and the observed values of $I(150°)/I(90°)$, a least-squares fit was made to the latter quantity for energies between 500 kev and 820 kev, in which range δ (the phase difference between the two resonance denominators) does not change by more than 5°. The above quoted value of $2c\cos\gamma$ was taken. The quantities determined from the least-squares fit are x^2 and F, where

$$F=\{\cos(\phi-\delta)-2c(p_2/p_0)^{1/2}\cos(\phi-\delta+\gamma)\}. \quad . \quad . \quad . \quad (3)$$

The fit is shown in fig. 2 (*a*). Extrapolation to higher and lower energies involves a strong variation of δ and in consequence a variation of F. A knowledge of γ itself then becomes necessary; because of our condition $0{\cdot}34<\cos\gamma<1$ the extrapolation can be made without great uncertainty.

Some disagreement between theory and experiment, of the order of 10% at the higher energies and 1% at the lower energies, might be expected because of the effects of the level at 1210 kev. If we use only our knowledge that $\cos\gamma>0{\cdot}34$, then $\phi=(20°\pm20°)$ *or* $(116°\pm20°)$. If one makes the extreme assumption that $\cos\gamma=1$, one finds $\phi=(15°\pm5°)$ or $(121°\pm5°)$; because of the possible effects caused by the 1210 kev level, one cannot decide between these alternative extrapolations, which are both shown in fig. 2 (*a*).

5.3. *Excitation Curves*

The extrapolated interference patterns are such that a level at 1050 kev of 150 kev width would appear, if established by observation at 138° to the incident proton beam, to be at about 1025 kev if $\phi=20°$, and at 1030 kev if $\phi=116°$. Although the magnitude of this shift is uncertain, its existence would suggest that the 1020 kev resonance observed at 138° in ^{15}N(p, α) and the 1050 kev resonance in ^{15}N(p, γ) (see Schardt *et al.*, *loc. cit.*) represent the same level.

The value of x^2 (the relative inherent excitation of the two levels) obtained from the $I(150°)/I(90°)$ curve is $(0{\cdot}033\pm0{\cdot}006)$; this is in reasonable agreement with the figure $(0{\cdot}06_8\pm0{\cdot}03)$ required to account for the observed $\cos^2\theta$ term. It is worth noting that the value of x^2 determines the excitation curve of the reaction at 90°, provided the penetrabilities are known. (At 90° interference between levels, of the type discussed by us, vanishes completely as may be seen by putting $\cos\theta=0$ in eqn. (2).) It is thus possible to derive yet another value of x^2

from the observed excitation function; using the published results of Schardt *et al.* (*loc. cit.*) we find $x^2=0{\cdot}12$, which seems significantly higher than our values. With this value the relative heights of the resonant peaks are well fitted, but the ' saddle ' in the 90° excitation curve in the neighbourhood of 450 kev is higher than one would expect. This was ascribed by Schardt *et al.* (*loc. cit.*) and by Fowler and Thomas (1953) to constructive interference of the type treated by Wigner (1946). It seems quite possible, however, that this discrepancy, as well as the anomalous value of x^2, simply represents a shortcoming of conventional penetrability calculations when the conditions at widely different energies are being compared.

§ 6. Further Discussion of Results

6.1. *Application of Modern Dispersion Theory*

The phases ϕ and γ may be predicted from the dispersion theory of Wigner and Eisenbud (see Thomson *et al.* (*loc. cit.*) and Seed and French 1952). The predicted value of γ is 84° with little dependence on energy and nuclear radius; this is in disagreement with the observed condition $\cos\gamma>0{\cdot}34$, $\gamma<70°$. The predicted value of ϕ is 25° for an interaction radius a of $5{\cdot}05\times10^{-13}$ cm, and 16° for $a=4{\cdot}22\times10^{-13}$ cm, with little dependence on energy. One of our values for ϕ does not disagree with this, though it is evident that too much reliance should not be placed on the theoretical predictions.

Fowler and Thomas (1953) have suggested that the level at 340 kev is $(1, -)$ formed by s-protons, because of the large width for proton emission. From the values of Schardt *et al.* for the width and the cross section at resonance we infer $\Gamma_p=(91\pm0{\cdot}5)$ kev or $(3{\cdot}3\pm0{\cdot}5)$ kev. We may reject the first alternative as being rather high even for s-protons. If we accept the value 3·3 kev and correct it for the effects of level shift (Lane 1951, and Thomas 1953) we find

$$\Gamma_p\,(\text{true})=12\text{ kev for p-protons, and }3{\cdot}3\text{ kev for s-protons.}$$

We now use the criterion given by Teichmann and Wigner (1952):

$$\Gamma_p\,(\text{true})\leqslant\left(\frac{3\hbar^2}{\mu a}\right).2kp_l$$

where

μ=reduced mass of system,

a=interaction radius,

k=wave-number of incoming proton,

p_l=penetrability coefficient.

This requires Γ_p (true)$\leqslant$50 kev for s-protons, and $\leqslant$9·5 kev for p-protons, assuming in our calculations that $a=5{\cdot}05\times10^{-13}$ cm. Thus the Wigner criterion is just violated if we assume p-protons are responsible for forming the level at 340 kev.

The calculation, in particular the correction of Γ_p for level-shift, is peculiarly sensitive to the assumed penetrability coefficient. In our calculations, we have assumed that the Coulomb potential is valid right

down to the nuclear boundary, a condition that is unlikely to hold. It may well be that Γ_p (true) is in fact less than Wigner's upper limit, but that our knowledge of penetrabilities is not exact enough for us to use this criterion in marginal cases. On this view it would seem that there is no strong argument against our supposition that the 340 kev resonance is (0, +) formed by s-protons.

6.2. *Isotopic Spin*

In the above discussion we have tentatively identified the alpha-emitting level formed at 1020 kev with the gamma-emitting level formed at about 1050 kev. From the yield of the radiative capture process $^{15}N(p, \gamma)$ (Schardt *et al.*, *loc. cit.*) we may infer that Γ_γ is (150 ± 22) ev at 1050 kev. Now the maximum expected width for gamma-radiation of this energy is 2000 ev for electric dipole, and 45 ev for magnetic dipole, using the formulae of Blatt and Weisskopf (1952). For any higher order of radiation it is of course much less. It is thus almost certain that the gamma-emitting level is (1, −), and that therefore it is indeed identical with the alpha-emitting state. One cannot, however, quite exclude the possibility that it is (1, +) and proceeds to the ground state by a magnetic dipole transition.

If isotopic spin T is a good quantum number, the alpha-emitting state must have $T=0$ (Adair 1952). Wilkinson (1953) has pointed out that if this is so, and if one identifies the alpha- and the gamma-emitting levels, as we have done, there is a clear violation of the isotopic spin selection rule ΔT $0 \rightarrow 0$ *forbidden for electric dipole transitions* (Radicati 1952 and 1953). If the selection rule is to hold, then we must postulate two distinct levels, separated by less than 30 kev, and of the same width and spin, though possibly of opposite parity. This seems unlikely, and it is probable that isotopic spin is not a good quantum number for this level, which perhaps is not surprising at such a high excitation of the compound nucleus.

§ 7. Conclusion

The results provide yet another example of 'interference' between nuclear levels. It seems reasonably well established that the level formed at 340 kev is (0, +) and that the resonance at 1020 kev corresponds to a (1, −) level near 1050 kev. We seem to have a clear exception to the isotopic spin selection rules. Of the two observed phase-differences between coherent proton-waves in this reaction, one possibly agrees and the other probably disagrees with the predictions of the theory of Wigner and Eisenbud.

Acknowledgments

One of us (A. V. C.) is indebted to Trinity College, Cambridge, for a scholarship, and to the Department of Scientific and Industrial Research for a grant, while this work was being done.

We wish to acknowledge helpful correspondence with Dr. R. G. Thomas, of Los Alamos Laboratory, on the implications of the results.

References

Adair, R. K., 1952, *Phys. Rev.*, **87,** 1041.

Blatt, J. M., and Weisskopf, V. F., 1952, *Theoretical Nuclear Physics* (New York : John Wiley).

Burcham, W. E., and Smith, C. L., 1939, *Nature, Lond.*, **143,** 795.

Cochrane, W., and Hester, R. G., 1949, *Proc. Roy. Soc.* A, **199**, 458.

Cohen, A. V., 1953, *Phil. Mag.* [7], **44,** 583.

Devons, S., and Hine, M. G. N., 1949, *Proc. Roy. Soc.* A, **199**, 56.

Fowler, W. A., and Thomas, R. G., 1953, *Bull. Amer. Phys. Soc.*, **28,** 49.

Freeman, J. M., 1950, *Phil. Mag.* [7], **41,** 1225.

Hornyak, W. F., Lauritsen, T., Morrison, P., and Fowler, W. A., 1950, *Rev. Mod. Phys.*, **22,** 291.

Kraus, A. A., French, A. P., Fowler, W. A., and Lauritsen, C. C., 1953, *Phys. Rev.*, **89,** 299.

Krüger, H., 1938, *Zeit. für Physik*, **111,** 467.

Lane, A. M., 1951, *The Theory of Nuclear Resonance Reactions* (privately circulated).

Mileikowsky, C., and Pauli, R. T., 1952, *Arkiv. för Fysik*, Band 4, no. 13.

Radicati, L. A., 1952, *Phys. Rev.*, **87,** 521 ; 1953, *Proc. Phys. Soc.* A, **66,** 139.

Schardt, A., Fowler, W. A., and Lauritsen, C. C., 1952, *Phys. Rev.*, **86,** 527.

Seed, J., and French, A. P., 1952, *Phys. Rev.*, **88,** 1007.

Teichmann, T., and Wigner, E. P., 1952, *Phys. Rev.*, **87,** 123.

Thomas, R. G., 1953, private communication.

Thomson, D. M., Cohen, A. V., French, A. P., and Hutchinson, G. W., 1952, *Proc. Phys. Soc.* A, **65,** 745.

Wigner, E. P., 1946, *Phys. Rev.*, **70,** 606.

Wilkinson, D. H., 1953, *Phys. Rev.*, **90,** 721.

Wood, R. W., and Dieche, G. H., 1938, *J. Chem. Phys.*, **6,** 928.

CXXXII. *Isotopic Spin Selection Rules—III: Radiations from* ^{14}N

By A. B. Clegg and D. H. Wilkinson
Cavendish Laboratory, Cambridge*

[Received July 28, 1953]

Abstract

It is pointed out that the 8·06 mev (1−) state of ^{14}N is of $T=1$, corresponding with the 6·10 mev state of ^{14}C. The electric dipole transition to the 2·31 (0+) $T=1$ state of ^{14}N is therefore forbidden by the isotopic spin selection rules. It is shown that the strength of this forbidden electric dipole transition is less than 0·7% of that of the allowed electric dipole transition to the (1+) $T=0$ ground state of ^{14}N; this implies that the contamination of the 8·06 mev state by a state of $T=0$ is less than 2% in *intensity*.

§ 1. Introduction

This paper continues the series (Wilkinson and Jones 1953—I; Wilkinson 1953 a—II) in which the stringency and general applicability of the isotopic spin selection rules is being investigated. The present work —as I—concerns the rule (Radicati 1952, Gell-Mann and Telegdi 1953) that electric dipole transitions in self-conjugate nuclei must be accompanied by a change of unity in the isotopic spin, i.e., transitions with $\Delta T=0$ are there forbidden. This rule is seen to operate in several instances (in ^{16}O (one example)—see I; in ^{10}B (four examples)—Jones and Wilkinson 1953 and forthcoming paper; in ^{14}N (one example)—present paper; in ^{20}Ne (one example)—forthcoming paper) in suppressing such transitions without change of isotopic spin. It is unlikely that this suppression is due to chance fluctuations in the electric dipole matrix elements since such fluctuations appear to be rather small as a rule in light nuclei (Wilkinson 1953 b). That the inhibition may in fact be ascribed to the isotopic spin rule is made probable by the observation (in II) that electric dipole transitions without change of isotopic spin are not discouraged in nuclei of $T_z=+1$.

§ 2. States of ^{14}N

When protons of 550 kev bombard ^{13}C a state of width 32·5 kev is formed in ^{14}N at 8·06 mev (see Ajzenberg and Lauritsen 1952 for most references to level characteristics). This width is about 12% of the Wigner limit (Teichmann and Wigner 1952) if we assume s-wave proton capture and approaches or exceeds the single-particle reduced width if we assume p-wave proton capture. Since s-wave interactions in light nuclei show

* Communicated by the Authors.

large reduced widths while p-wave interactions show relatively small widths (A. M. Lane—private communication) this observation makes it very probable that we are dealing with s-wave protons and that the 8·06 Mev state is therefore (0−) or (1−). This conclusion is strengthened by the observation that the emission of gamma radiation by this state is isotropic with respect to the proton beam (Devons and Hine 1949). This level de-excites by radiation to the (1+) $T=0$ ground state of ^{14}N with a value of $(2J+1)\,\Gamma_\gamma=31$ ev. This corresponds to a value of $(2J+1)\,|M|^2=0{\cdot}09$ where M is the matrix element relative to that of the single particle model (Weisskopf 1951); this value is appropriate to an allowed electric dipole transition (Wilkinson 1953 b) and so demands that, for the 8·06 Mev state, $T=1$. Now the first $T=1$ state of ^{14}N is (0+) and is at 2·31 Mev, so we might expect to find the companion to the 8·06 Mev state of ^{14}N in ^{14}C at about 5·7 Mev. There is a state well established in ^{14}C at 6·10 Mev: Benenson (1953) has shown that it is formed by s-wave neutron transfer in the reaction ^{13}C (dp) ^{14}C and so must be (0−) or (1−); but Thomas and Lauritsen (1952) have shown that this state emits gamma-rays to the (0+) ground state of ^{14}C and so it must be (1−)—an observation supported by the fact that these workers also find that the internal pair-formation suggests an electric dipole transition. Thomas and Lauritsen also remark that the difference between 6·10 Mev, the excitation of the state in ^{14}C, and 8·06–2·31 Mev, the separation of the $T=1$ states in ^{14}N, may be quantitatively correlated with the large reduced width of the 8·06 Mev state of ^{14}N—the Wigner–Thomas shift (see Thomas 1952). It is therefore highly probable that the 8·06 Mev state of ^{14}N is (1−) $T=1$. This is made certain by the work of E. Milne (private communications from R. G. Thomas and H. H. Woodbury) on ^{13}C (pp′) ^{13}C which shows the state to be of $J=1$.

We must now note that the transition from the 8·06 Mev (1−) $T=1$ state to the 2·31 Mev (0+) $T=1$ state is an electric dipole transition that, on the basis of energetics alone, we should expect to be about 0·4 times as strong as the electric dipole transition to the ground state. But it is forbidden by the isotopic spin selection rule since $\Delta T=0$.* The history of this possible 5·75 Mev transition is a curious one, during which its reported intensity has steadily dwindled. Lauritsen and Fowler (1940) and Fowler and Lauritsen (1949) reported the intensity to equal that of the ground state transition; Carver and Wilkinson (1951) (see Barnes, Carver, Stafford and Wilkinson (1952) for details) showed that this was not so and reported radiation of $5{\cdot}81\pm0{\cdot}25$ Mev in about 7% of the intensity of the ground state transition but entered the caveat that this might be contamination from the 6·14 Mev gamma-rays arising in the reaction ^{19}F (pα) ^{16}O; Woodbury and Fowler (1952) and Woodbury, Day and Tollestrup (1953) showed that 7% was indeed too generous an allowance and placed an upper limit of 2% on the relative abundance; Hicks, Husain, Sanders and

* This has also been noticed by Gell-Mann and Telegdi (1953) and Benenson (1953).

Beghian (1953) also failed to find the transition (corresponding to a limit of about 4%).

We may now understand the absence of this transition as an isotopic spin effect as remarked above, and it becomes of considerable interest to try and find it or place a closer limit on its occurrence in order to be able to make as strong a statement as possible about the contamination of the $T=1$ state at 8·06 MeV with a $T=0$ component such as would enable the transition to take place. (We may suppose the $T=1$ state at 2·31 MeV to be relatively pure since it is certainly removed by several MeV from any suitable $(0+)$ $T=0$ contaminant.)

It is appropriate to remark here that the discovery of such transitions of determinable radiative width that violate the isotopic spin selection rule is the best way of actually determining isotopic spin impurity as opposed to setting a limit on this quantity. This is because the uninhibited electric dipole transitions seem as a rule to show a constancy of $(2J+1)\,|\,M\,|^2$ to within a factor of about 2·5 (Wilkinson 1953 b) and so the measurement of an inhibited radiative width would determine the isotopic spin impurity with comparable precision. The other form of violation of the isotopic spin rules, the formation of, say, a $T=1$ state from $T=0$ particles such as is observed in ^{6}Li $(\alpha\gamma)$ ^{10}B (Jones and Wilkinson 1953 and forthcoming paper) is less helpful since uninhibited reduced widths are subject to much greater fluctuations (of the order of a factor of 100) and the correction for the penetration of the Coulomb barrier is also often rather uncertain. This second form of violation can only properly be interpreted as placing a lower limit on the isotopic spin impurity (through the use of the Wigner limit for the reduced width).

It was for this reason that we undertook a more extensive search for the forbidden transition than those referred to above.

§ 3. The Reaction ^{13}C (pγ) ^{14}N

We bombarded a thin target of electromagnetically-separated ^{13}C with protons of 560 kev and observed the gamma-rays at 90° to the proton beam* with the aid of a 1″ cube of NaI(Tl) and an EMI multiplier type 6262. Eight runs were made, separated by standardizing irradiations using sources of ^{137}Cs (662 kev), ^{60}Co (1·172 and 1·332 MeV), ^{12}C (4·43 MeV) and ^{16}O (6·14 MeV).

The combined irradiations are shown in the figure.

The standard deviations may be estimated from the number of counts per channel and are everywhere smaller than the radius of the circles. Peak A is due to the 8·06 MeV gamma-rays produced in the direct transition to the ground state of ^{14}N; it is due to pair creation with subsequent escape from the crystal of both annihilation quanta (the two-quantum escape peak).

* The angle of observation is of no consequence since, as we have seen, the reaction is induced by s-wave protons.

It had been reported by Woodbury and Fowler (1952) and Woodbury *et al.* (1953) that, in addition to this principal ground state transition, there is a weak transition to the state at $3{\cdot}948 \pm 0{\cdot}015$ MeV* giving a gamma-ray of energy about 4·1 MeV. This transition is well seen in our spectrum as peak B, due, as peak A, to pair creation with escape of both annihilation quanta ; at C we have the step due to capture of one annihilation quantum (the one-quantum escape peak), and at D the final step due to capture of both quanta (the no-quantum escape peak). At E we have the two-quantum escape peak due to the unhappily-ubiquitous 6·14 MeV gamma-rays from fluorine contamination (see the calibration distribution Y below it); at F we see signs of the one-quantum escape peak of the same radiation.

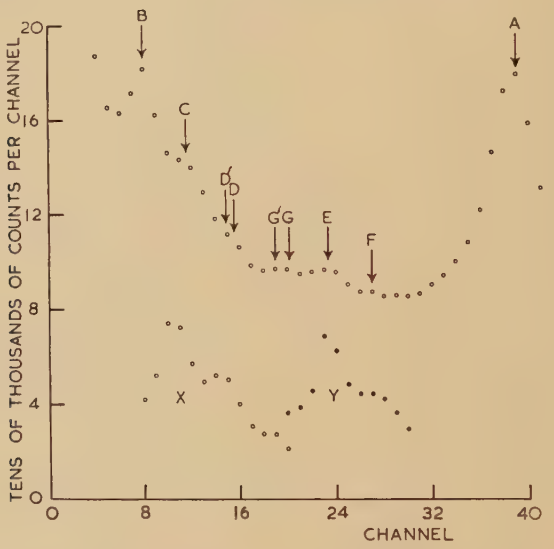

Pulse distribution due to the gamma-rays from ^{14}N detected in a NaI(Tl) crystal. For the meaning of the arrows see the text. Distribution X is part of that due to the 4·43 MeV gamma-rays from ^{12}C following $^{15}N(p\alpha)^{12}C$; distribution Y is part of that due to the 6·14 MeV gamma-rays from ^{16}O following $^{19}F(p\alpha)^{16}O$. (Distributions X and Y do not have the same ordinate scale or zero as the main distribution.)

At G we have placed an arrow in the position expected of the two-quantum escape peak from the forbidden 5·75 MeV transition that we seek. There is certainly a significant rise at about this position and we may be tempted to identify it with this forbidden transition. If we do this then the intensity of the supposed transition is about 0·7% of that to the ground state. But there is an alternative explanation of the peak G. ^{14}N possesses a state at $5{\cdot}08 \pm 0{\cdot}02$ MeV† which combines directly with the

* This value is derived from measurements by Thomas and Lauritsen (1952) on gamma-rays from $^{13}C(dn)^{14}N$.

† This energy derives from measurements of Thomas and Lauritsen on $^{13}C(dn)^{14}N$ and Woodbury *et al.* on $^{13}C(p\gamma)^{14}N$.

(1+) ground state and also shows a competing branch of intensity 26% to the (0+) $T=1$ state at 2·31 MeV (Woodbury *et al.* 1953); no corresponding state is known in ^{14}C so it is probably $T=0$. This makes it probable that it is (1+) since $J=0$ is excluded by the transition to the 2·31 MeV (0+) $T=1$ state which also makes $J\geqslant 2$ improbable, while (1−) would give two electric dipole transitions of which that to the ground state would be isotopic spin forbidden. This parity assignment agrees with Benenson's (1953) tentative conclusion from ^{13}C (dn) ^{14}N stripping while Woodbury *et al.* suggest $J=1$ or 2. If our suggestion of (1+) is correct we must expect a number of transitions to take place to this level from our (1−) level at 8·06 MeV—by the energy alone about 5% of the number to the ground state. Indeed Barnes *et al.* (1952) reported a possible gamma-ray of energy about 5·2 MeV in about 1·5% abundance while Hicks *et al.* (1953) reported a $5{\cdot}1\pm 0{\cdot}2$ MeV line in 4% abundance. These figures, corrected for the branching ratio observed by Woodbury *et al.* are well consistent with the expected abundance of about 5% for the transition to the 5·08 MeV state. Now if this 5·08 MeV line is really there its one-quantum escape peak will fall at 4·57 MeV, rather close to the principal two-quantum escape peak at 4·73 MeV from our forbidden transition. The position of this one-quantum escape peak is indicated by the arrow at G′ which fits the observed peak about as well as that at G corresponding to the forbidden transition. The principal two-quantum escape peak of the possible 5·08 MeV line would fall at 4·06 MeV at the position indicated by the arrow D′ and so be largely hidden by the no-quantum escape peak from the 4·1 MeV line. If we interpret the peak GG′ as a one-quantum escape peak it implies a relative intensity for the 5·08 MeV line of 2% which agrees well with the earlier estimates. A slight argument against accepting the peak GG′ as due wholly to a 5·08 MeV line is that the form of the successive peaks B, C and D is in excellent agreement with what is expected of a 4·1 MeV line (the nearby 4·43 MeV line of ^{12}C provides a good measure of this—see distribution X of the figure); if we subtract from the BCD group the two quantum escape peak at D′ appropriate to the one-quantum escape peak G′ the remaining BCD group becomes a little mis-shapen. A 2% abundance of a 5·08 MeV line implies, using the branching ratio of Woodbury *et al.* (1953), a 2·7% abundance of the preceding 3·0 MeV line. We have sought this line but not found it. The search is made difficult by the fact that the photo-peak of this line is hidden by the two-quantum escape peak of the 4·11 MeV line, while the principal two-quantum escape peak almost coincides with the Compton edge due to the 2·31 MeV line. A 3% abundance would have escaped detection. Hicks *et al.* have reported a $3{\cdot}05\pm 0{\cdot}1$ MeV line in 15% abundance; this appears to be excluded by our results and by those of Woodbury *et al.*

We must also bear in mind the possibility that this bump GG′ is indeed the two-quantum escape peak of a gamma-ray of about 5·7 MeV, but one that follows a transition from the initial 8·06 MeV level to one of the known states at about this excitation.

§ 4. The Isotopic Spin Impurity

The present results, therefore, are not conclusive. We have seen that it is very reasonable that the 5·08 MeV line should exist and that there is some evidence for it so we must leave our 0·7% as a limit rather than as a determination of an abundance. This corresponds to a contamination of the 8·06 MeV $T=1$ state with less than 2% of $T=0$ in *intensity*; in the notation of Radicati (1953) $\alpha_1^2(0)<0{\cdot}02$.

If the evidence in favour of the 5·75 MeV line were acceptable we would say $\alpha_1^2(0)\sim 0{\cdot}02$. This would be a rather large contamination but perhaps not unreasonable in view of the fairly high density of states at this excitation in ^{14}N. A higher contamination has been observed at 13·09 MeV in ^{16}O where $\alpha_1^2(0)>0{\cdot}03$ (Wilkinson 1953 c). (As always, when we are concerned with a self-conjugate nucleus, we must bear in mind that these results in themselves are explicable in terms of charge-symmetry and the charge-parity rules alone (Kroll and Foldy 1952) though the identification that we have made in § 2 between the 8·06 MeV state of ^{14}N and the 6·10 MeV state of ^{14}C tells of course, for charge-independence.)

§ 5. Other Gamma-Rays

Woodbury *et al.* (1953) report the energy of the cascade gamma-ray as $4{\cdot}0\pm 0{\cdot}1$ MeV; Hicks *et al.* (1953) give $4{\cdot}45\pm 0{\cdot}1$ MeV and hypothesize a new level in ^{14}N in explanation. This is a serious discrepancy. We have measured this energy as $4{\cdot}11\pm 0{\cdot}02$ MeV from the data presented in the figure and also from a further series of 14 runs interleaved with calibrations from the nearby 4·43 MeV gamma-ray from ^{12}C made by ^{15}N (pα) ^{12}C; these runs were made with high dispersion in order to examine the 4·1 MeV peak alone in more detail. This energy agrees perfectly with what is expected of a transition between the 8·06 and 3·95 MeV states. Woodbury *et al.* (1953) have reported the branching from the 3·85 MeV state to that at 2·31 MeV to be twice as probable as the direct transition to the ground state. This would imply that the 3·95 MeV gamma-ray should be present in one third the intensity of the 4·11 MeV line and it would therefore be rather difficult to separate from that line. We have seen no sign of the 3·95 MeV line and believe that its intensity may be slightly less than Woodbury *et al.* claim, though we do not feel strongly on this point.

We have, incidentally to our accurate measurement of the 4·11 MeV line, observed the last element of the cascades and determined its energy to be $2{\cdot}307\pm 0{\cdot}015$ MeV. Thomas and Lauritsen (1952) from a study of ^{13}C (dn) ^{14}N find $2{\cdot}310\pm 0{\cdot}012$ MeV as the energy of this transition; Woodbury *et al.* find $2{\cdot}32\pm 0{\cdot}02$, $2{\cdot}35\pm 0{\cdot}04$, $2{\cdot}32\pm 0{\cdot}04$ and $2{\cdot}32\pm 0{\cdot}02$ MeV yielding an average of $2{\cdot}323\pm 0{\cdot}015$ MeV. These estimates are consistent with our own and may be averaged to give an energy for the state of $2{\cdot}313\pm 0{\cdot}007$ MeV.

Acknowledgments

We would like to express our thanks to Sir John Cockcroft and Dr. Ralph Dawton of the Atomic Energy Research Establishment, Harwell,

for the supply of the separated ^{13}C; to Drs. Woodbury, Day and Tollestrup for the communication of their paper before publication and to Drs. R. G. Thomas and H. H. Woodbury for informing us of E. Milne's experiment.

References

Ajzenberg, F., and Lauritsen, T., 1952, *Rev. Mod. Phys.*, **24,** 321.
Barnes, C. A., Carver, J. H., Stafford, G. H., and Wilkinson, D. H., 1952, *Phys. Rev.*, **86,** 359.
Benenson, R. E., 1953, *Phys. Rev.*, **90,** 420.
Carver, J. H., and Wilkinson, D. H., 1951, *Proc. Phys. Soc.* A, **64,** 199.
Devons, S., and Hine, M. G. N., 1949, *Proc. Roy. Soc.* A, **199,** 56, 73.
Fowler, W. A., and Lauritsen, C. C., 1949, *Phys. Rev.*, **76,** 314.
Gell-Mann, M., and Telegdi, V., 1953, *Phys. Rev.* (in course of publication).
Hicks, D., Husain, T., Sanders, L. G., and Beghian, L. E., 1953, *Phys. Rev.*, **90,** 163.
Jones, G. A., and Wilkinson, D. H., 1953, *Phys. Rev.*, **90,** 722.
Kroll, N. M., and Foldy, L. L., 1952, *Phys. Rev.*, **88,** 1177.
Lauritsen, T., and Fowler, W. A., 1940, *Phys. Rev.*, **58,** 193.
Radicati, L. A., 1952, *Phys. Rev.*, **87,** 521; 1953, *Proc. Phys. Soc.* A, **66,** 139.
Teichmann, T., and Wigner, E., 1952, *Phys. Rev.*, **87,** 123.
Thomas, R. G., 1952, *Phys. Rev.*, **88,** 1109.
Thomas, R. G., and Lauritsen, T., 1952, *Phys. Rev.*, **88,** 969.
Weisskopf, V. F., 1951, *Phys. Rev.*, **83,** 1073.
Wilkinson, D. H., 1953 a, *Phil. Mag.*, **44,** 1019 (II); 1953 b, *Ibid.*, **44,** 450; 1953 c, *Phys. Rev.*, **90,** 721.
Wilkinson, D. H., and Jones, G. A., 1953, *Phil. Mag.*, **44,** 542 (I).
Woodbury, H. H., Day, R. B., and Tollestrup, A. V., 1953, *Phys. Rev.* (in course of publication).
Woodbury, H. H., and Fowler, W. A., 1952, *Phys. Rev.*, **85,** 51.

CXXXIII. *Dielectric Polarization of a Dipolar Lattice*

By J. A. Pople
Department of Theoretical Chemistry, University of Cambridge*

[Received August 5, 1953]

Summary

This paper is concerned with a rigorous treatment of the dielectric polarization of a model consisting of unpolarizable point dipoles fixed on the sites of a lattice but free to rotate. The dielectric constant of this system is expanded in inverse powers of the temperature as far as T^{-3}. It is shown that for small dipole moments the Debye and Onsager approximate formulae both overestimate the polarization, the Onsager result being the more accurate of the two. Previous treatments of this problem did not make adequate allowance for the long-range effects of boundary field polarization.

§ 1. Introduction

One of the simplest statistical models that can be used as a basis for a theory of dipolar interaction in condensed polar media is the dipolar lattice. In this model each molecule is represented by a point dipole fixed at a lattice site but free to rotate in the electric field of all the others. Although the partition function cannot be evaluated in closed form, considerable progress can be made with a high temperature expansion (Van Vleck 1937, Pople 1952) and the model has been used for a discussion of the cohesion of polar liquids.

The present paper is devoted to the calculation of the polarization of the dipolar lattice model in a uniform electric field, the aim being to expand the dielectric constant in inverse powers of the temperature by a method analogous to that used in the free energy treatment. We shall only consider the problem of a lattice of permanent dipoles and shall not be concerned with modifications (such as inclusion of polarizability or quadrupole interactions) which may make the model more realistic. The results for the simple model are of considerable interest, however, for, being rigorously derived, they can be used as a significant test of the approximate formulae of Debye (1929) and Onsager (1936).

This model for dielectric polarization has been investigated previously by Van Vleck (1937) and Rosenberg and Lax (1953). These authors, however, do not make adequate allowance for the effect of boundary

* Communicated by the Author.

field polarization. Kirkwood (1939), in an important paper on this topic, showed that the dielectric constant ϵ of a system consisting of N permanent dipoles in a volume V is given by

$$\epsilon-1=\frac{4\pi N}{V}\frac{\epsilon+2}{3}\frac{\boldsymbol{\mu}\,.\,\bar{\mathbf{M}}}{3kT}, \qquad \ldots\ldots \quad (1.1)$$

where $\bar{\mathbf{M}}$ is the total moment induced in a spherical specimen by any one of its dipoles maintained in a fixed position and orientation $\boldsymbol{\mu}$. Because of the reaction field due to the external boundary, $\bar{\mathbf{M}}$ is not concentrated near $\boldsymbol{\mu}$. Kirkwood therefore introduces a local moment $\bar{\boldsymbol{\mu}}$ which may be defined as the moment of a sphere surrounding $\boldsymbol{\mu}$ which is large compared with molecular dimensions but small compared with the whole specimen. In terms of this moment, ϵ is given by

$$\epsilon-1=\frac{4\pi N}{V}\frac{3\epsilon}{2\epsilon+1}\frac{\boldsymbol{\mu}\,.\,\bar{\boldsymbol{\mu}}}{3kT}. \qquad \ldots\ldots \quad (1.2)$$

Now the procedure of Van Vleck and Rosenberg–Lax is equivalent to a direct attempt to obtain a high temperature expansion for $\boldsymbol{\mu}\,.\,\bar{\mathbf{M}}$. As the coefficients are obtained as rapidly convergent lattice sums, it seems possible that they are really obtaining the local moment $\bar{\boldsymbol{\mu}}$ rather than the total $\bar{\mathbf{M}}$. The details of the analysis later in this paper indicate that this is so and the results have to be modified accordingly.

§ 2. High Temperature Expansions for the Dielectric Constant

Before obtaining the rigorous expansion for the dipolar lattice model, we shall give the corresponding expressions for the approximate formulae of Debye and Onsager. The Debye formula, corresponding to putting $\bar{\mathbf{M}}=\boldsymbol{\mu}$ in (1.1) can be written

$$3(\epsilon-1)/(\epsilon+2)=x, \qquad \ldots\ldots \quad (2.1)$$

where x is the non-dimensional quantity $4\pi N\mu^2/3VkT$. We shall find it convenient to expand the quantity $3(\epsilon-1)/(\epsilon+2)$ rather than $\epsilon-1$ in all formulae. $3(\epsilon-1)/(\epsilon+2)$ is 4π times the resultant moment of a spherical specimen per unit volume per unit field *before insertion of the dielectric material.*

The Onsager formula, obtained by putting $\bar{\boldsymbol{\mu}}=\boldsymbol{\mu}$ in (1.2) can be written

$$3(\epsilon-1)/(\epsilon+2)=\tfrac{3}{2}(1+\tfrac{2}{3}x)^{-1}\{(1+\tfrac{2}{3}x+x^2)^{1/2}-1+\tfrac{1}{3}x\}, \quad \ldots \quad (2.2)$$

or, expanding for small x

$$3(\epsilon-1)/(\epsilon+2)=x-\tfrac{2}{9}x^3+O(x^4). \qquad \ldots\ldots \quad (2.3)$$

The two formulae are seen to agree in giving no term in x^2 but differ in the coefficient of x^3.

The treatment of the dipolar lattice model will be based on the exact Kirkwood equation (1.2). If we write x' for $4\pi N\boldsymbol{\mu}\,.\,\bar{\boldsymbol{\mu}}/3VkT$ we have

$$3(\epsilon-1)/(\epsilon+2)=x'-\tfrac{2}{9}x'^3+O(x'^4), \qquad \ldots\ldots \quad (2.4)$$

so that it only remains to find x' in terms of x.

Suppose that we have N dipoles, fixed in position at points $\mathbf{R}_1 \ldots \mathbf{R}_n$ of a lattice, but free to rotate. The dipolar interaction energy is then given by

$$W=\sum_{i<j} w_{ij}, \quad . \quad . \quad . \quad . \quad . \quad . \quad . \quad (2.5)$$

where

$$w_{ij}=\epsilon_{\alpha\beta}^{(ij)}\mu_{i\alpha}\mu_{j\beta}. \quad . \quad . \quad . \quad . \quad . \quad . \quad . \quad . \quad (2.6)$$

Here Greek suffixes are used as tensor suffixes and $\epsilon_{\alpha\beta}^{(ij)}$ is the dipole interaction tensor

$$\left.\begin{aligned} &\epsilon_{\alpha\beta}^{(ij)}=R_{ij}^{-5}\{R_{ij}^{2}\delta_{\alpha\beta}-3R_{ij\alpha}R_{ij\beta}\}, \\ &\mathbf{R}_{ij}=\mathbf{R}_j-\mathbf{R}_i. \end{aligned}\right\} \quad . \quad . \quad . \quad . \quad (2.7)$$

Now suppose that v_i is a region surrounding the site $\mathbf{R}_i$ which is of the required intermediate dimensions. Then we may write

$$\boldsymbol{\mu} \cdot \bar{\boldsymbol{\mu}}-\mu^2=\sum_{j(\neq i)}^{*} \overline{\boldsymbol{\mu}_i \cdot \boldsymbol{\mu}_j}, \quad . \quad . \quad . \quad . \quad . \quad . \quad . \quad (2.8)$$

where Σ^* indicates summation over lattice sites in v_i and the bar represents an average over the canonical ensemble for the whole specimen (in the absence of an external field). Now

$$\overline{\boldsymbol{\mu}_i \cdot \boldsymbol{\mu}_j}=\int \boldsymbol{\mu}_i \cdot \boldsymbol{\mu}_j \exp\left\{-\sum_{k<l}^{N} w_{kl}/kT\right\} d\omega \Big/ \int \exp\left\{-\sum_{k<l} w_{kl}/kT\right\} d\omega, \quad (2.9)$$

$\int d\omega$ having been written for integration over the angular co-ordinates of all dipoles. The numerator and denominator of (2.9) can now be expanded in powers of x. The denominator is $(4\pi)^N\{1+O(x^2)\}$ and the leading terms occurring in the numerator are (for $i \neq j$)

$$\left.\begin{aligned} &\boldsymbol{\mu}_i \cdot \boldsymbol{\mu}_j \, d\omega=0, \\ &\int \boldsymbol{\mu}_i \cdot \boldsymbol{\mu}_j w_{ij} \, d\omega=\int \mu_{i\alpha}\mu_{j\alpha}\epsilon_{\beta\gamma}^{(ij)}\mu_{i\beta}\mu_{j\gamma} d\omega=\tfrac{1}{9}(4\pi)^N\mu^4\epsilon_{\alpha\alpha}^{(ij)}=0, \\ &\int \boldsymbol{\mu}_i \cdot \boldsymbol{\mu}_j w_{kl} \, d\omega=0. \end{aligned}\right\} \quad . \quad . \quad (2.10)$$

It follows that $(\boldsymbol{\mu} \cdot \bar{\boldsymbol{\mu}}/\mu^2)-1$ is at least as small as $O(x^2)$. The only non-vanishing integrals in the next term of the expansion have integrands $\boldsymbol{\mu}_i \cdot \boldsymbol{\mu}_j w_{ik} w_{jk}$ $(k \neq i, j)$ and we find that

$$(\boldsymbol{\mu} \cdot \bar{\boldsymbol{\mu}}/\mu^2)-1=(4\pi)^{-N}(\mu^2k^2T^2)^{-1}\sum_{j(\neq i)}^{*}\sum_{k} \int \boldsymbol{\mu}_i \cdot \boldsymbol{\mu}_j w_{ik} w_{jk} \, d\omega. \quad (2.11)$$

It should be noted that the sum over k in (2.11) is over all the lattice sites in V (except i and j) whereas the sum over j is only over those in v_i (except i). Integration over angle gives

$$(\boldsymbol{\mu} \cdot \bar{\boldsymbol{\mu}}/\mu^2)-1=\tfrac{1}{27}(\mu^4/k^2T^2)\sum_{j(\neq i)}^{*}\sum_{k} \epsilon_{\alpha\beta}^{(ik)}\epsilon_{\alpha\beta}^{(jk)}, \quad . \quad . \quad . \quad . \quad . \quad . \quad (2.12)$$

$$\epsilon_{\alpha\beta}^{(ik)}\epsilon_{\alpha\beta}^{(jk)}=3R_{ik}^{-5}R_{jk}^{-5}\{3(\mathbf{R}_{ik} \cdot \mathbf{R}_{jk})^2-R_{ik}^{2}R_{jk}^{2}\}. \quad . \quad . \quad . \quad (2.13)$$

The evaluation of the double summation in (2.12) requires some care. For any given value of j in v_i the k-summation is over a large region

round both i and j. Thus k-summation (again for fixed j) converges if extended to infinity (by inspection of (2.13)) and the sum will be a function of R_{ij}. Since the region v_i itself is macroscopic, we can then carry out a second infinite summation over j. As a result we may write (2.12) as a doubly infinite summation, the k-summation being carried out first.

$$(\boldsymbol{\mu}\,.\,\bar{\boldsymbol{\mu}}/\mu^2)-1=\tfrac{1}{27}(\mu^4/k^2T^2)\sum_{j(\neq i)}^{\infty}\sum_{k}^{\infty}\epsilon_{\alpha\beta}^{(ik)}\epsilon_{\alpha\beta}^{(jk)}. \quad . \quad . \quad . \quad . \quad . \quad (2.14)$$

(Infinite summation in this context means summation over sites extending infinitely from the neighbourhood of i.)

It should be emphasized that this clear separation as a consecutive doubly infinite summation is only possible because of the introduction of the two regions v_i and V. If both summations were over V this argument would break down, for there would no longer always be a large region of k-summation outside both i and j. This is the point that has not been sufficiently considered by Van Vleck (1937) and Rosenberg and Lax (1953). They assume, in effect, that the double series on the right-hand side of (2.14) gives $(\boldsymbol{\mu}\,.\,\overline{\mathbf{M}}/\mu^2)-1$ (eqn. (1.1)) and includes the contribution of the boundary field polarization.

It is convenient to add the term $j=i$ to (2.14) and subtract again

$$(\boldsymbol{\mu}\,.\,\bar{\boldsymbol{\mu}}/\mu^2)-1=\tfrac{1}{27}(\mu^4/k^2T^2)\left\{\sum_{j}^{\infty}\sum_{k}^{\infty}\epsilon_{\alpha\beta}^{(ik)}\epsilon_{\alpha\beta}^{(jk)}-\sum_{k}^{\infty}\epsilon_{\alpha\beta}^{(ik)}\epsilon_{\alpha\beta}^{(ik)}\right\}. \quad . \quad . \quad . \quad . \quad (2.15)$$

We next show that the double summation in (2.15) is zero. This is on account of the following two results :

1. $\sum_{k}^{\infty}\epsilon_{\alpha\beta}^{(ik)}\epsilon_{\alpha\beta}^{(jk)}$ is convergent for all j ($\epsilon_{\alpha\beta}^{(ik)}\epsilon_{\alpha\beta}^{(jk)}$ being asymptotically proportional to R_{ik}^{-6} for k far from both i and j).

2. $$\sum_{j}^{\infty}\epsilon_{\alpha\beta}^{(ik)}\epsilon_{\alpha\beta}^{(jk)}=\epsilon_{\alpha\beta}^{(ik)}\sum_{j}^{\infty}\epsilon_{\alpha\beta}^{(jk)}=0. \qquad \text{(all } k\text{)}. \quad . \quad . \quad . \quad . \quad . \quad . \quad . \quad . \quad . \quad (2.16)$$

This follows directly from (2.7) and the symmetry of the lattice.

From the second of these results it is clear that $\sum_{j}^{\infty}\sum_{k}^{p}\epsilon_{\alpha\beta}^{(ik)}\epsilon_{\alpha\beta}^{(jk)}$ converges uniformly for all p (that is for all finite k-summations). We therefore have sufficient conditions to interchange the order of summation (Jeffreys and Jeffreys 1950, § 1.125) and the double summation vanishes.

Evaluating the remaining term in (2.15) using (2.7) we now have

$$\begin{aligned}\boldsymbol{\mu}\,.\,\bar{\boldsymbol{\mu}}/\mu^2&=1-\tfrac{2}{9}(\mu^4/k^2T^2)\sum_{k(\neq i)}R_{ik}^{-6}+\ldots\\&=1-bx^2+O(x^3), \quad . \quad . \quad . \quad . \quad . \quad . \quad (2.17)\end{aligned}$$

where $$b=2(V/4\pi N)^2\sum_{k(\neq i)}R_{ik}^{-6}, \quad . \quad . \quad . \quad . \quad . \quad . \quad (2.18)$$

is a number depending on the type of lattice. For the simple, body-centred and face-centred cubic lattices b has the values 0·10642, 0·09196 and 0·09154.

§ 3. Discussion

The high temperature expansions for dielectric polarization obtained in this paper are

Debye formula $3(\epsilon-1)/(\epsilon+2)$	$=x.$
Onsager formula	$=x-0{\cdot}22222x^3+\ldots.$
Simple cubic lattice	$=x-0{\cdot}32864x^3+\ldots.$
Body-centred cubic lattice	$=x-0{\cdot}31418x^3+\ldots.$
Face-centred cubic lattice	$=x-0{\cdot}31376x^3+\ldots.$

For reasons discussed in the previous section, these differ from the figures given by Van Vleck (1937) and by Rosenberg and Lax (1953).

It should be noted that the expansions for the three lattices differ only slightly. This suggests that the lattice formulae should, in fact, give a good approximation to the polarization for any isotropic arrangement of dipoles as in a liquid. When the accurate results are compared with the corresponding expansions of the approximate formulae, it is clear that, for small dipole moments at least, both the Debye and Onsager equations overestimate the polarization, the latter being the more accurate of the two. The dielectric constants of actual polar liquids will also be influenced by other factors such as polarizability and other short range intermolecular forces, but the results of this paper suggest that the Onsager equation may be substantially in error even for molecules interacting as permanent point dipoles.

The author is indebted to Dr. S. F. Boys for discussion on this subject.

References

Debye, P., 1929, *Polar Molecules* (Chem. Catalog. Co.).
Jeffreys, H., and Jeffreys, B., 1950, *Methods of Mathematical Physics* (Cambridge : University Press).
Kirkwood, J. G., 1939, *J. Chem. Phys.*, **7**, 911.
Onsager, L., 1936, *J. Amer. Chem. Soc.*, **58**, 1486.
Pople, J. A., 1952, *Proc. Roy. Soc.* A, **215**, 67.
Rosenberg, R., and Lax, M., 1953, *J. Chem. Phys.*, **21**, 424.
Van Vleck, J. H., 1937, *J. Chem. Phys.*, **5**, 556.

CXXXIV. *Superconductivity at Very High Pressures*

By P. F. Chester and G. O. Jones
Queen Mary College, University of London*

[Received August 24, 1953]

Abstract

A method is described for the realization of very high pressures at liquid helium temperatures. First results are given of its application to studies of superconductivity under pressures up to 44 000 atm. Bismuth is shown to become superconducting under pressure. T_c for tin is shown to vary approximately linearly with volume up to 17 500 atm. The value of dT_c/dp for thallium is found to be negative, in disagreement with previous work.

§ 1. Introduction

Recent theories of the origin of superconductivity make it desirable to obtain more experimental information on the effect of varying the pressure on the properties of superconductors, to supplement the growing mass of data on the effect of varying the isotope in a given superconducting metal. Indeed, the pressure (or volume) and the mass number would seem to be the only variables whose effect might be capable of immediate theoretical interpretation. In particular, it is of interest to determine the influence of pressure on the transition temperature, T_c, and on the value of the quantity dH_c/dT at T_c (where H_c is the threshold field at temperature T), and also to find whether the application of high pressures can destroy superconductivity, or cause it to appear in metals not normally superconducting.

The present paper describes some experiments of this kind which we have carried out at pressures up to about 40 000 atm.—over twenty times higher than the maximum pressures previously employed in similar investigations. The increase in the working range of pressure has been made possible by the use of a technique due to Bridgman adapted in a special way for use in low-temperature enclosures.

In a further paper the implications of some of the results obtained will be examined from the general standpoint adopted in the theories of Fröhlich (1950 a, b, 1951) and Bardeen (1950 a, b, 1951 a, b, c), in which superconductivity is attributed to interactions between electrons *via* their interactions with the lattice.

* Communicated by the Authors.

§ 2. Summary of Previous Work

The earliest systematic study of the effect of compression on the properties of superconductors was carried out by Sizoo and Onnes (1925), who applied pressure to wires of tin and indium by compressing helium into the vessel in which they were mounted. For both metals the transition temperature (T_c), at which the resistance fell to half its residual value, was found to be depressed. However, the maximum pressures used were no greater than 300 atm., and the maximum observed depression of T_c was about 0·005°. The later discovery by Keesom (1926) of the solidification of helium under pressure threw doubt on the results obtained by Sizoo and Onnes for all but the lowest pressures used, and removed the last hope of using a transmitting fluid for the application of conventional high-pressure techniques to experiments at liquid helium temperatures.

An advance in technique which enabled appreciably higher pressures to be reached at low temperatures was made by Lazarew and Kan (1944), who generated pressures of about 1750 atm. by allowing water to freeze in a thick-walled ' bomb '. Electrical leads leading out of the ' bomb ' made it possible to measure the resistance of wires mounted in it as they were cooled, under pressure, to liquid helium temperatures. Of the metals (thallium, indium, tin, mercury, tantalum and lead) subsequently investigated by Kan, Sudovstov and Lazarew (1948, 1949), all but thallium showed a depression of T_c under pressure. Using the same technique, Alekseyevski and Brandt (1949, 1952) investigated the non-superconducting metal bismuth and its superconducting compounds $RhBi_4$, $NiBi_3$, KBi_2, LiBi and Au_2Bi. No signs of superconductivity could be observed in metallic bismuth at pressures up to 1050 atm. Compression lowered the transition temperatures of LiBi and Au_2Bi but raised those of the other compounds named. The absolute magnitude of the quantity dT_c/dp in these experiments ranged from $5{\cdot}8\times10^{-11}$ deg. dyne^{-1} cm^2 for tin to almost zero for $RhBi_4$. The maximum observed change in T_c was therefore about 0·1° ; in most cases the total change was much smaller. The fact that the transitions observed were fairly sharp was taken to imply that the pressure was uniform throughout the volume of the superconductor.

A number of other experiments, on specimens under non-uniform distributions of stress (such as linear extension), have also been carried out by the authors named above, but we do not discuss the results here.

§ 3. Experimental Method

In order to reach much higher pressures it was decided to adapt for our purpose the technique due to Bridgman (1935 a, 1949, 1950, 1952) by which quasi-hydrostatic pressures up to about 400 000 atm. may be generated in thin solid specimens. This technique depends on the fact that a small area of a massive block of metal is able to withstand stresses far greater than the normal breaking stress of the bulk material, because of the support afforded by the surrounding metal. In applying this principle to the study of the shear strength or electrical resistance of

metals under very high pressures, Bridgman interposes a disc-shaped specimen between the plane faces of two truncated conical bosses, each machined on massive blocks of steel or Carboloy. As the blocks are forced together, very intense stresses are developed over the small area of contact, and the specimen and compressing surfaces deform in such a way that the pressure in the specimen approaches a hydrostatic distribution locally, with a value which decreases radially from the centre to the perimeter. The actual form of the variation is difficult to estimate, but it was believed by Bridgman that a large central part of such a specimen would be under fairly uniform pressure. This question is discussed elsewhere (Chester 1953), and we shall only mention here certain indications arising from the present results which suggest that this is true for the metallic specimens so far investigated by us. (The values of mean pressure quoted in the present paper are equal to the total force applied in a given experiment divided by the area of the specimen under stress.)

In order to avoid the necessity for cooling to the working temperature the rather bulky apparatus which would be required to transmit a sufficient force to the specimen, we have mounted our specimens in a small self-contained device, which we refer to here as a ' clamp '. Pressure may be generated in the specimen at room temperature by applying a force to the clamp by means of a hydraulic press, and after a suitable adjustment the clamp may be removed from the press and transferred to a small cryostat, with the state of stress in the specimen still maintained. Apart from the simplification in technique wich results, there is an important advantage in the fact that the force is applied to the specimen at room temperature, and not at the working temperature in the liquid helium region. With this procedure the specimen, particularly if of a soft metal, remains in a fairly well annealed condition throughout. If the force were applied at liquid helium temperatures, annealing would not occur and the specimens stressed in the way described would be, if not actually disrupted, severely ' cold-worked '—a condition which is known (Hilsch 1951) to affect the superconducting properties profoundly.

The design of the clamp is illustrated in fig. 1. The specimen, in the form of a thin disc, is set between the truncated compressing cones C. For the application of pressure, the clamp is supported by its rim R in the cylindrical jig J, a plunger G is inserted in the axial hole H in the screw W, and the whole unit placed between the rams of the press. When force is applied between the plunger and the base of the jig, the pistons P of the clamp—and therefore the specimen—are put under compression, whilst the outer wall of the clamp is put into tension. The various members can now be ' locked ' in their state of stress by tightening the screw.

In practice it is not possible to preserve the full stress because of friction in the screw-thread, and the following procedure is adopted to ensure that the fraction preserved is as large as possible and is accurately known : When a suitable value of the force is reached, the screw is tightened progressively

and the hydraulic press relaxed at such a rate as to keep constant the strain in the clamp—as indicated by a resistance strain-gauge cemented to its outer wall. As the press is relaxed further, the screw becomes more difficult to turn and after a certain stage no further tightening is attempted. At this point the press is relaxed completely and the fraction of the original strain which has been retained (in practice never less than 90%) is noted from the indication of the strain-gauge. The clamp is now transferred to the cryostat. No change in the pressure applied to the specimen is to be expected on subsequently cooling the clamp to the working temperature because its load-bearing members are made wholly of one material, and therefore contract equally.

Fig. 1

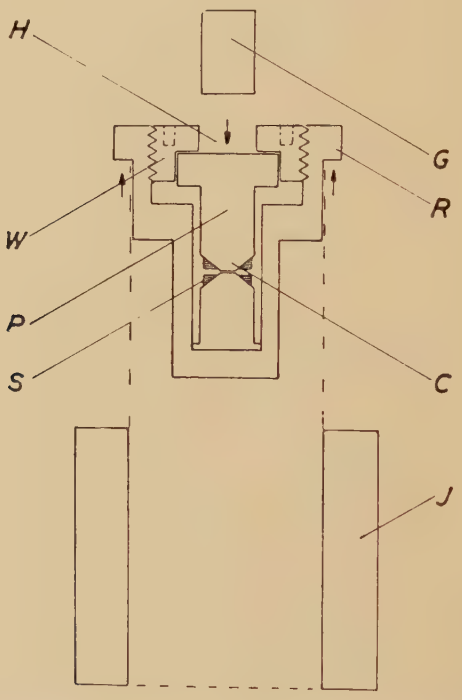

Schematic diagram of clamp (for explanation of symbols see text).

The superconducting transition of the compressed specimen is observed by a magnetic method. This is to be preferred to a method depending on the measurement of resistance, because it avoids the difficulties of electrical insulation at high pressure, and is less likely to lead to the spurious effects associated with the existence of filaments of abnormally high critical field—as reported by Lazarew and Galkin (1944) for inhomogeneously strained superconductors and by de Haas and Voogd (1930) for inhomogeneous superconducting alloys. The method best suited to the geometry of the clamp is to wind secondary coils S, in series, round each

cone and to apply an alternating field along the axis of the clamp by means of a solenoid coaxial with it. The e.m.f. induced in the secondary coils is amplified, rectified and displayed on a micro-ammeter. Because of the large demagnetizing factor of a transverse disc, reasonably sharp transitions are to be expected only if the alternating field is of small amplitude. We have found also that it is not possible to make use of the increased sensitivity to be expected of high-frequency measurements because of skin effects in the material of the clamp. In consequence, most of the work has been done with alternating fields of amplitude about 0·1 gauss and frequency 30 c/s.

Preliminary investigations, made with clamps of various steels, indicated that the proximity of ferromagnetic materials complicated the transition of the superconductor and made accurate determination of T_c difficult. All the quantitative work to be described has therefore been carried out with a clamp of beryllium-copper—a material which remains weakly paramagnetic down to liquid helium temperatures. For experiments up to mean pressures of 16 000 atm., the circular area in contact with the specimen was about 5 mm in diameter, and the thickness of the specimen after compression was usually less than 0·01 mm. Some rough work up to higher pressures (about 40 000 atm.), has been carried out, using conical tips of smaller area, of ' Vibrac ' steel.

Because of the existence of a radial pressure gradient in the specimen it was expected that for most superconductors under pressure the outer part of the disc would become superconducting at a higher temperature than would the centre part, and it was thought that the superconducting rings thus formed might tend to mask the transition of the centre. To avoid this complication a small wedge of a metal, known to be not superconducting under the conditions of the experiments, is inserted into a suitable cut in the circumference of the disc before compression, to prevent the formation of complete superconducting rings in the periphery. Aluminium, normally a superconductor below 1·2°K, has been found suitable for use with the metals so far studied. (An independent test was carried out to ensure that aluminium did not become superconducting under pressure above 2°K—the lower limit of temperature of the present experiments.) This precaution was not, of course, necessary in the exploratory work on non-superconductors.

A Helmholtz pair located outside the cryostat, with the axis of its coils in the plane of the specimen, permitted transitions to be observed in known magnetic fields. The demagnetizing factor of the disc in this direction appears to be sufficiently small to be ignored, because the form of transition curve obtained—though not of course its location on the temperature axis—is not sensibly altered by varying the field (see fig. 4).

Temperature control in the region 2° to 4·2°K was effected by varying the pressure over a bath of liquid helium in which the clamp was immersed, the temperature being deduced from the value of vapour pressure. Above 4·2°K a charcoal desorption method was used and temperatures measured

by means of a carbon resistance thermometer of the type described by Clement and Quinnell (1952).

§ 4. Experimental Results and Discussion

The results on the metals studied are now presented and discussed separately.

Tin

Tin, according to the Russian workers, shows the largest change in T_c under pressure. It is the most extensively studied superconductor, having its transition temperature in a range where very accurate control of temperature is possible, and it was therefore the obvious choice for a first detailed investigation.

Superconducting transitions were observed by cooling through the transition temperature under mean pressures of 1, 10 500 and 16 000 atm. The results are shown in fig. 2, where the alternating flux in the secondary

Fig. 2

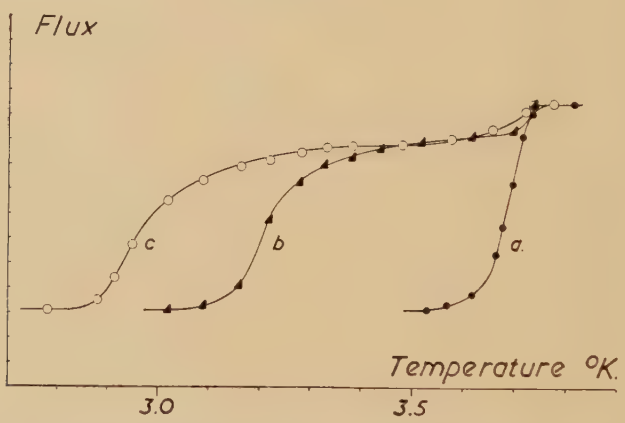

Transitions of tin in zero field at differing pressures : (*a*) 1 atm., (*b*) 10 500 atm., and (*c*) 16 000 atm. mean pressure. Flux in arbitrary units.

coils is plotted, in arbitrary units, against temperature. The width of the curve at 1 atm. provides a reasonable measure of the limit of resolution of the method for a given alternating field, and we then interpret the spreading of the curves at high pressure as due to the pressure gradient in the specimen. Inspection of the curves suggests that over about three-quarters of the area the pressure is uniform within our limits of resolution (the small drop in flux at the high-temperature end of the curves is probably due to metal extruded beyond the area of the compressing cones). By assuming a linear gradient over the remaining area we can arrive at estimates of the maximum pressure in the specimen. For a mean pressure of 16 000 atm., for instance (curve c), we estimate that the pressure over the central three-quarters of the specimen lies between 16 000 and

19 000 atm., which we write as 17 500±1 500 atm. We believe the results may fairly be stated as follows :

At 1 atm., the value of T_c determined by us agrees with the normal value (3·73°K), within experimental error.

At 11 500±1000 atm., T_c=3·21±0·07°K.

At 17 500±1500 atm., T_c=2·9±0·1°K.

It is important to emphasize that the curves represent reversible behaviour and the effects shown are therefore not due to work-hardening (or ' cold-working '). After relaxing the pressure the curve obtained with a given specimen is indistinguishable from that obtained before the application of pressure.

Combining these with the results of Kan, Sudovstov and Lazarew (1948), and making use of Bridgman's values (Bridgman 1949) for the compressibility of tin, it is possible to plot T_c against $\Delta V/V$, where ΔV is the change in volume due to the increase in pressure. This is done in fig. 3, where it

Fig. 3

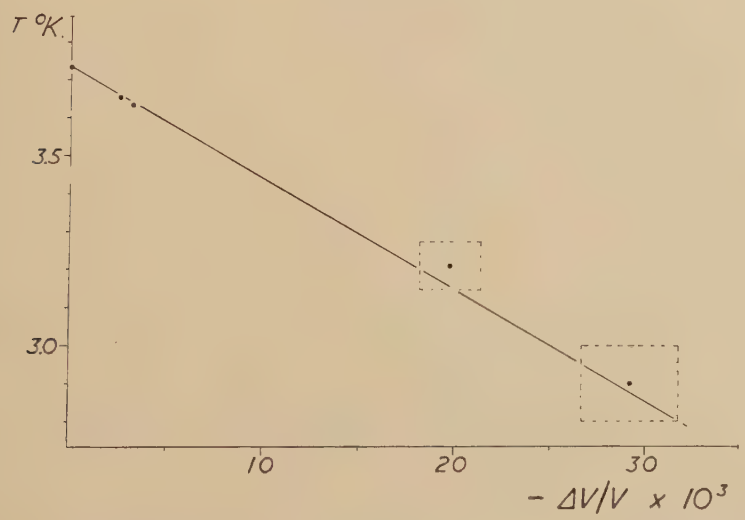

Relation between transition temperature and change in volume for tin under pressure. The areas enclosed by the dotted lines indicate the estimated experimental uncertainty in the present work.

may be seen that the variation is linear, within experimental error, and that the earlier and the present results lie on the same line.

The relation derived from the graph is

$$T_c\,(°\text{K}) = 3{\cdot}73 + 29\,(\Delta V/V)$$

where the coefficient of $\Delta V/V$ may be in error by ±10% at the lower pressures and by ±20% at the higher pressures.

We have also observed transitions under the highest of these pressures for a number of differing values of magnetic field (in the plane of the disc).

The curves obtained are shown in fig. 4. A field of 50 gauss depresses the foot of the curve by about 0·37°. The corresponding depression at 1 atm. (see for instance Shoenberg 1952) would be 0·35°. Thus the quantity dH_c/dT at the temperature T_c remains substantially constant under pressure. At a given temperature H_c is of course lowered by pressure.

The magnitude of the quantity H_0, equal to $(H_c)_{T=0}$, is of theoretical significance since it is related to the difference in energy between the normal and superconducting states at absolute zero. Our experiments have not yet been carried to a sufficiently low temperature to determine the form of the curve of H_c against T, but we may point out that if it has

Fig. 4

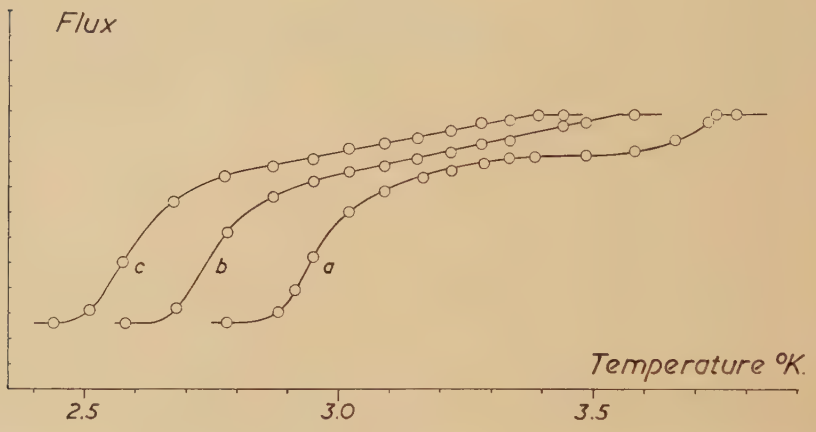

Transitions of tin under 16 000 atm. mean pressure in differing magnetic fields : (*a*) zero field, (*b*) 23·6 gauss, (*c*) 47·2 gauss. Flux in arbitrary units.

the approximately parabolic form characteristic of tin at 1 atm., then the present results imply that H_0—and therefore the energy difference between the normal and superconducting states—is lowered by compression.

Lead

We have confirmed that T_c for lead is lowered by compression, but have not yet obtained detailed results on this metal.

Thallium

Because of the anomalous behaviour reported for thallium by the previous workers (Kan, Sudovstov and Lazarew 1949), using resistance measurements, we have investigated it by our method up to higher pressures.

In two runs under mean pressures of 11 700 atm. and 13 400 atm. respectively, no signs of superconductivity could be observed above 2·35°K although an uncompressed specimen began to show superconductivity at 2·39°K. The whole transition curve was displaced by pressure

to a lower temperature, T_c being lowered by about 0·06° under 13 400 atm. The change is much smaller than that observed for tin, but is in the same direction. This result disagrees with the observation of Kan, Sudovstov and Lazarew ; we may mention that the behaviour of thallium in the experiments of these workers was stated to be very sensitive to the method of mounting the specimen.

Bismuth

Bismuth, though not normally a superconductor, is obviously very close to being one. Hilsch (1951) has shown that very thin films of bismuth deposited from the vapour on to a surface at liquid helium temperatures exhibit superconductivity, with T_c at about 5°K (although annealing at room temperature destroys this property of the film) and a large number of alloys containing bismuth have been found to be superconductors. The positive value of dT_c/dp found by Alexeyevski for the bismuth-rich compounds $RhBi_4$, $NiBi_3$ and KBi_2, together with the vanishingly small electronic specific heat of the pure metal at low temperatures led him to suggest that bismuth might be a ' virtual ' superconductor and that sufficient pressure might bring its transition temperature into the liquid helium region. Another interesting pointer arises from the curve of atomic volume of the elements plotted against atomic number ; the superconducting metals are found to occupy a fairly well defined range of atomic volumes intermediate between the peaks and troughs of the curve (see for instance Mendelssohn 1952). Bismuth at ordinary pressures would appear to have just too great an atomic volume to take its place in this group.

A number of runs were made under pressure with samples of bismuth of purity stated to exceed 99·999%. No signs of superconductivity could be observed (down to 2°K) at mean pressures less than 20 000 atm., but at all pressures tried between 20 000 atm. and 41 000 atm., a superconducting transition was observed at about 7°K, the value of T_c not varying by more than 0·1°K throughout the range of pressures covered. This behaviour was reversible ; that is, after relaxation of the pressure at room temperature the specimen was again non-superconducting.

It is of interest to consider this result in conjunction with the phase-equilibrium diagram for bismuth at high pressures determined by Bridgman (1935 b), in which polymorphic transitions are shown at room temperature at about 25 500 atm. and 27 000 atm. In view of the uncertainty about the distribution of pressure in our experiments, it seems reasonable to associate the onset of superconductivity with the changes to more close-packed crystalline forms of bismuth discovered by Bridgman.

Calcium and Strontium

Strontium satisfies the criteria for superconductivity arising in the theories of Fröhlich and Bardeen, and although calcium does not satisfy these criteria, both metals are exceptional in that their electrical resistance

at room temperature increases with pressure (Bridgman 1949, 1952)—a property which would be expected to favour the appearance of superconductivity at high pressure.

We have subjected samples of calcium of purity 97% and strontium of purity 99·85% to mean pressures of 44 000 and 42 000 atm. respectively, and examined them down to 2·1°K. No signs of superconductivity could be observed in either metal.

The work is to be extended to other superconductors and non-superconductors, and to higher pressures.

Acknowledgments

Acknowledgments are due to Professor H. R. Robinson, F.R.S. for the facilities provided in the Department of Physics at Queen Mary College, to the Department of Scientific and Industrial Research for a maintenance allowance to one of us and for a grant-in-aid, and to the Central Research Fund of the University of London for the loan of apparatus.

We are indebted to the Ministry of Supply and to Mining and Chemical Products Ltd., for kindly supplying samples of calcium and bismuth respectively, to Mr. W. Doy and Mr. W. A. G. Baldock of the College and Departmental workshops for the constructional work and to Mr. W. Eagers for ready assistance.

References

Alekseyevski, N. E., 1949, *J. Exp. Theor. Phys., U.S.S.R.*, **19,** 358.

Alekseyevski, N. E., and Brandt, N. B., 1952, *J. Exp. Theor. Phys., U.S.S.R.*, **22,** 200.

Bardeen, J., 1950 a, *Phys. Rev.*, **79,** 167 ; 1950 b, *Ibid.*, **80,** 567 ; 1951 a, *Ibid.*, **81,** 469 ; 1951 b, *Ibid.*, **81,** 829 ; 1951 c, *Ibid.*, **81,** 1070.

Bridgman, P. W., 1935 a, *Phys. Rev.*, **48,** 825 ; 1935 b, *Ibid.*, **48,** 896 ; 1949, *The Physics of High Pressure* (London : Bell) ; 1950, *Proc. Roy. Soc.* A, **203,** 1 ; 1952, *Proc. Amer. Acad. Arts Sci.*, **81,** 228.

Chester, P. F., 1953, *Thesis*, London.

Clement, J. R., and Quinnell, E. H., 1952, *Rev. Sci. Instrum.*, **23,** 213.

de Haas, W. J., and Voogd, J., 1930, *Leiden Comm.*, 208b.

Fröhlich, H., 1950 a, *Phys. Rev.*, **79,** 845 ; 1950 b, *Proc. Phys. Soc.* A, **63,** 778 ; 1951, *Ibid.*, **64,** 129.

Hilsch, R., 1951, *Proceedings of the International Conference on Low Temperature Physics* (Oxford), p. 119.

Kan, L. S., Sudovstov, A. L., and Lazarew, B. G., 1948, *J. Exp. Theor. Phys., U.S.S.R.*, **18,** 825 ; 1949, *Doklady*, **69,** 173.

Keesom, W. H., 1926, *Leiden Comm.*, 184b.

Lazarew, B. G., and Galkin, A. A., 1944, *J. Phys., U.S.S.R.*, **8,** 371.

Lazarew, B. G., and Kan, L. S., 1944, *J. Phys., U.S.S.R.*, **8,** 193.

Mendelssohn, K., 1952, in *Low Temperature Physics by* Simon *et al.* (London : Pergamon Press).

Shoenberg, D., 1952, *Superconductivity* (Cambridge : University Press).

Sizoo, G. J., and Onnes, H. K., 1925, *Leiden Comm.*, 180b.

CXXXV. *A Note on the Range-Scattering Method of Mass Estimation of Ionizing Particles*

By M. G. K. Menon and C. O'Ceallaigh
H. H. Wills Physical Laboratory, University of Bristol*

[Received August 4, 1953]

Summary

The applicability of the method of Menon and Rochat to the estimation of the mass of singly-ionizing particles arrested in photographic emulsion is examined and modifications necessary to take account of (*a*) dip and (*b*) the variation of scattering constant with cell-size and velocity, are discussed. The 'sliding cut-off' method of eliminating large unrepresentative signals is described in detail.

§ 1. Introduction

The range-scattering technique permits of very easy and rapid identification of particles which happen to come to rest in the emulsion. The scattering method has the additional advantage of yielding estimates of mass which are independent of variations in the degree of development of the plates.

In the method as described by Menon and Rochat (1951), the mass estimate depends on the experimental value of a statistical parameter P, which is a logarithmic function of the mass. P is defined as

$$P=1{\cdot}37 \log R+2{\cdot}37 \log \hat{\alpha}, \quad . \quad . \quad . \quad . \quad . \quad (1)$$

when R is the residual range, in microns of the particle, and $\hat{\alpha}$ is the experimental value of the mean absolute angle of scattering per 100 microns, measured along the faster half of the trajectory. For Ilford G5 emulsions, the calibration measurements of Menon and Rochat using identified particles, yield the following expression.

$$P=7{\cdot}243-\log \mu, \quad . \quad . \quad . \quad . \quad . \quad . \quad . \quad (2)$$

where μ is the mass of the particle expressed in mev.

This method has been used to estimate the masses of particles K1 and K2 (O'Ceallaigh 1951) and has been employed in subsequent work on charged heavy mesons (Crussard *et al.* 1952, Menon and O'Ceallaigh 1953, Friedlander, Harris and Menon 1953).

Certain simplifying assumptions are made in using the parameter P to estimate mass. For instance, it can be shown that P depends on $K^{2{\cdot}37}$, where K is the scattering constant, but in the method as it exists, the variation of K with cell size and velocity has been neglected. These are

* Communicated by Professor C. F. Powell, F.R.S.

without significant influence in the application for which the method was originally conceived, but must be avoided in critical work such as mass estimates of particles of unknown mass, particularly when such measurements are carried out on long lengths of track. The method of taking into account such variations of the scattering constant, and a few modifications in the experimental procedure are considered in the following sections.

§ 2. Effect of the Variation of the Scattering Constant on P

Following Gottstein *et al.* (1951), we may write for singly-charged particles

$$\langle \Phi \rangle_s = \frac{K_{(B,s)} s^{1/2}}{pv} = \frac{K_{(B,s)} B s^{1/2}}{\mu(B^2-1)}, \quad \ldots\ldots (3)$$

where $\langle \Phi \rangle_s$ is mean absolute angle of scattering measured in cell-size s, s being expressed in units of $100\,\mu$, p, v=momentum and velocity, $B=(1-\beta^2)^{-1/2}$, μ=mass of the particle in Mev and $K_{(B,s)}$, expressed in (degrees$\times$Mev)/$(100\,\mu)^{1/2}$, is the value of the scattering constant appropriate to B and s. We have, by definition

$$\hat{\alpha}_{100\mu} = \frac{1}{B_1 - B_2} \int_{B_2}^{B_1} \langle \Phi \rangle_s s^{-1/2}\, dB, \quad \ldots\ldots (4)$$

where B_1 and B_2 are the values of B corresponding to residual ranges R and $R/2$ respectively. Hence

$$\hat{\alpha}_{100\mu} = \frac{1}{\mu(B_1 - B_2)} \int_{B_2}^{B_1} \frac{K_{(B,s)} B\, dB}{(B^2-1)}. \quad \ldots\ldots (5)$$

Since $K_{(B,s)}$ is not strongly dependent on B, it will be sufficient to regard it as constant and equal to $\overline{K}_{(B,s)}$ the value corresponding to $3R/4$.

Integrating and neglecting powers of (B_1-B_2) greater than the first, we have with sufficient approximation

$$\hat{\alpha}_{100\mu} = \frac{\overline{K}_{(B,s)}}{2\mu(B_1-B_2)} \ln\left[\frac{B_1-1}{B_2-1}\right] + \frac{\overline{K}_{(B,s)}}{4\mu}. \quad \ldots\ldots (6)$$

We assume as valid for all singly charged particles, the range-velocity relation

$$(B-1) = 1{\cdot}3975 \times 10^{-2} (R/\mu)^{0{\cdot}578}. \quad \ldots\ldots (7)$$

Substituting (7) in (6) and rearranging we have

$$\mu^{0{\cdot}422} = 43{\cdot}4 \overline{K}_{(B,s)} R^{-0{\cdot}578} \Big/ \left(\hat{\alpha}_{100\mu} - \frac{\overline{K}_{(B,s)}}{4\mu}\right). \quad \ldots (8)$$

If now we set $\overline{K}_{(B,s)} \equiv K$, regarding it as a constant and independent of B and s, and also neglect the small corrective term $\overline{K}_{(B,s)}/4\mu$ which is equivalent to setting

$$\frac{B_1+1}{B_2+1} \sim 1,$$

we have

$$\mu^{0{\cdot}422} = 43{\cdot}4 K R^{-0{\cdot}578} / \hat{\alpha}_{100\mu}, \quad \ldots\ldots (9)$$

which reduces to

$$\log \mu = 2{\cdot}37 \log (43{\cdot}4\, K) - 1{\cdot}37 \log R - 2{\cdot}37 \log \hat{\alpha}. \quad \ldots (10)$$

Introducing the definition of P given in eqn. (1) we obtain

$$P=2{\cdot}37\log(43{\cdot}4K)-\log\mu. \quad . \quad . \quad . \quad . \quad . \quad . \quad (11)$$

Substituting $K=26{\cdot}2$ (degrees$\times$Mev)/$(100\,\mu)^{1/2}$ in (11) we obtain (2) which is Menon and Rochat's expression.

Recently, extensive calculations of stopping power for Ilford C2 nuclear research emulsions have been presented by Vigneron and Bogaardt (1951) and Vigneron (1953). We find that the results of Vigneron (1953) may be very well fitted by the range-velocity relationship

$$B-1=1{\cdot}460\times10^{-2}(R/\mu)^{0{\cdot}568} \quad . \quad . \quad . \quad . \quad . \quad (12)$$

for $1{\cdot}01\leqslant B\leqslant1{\cdot}16$. This would correspond to a modified value of (11)

$$P=2{\cdot}32\log(41{\cdot}4K)-\log\mu. \quad . \quad . \quad . \quad . \quad . \quad (11\,b)$$

These results are in good agreement with those of experiment over the limited region hitherto examined ($B\leqslant1{\cdot}043$), but there is a need for further experiments with faster particles.

To deal with the case of G5 emulsions, and to allow for variation in moisture content of the emulsion, it would seem sufficient to modify the value of the constant in (12) choosing always the value 0·568 for the exponent.

It is thus clear that the value of P depends on $K^{2{\cdot}37}$, and accurate estimates of mass require exact knowledge of the value of K. Furthermore, its variation with s and B cannot be neglected.

A theory of the variation of K with s and B has been given by Molière (1947, 1948, 1951), and is discussed at length by Gottstein *et al.* (1951), to which reference may be made.

It is shown there that the value of $K_{(B,\,s)}$ is determined by a parameter Ω_b, where Ω_b/s is dependent only on the velocity of the particle. Figure 2 of Gottstein *et al.* gives Ω_b/s as a function of β^2, and fig. 1 of the same paper gives $K_{(B,\,s)}$ as a function of Ω_b. The value $K=26{\cdot}2$ is based on Menon and Rochat's (1951) calibration point marked 5 in this figure, and corresponds to a value $\Omega_b\sim500$, and thus to protons of residual range about 1 mm. Various calibration measurements that have been carried out in different laboratories suggest that the theoretical slope (e.g. shown in fig. 1 of Gottstein *et al.* 1951) may be taken with reasonable confidence as representing the variation of $K_{(B,\,s)}$ with Ω_b.

The method of calculating the value of μ from (7) is therefore as follows. An approximate value of μ is obtained from (1). This enables us to determine $(B-1)$ and hence, β^2 corresponding to $3R/4$, by use of (7). The value of Ω_b/s is then found from fig. 2 of Gottstein *et al.* From fig. 1, we may obtain the appropriate $K_{(B,\,s)}$ for the value of Ω_b/s used in making the experimental estimate of $\hat{\alpha}_{100\mu}$. The value of the small corrective term $\overline{K}_{(B,\,s)}/4\mu$ can be found from the approximate mass choosing $\overline{K}_{(B,\,s)}=26$. A corrected value of μ can then be obtained by substitution of these values in (7). Usually it will not be necessary to repeat this procedure.

The effect of neglecting the variation of $K_{(B,\,s)}$ may be quite serious, and for particles of mass $\sim1000\,m_e$, on long lengths of track, may possibly

be greater than the statistical uncertainties associated with the experimental determination of $\hat{\alpha}_{100\mu}$.

§ 3. Signal/Noise Ratio and Noise Elimination

In the application of the method by Menon and Rochat, the cell-size s was chosen so that the ratio, signal/noise$=\rho$, was at least 4. This requirement is probably over stringent, since with good instruments and experienced observers, the noise level tends to remain very constant. The optimum value of ρ can be shown to be $\sim 2{\cdot}6$. Thus a value of $\rho \sim 2$ may well be used and the noise level determined for the conditions of the experiment. This may readily be done using the method of cross products suggested by Molière (1951) the experimental application of which is described by Menon *et al.* (1951) Appendix I. Small accidental variations in noise level will still be without significant effect on the accuracy of the results. We may set up an equation for the minimum cell size s such that $\rho \geqslant \epsilon$, ϵ being any value fixed in advance. The solution is

$$\log s = \tfrac{2}{3}[0{\cdot}578 \log R + \log \{g\sqrt{(\rho^2-1)}\} - P/2{\cdot}37] \quad . \quad . \quad (13)$$

where g=constant and $\sim 0{\cdot}15$ micron for good instruments, skilled observers, and well lined up tracks.

A plot of s on log-log paper will be linear, and may be used to find the desired value of s for selected ρ. The effect of changes in P on the choice of s is not great, and we may well use the same value of s for all particles.

§ 4. Corrections for 'Dip'

It is necessary to allow for the effect of 'dip' on the measured values of R and $\hat{\alpha}$. We require the value of these parameters in the unprocessed emulsion. Distinguishing these by the subscript u we have

$$\left.\begin{aligned} R_u &= R \sec \theta_u, \\ \hat{\alpha}_u &= \hat{\alpha} \sec^{-3/2} \theta_u. \end{aligned}\right\} \quad . \quad . \quad . \quad . \quad . \quad . \quad . \quad (14)$$

R and $\hat{\alpha}$ are the experimental values and are referred to the plane of the glass (x, y), the optic axis coinciding with the z axis. R_u and θ_u are the values referred to a plane containing the mean trajectory of the particle, the normal to which makes an angle θ_u with the z axis. We assume that the effect of processing is a uniform linear translation in the direction of z and hence that $\tan \theta_u = S \tan \theta$ where S is the shrinkage factor.

§ 5. Elimination of Large Angles

It is found occasionally in multiple scattering measurements, that large unrepresentation values of second difference occur which would have little effect on the value of the mean if the sample were of sufficient size. They can, however, lead to unreliable estimates of the scattering parameter, when they occur in a small sample of second differences, obtained from a limited length of track. It is customary therefore, to employ a 'cut-off'

procedure, to eliminate these large values of second difference. In the case of high energy particles, where the loss of energy along the track is negligible, it has been found convenient to employ what is known as a '$4\bar{D}$ cut-off' i.e. an angle is 'cut-off' if it is greater than four times the mean of the second differences obtained without including it.

In the Menon–Rochat method, this procedure is not permissible, since measurements are made on a section of track along which the energy of the particle, and hence the multiple scattering, is changing rapidly. In these circumstances, it is necessary to apply a 'sliding cut-off procedure' i.e., an angle α_i is 'cut-off' if it is greater than $c_i\hat{\alpha}_{c0}$ where $\hat{\alpha}_{c0}$ is the mean angle obtained after excluding α_i. c_i takes a sliding value, increasing continuously as one proceeds from R to $R/2$ and has a value c_{eff} at the range $R_{\text{eff}}=0{\cdot}72\,R$, to which corresponds the measured mean angle of multiple scattering $\hat{\alpha}$ (Menon and Rochat 1951). R is the true total range. Figure 1 of the present paper shows c_i plotted as a function of range

Fig. 1

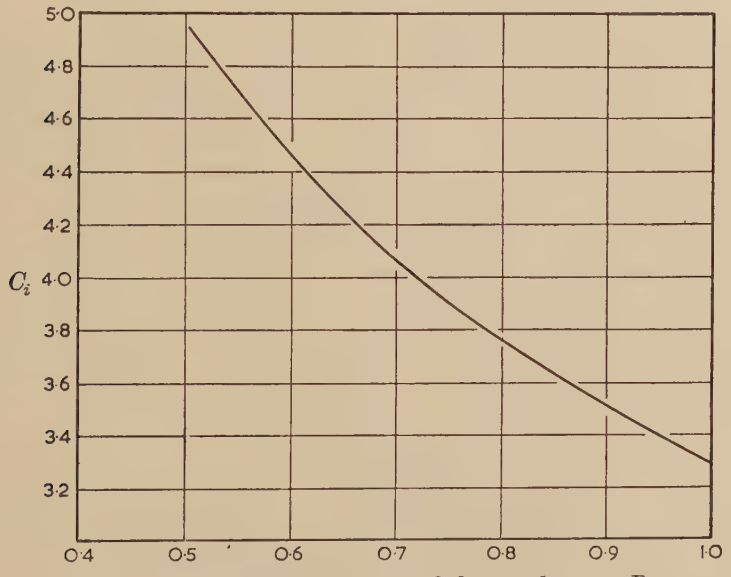

R_i expressed as a fraction of the total range R.

for a '$4\bar{D}$ sliding cut-off'. In this case $c_{\text{eff}}=4$ and c_i has a value 3·3 at R and 4·95 at $R/2$ and varies continuously in between. The calculation involved is based only on the energy loss by the particle along its trajectory.

The application of the cut-off procedure is comparatively simple. The range R_i at which the suspect value α_i occurs is determined; R_i may be expressed as a fraction of the total range R. The value of c_i corresponding to R_i is read off from the graph in fig. 1. α_i can then be excluded if it exceeds $c_i\hat{\alpha}_{c0}$ where $\hat{\alpha}_{c0}$ has been obtained without the inclusion of α_i.

It is clear, however, that the exclusion of an angle at a range near R would affect the mean to a lesser extent than the exclusion of an angle near

$R/2$. This difficulty can be partly overcome by a substitution procedure. After an angle α_i has been excluded, it is replaced by a value $\alpha_{i(\text{exp})}$, the angle to be expected at a range R_i when the determined mean angle along the track is $\hat{\alpha}_{c0}$. A new mean value $\hat{\alpha}$ may then be obtained after inclusion of this value $\alpha_{i(\text{exp})}$. In marginal cases, it is advisable to verify that the excluded α_i is greater than $c_i\hat{\alpha}$, where $\hat{\alpha}$ is the mean value finally obtained.

The suitability of $3{\cdot}5\overline{D}$, $4\overline{D}$, $4{\cdot}5\overline{D}$ and $5\overline{D}$ sliding cut-offs, corresponding to $c_{\text{off}}=3{\cdot}5$, 4, $4{\cdot}5$, 5 respectively, are being tested in the calibration measurements of Friedlander *et al.* (1953).

§ 6. Conclusions

The variation of $\overline{K}_{(B,\,s)}$ is probably well described by curves of the type given in fig. 1 of Gottstein *et al.* The method described in this note is thus probably adequate to allow for the variations of $K_{(B,\,s)}$ with Ω_b. Some doubt still exists, however, as to the precise value of the scattering constant for a given value of Ω_b. This uncertainty may lead to serious errors in absolute mass determinations.

In the calibration measurements of Menon and Rochat (1951) (point marked (5) in fig. 1 of Gottstein *et al.*) only large angles which definitely appeared to be individual ' single scatters ' were eliminated ; the procedure may thus be described as a $\sim 8\overline{D}$ cut-off. The position of point (5) is in better agreement with curve (*a*) which gives the theoretical values of the scattering constant for a ' no cut-off procedure '.

In the determinations of the mass of heavy charged mesons by Menon and O'Ceallaigh (1953), values of the scattering constant given by curve (*a*) of fig. 1 have been employed. We may remark that the estimates quoted may require revision on completion of the calibration measurements of Friedlander *et al.* (1953), which will give absolute values of the scattering constant for appropriate cut-off procedures.

References

Crussard, J., Morellet, D., Trembley, J., and Orkin-Lecourtois, A., 1952, *C. R. Acad. Sci., Paris*, **234**, 84.

Friedlander, M. W., Harris, G. G., and Menon, M. G. K., 1953, *Proc. Roy. Soc.* (in course of publication).

Friedlander, M. W., Harris, G. G., Menon, M. G. K., and O'Ceallaigh, C., 1953 (work in progress).

Gottstein, K., Menon, M. G. K., Mulvey, J. H., O'Ceallaigh, C., and Rochat, O., 1951, *Phil. Mag.*, **42**, 708.

Menon, M. G. K., O'Ceallaigh, C., and Rochat, O., 1951, *Phil. Mag.*, **42**, 932.

Menon, M. G. K., and O'Ceallaigh, C., 1953, *Proc. Roy. Soc.* (in course of publication).

Menon, M. G. K., and Rochat, O., 1951, *Phil. Mag.*, **42**, 1232.

Molière, G., 1947, *Zeit. f. Naturforschung*, 2A, 133 ; 1948, *Ibid.*, 3A, 78 ; 1951, unpublished.

O'Ceallaigh, C., 1951, *Phil. Mag.*, **42**, 1032.

Vigneron, L., 1953, *J. de Phys. et Rad.*, **14**, 145.

Vigneron, L., and Bogaardt, M., 1951, *C.R. Acad. Sci., Paris*, **233**, 941.

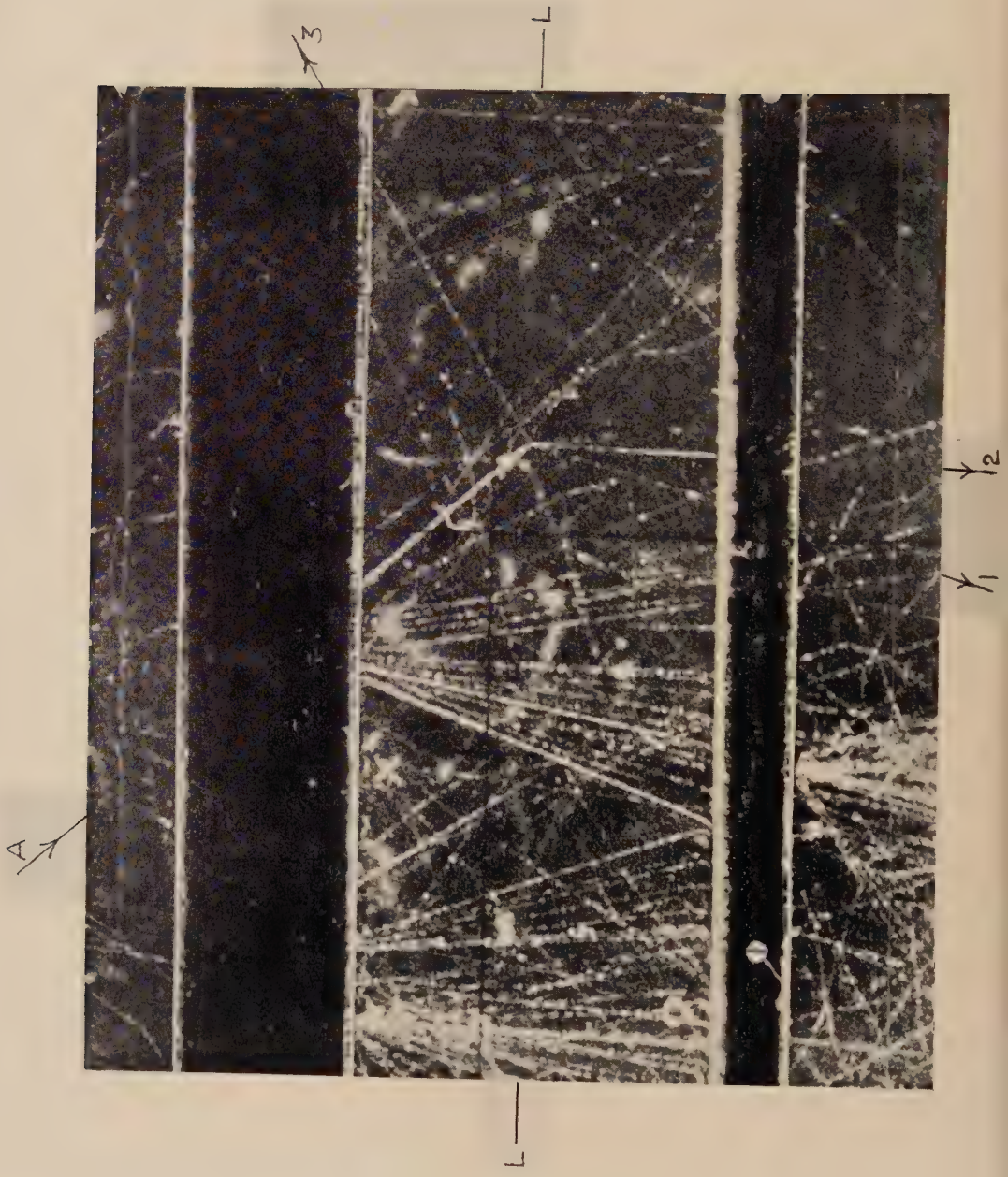
3
L
2
1
A
L

CXXXVI. *The Decay-in-Flight of a Heavily-Ionizing τ-Meson*

By D. B. GaythER
The Physical Laboratories, The University, Manchester*

[Received August 29, 1953]

Abstract

A τ-meson has been observed to decay in the gas of a cloud chamber operated without a magnetic field. The τ-meson was apparently created directly in an energetic nuclear interaction. Its energy at creation was about 100 Mev, and it lived for a proper time of $(7{\cdot}8 \pm 1{\cdot}0) \times 10^{-10}$ sec in the illuminated volume of the chamber.

Since the discovery of the τ-meson by Brown *et. al.* in 1949, several groups using photographic emulsions have established that this unstable particle decays into three charged particles which are probably π-mesons. The Q-value, or energy release, lies in the range (70–75) Mev and the mass of the τ-meson is about 975 m_e (assuming the mass of the charged π-meson to be 276 m_e). These results have been obtained from measurements on a small number of decays at rest. Four examples, however, of the decay of a τ-meson-in-flight have been reported (Leighton and Wanlass 1952, Annis and Harmon 1952, Van Lint and Trilling 1953). In each case the τ-meson decayed in the gas of a Wilson cloud chamber. The ionizations of these τ-mesons were indistinguishable from the minimum value. Recently, in an experiment on the Pic-du-Midi (2867 m), an event in the gas of a Wilson cloud chamber has been observed which is interpreted as the decay-in-flight of a heavily ionizing τ-meson.

The cloud chamber has an illuminated volume of $40 \times 30 \times 20$ cm and contains two lead plates ; the upper plate is 4 cm thick and the lower plate 1·5 cm thick. There is no heavy material above the chamber. An arrangement of enriched BF_3 proportional counters (see Barker *et. al.* 1952) is used to expand the chamber ; it selects nuclear interactions produced in the upper lead plate. No magnetic field is used. The lower lead plate is used to examine the penetrating power of the shower particles.

The event in the gas is shown in the plate (Plate 51) at level L. The heavily ionizing track A produces tracks 1, 2 and 3. Track A is copunctal, within errors of measurement, with the origin of the large interaction in the upper plate. Therefore, particle A must have been produced in this interaction and to have subsequently interacted or decayed in the gas at level L. No visible recoil track is produced and it therefore seems rather unlikely that particle A interacted with a gas nucleus. It is interesting to consider, therefore, whether the event could have been a decay process.

---

* Communicated by Professor P. M. S. Blackett, F.R.S.

The only known unstable particle which decays into three charged secondary particles is the τ-meson.

The secondary tracks, 1, 2 and 3, could all have been produced by π-mesons. For example, track 1 has an estimated ionization of less than twice the minimum value but the particle failed to penetrate 1·6 cm. of lead, thus its mass was less than 400 m_e. The measured angles between the various tracks and the estimated ionizations are given in rows (2), (3) and (4) of the table. ϕ is the angle between track A and a given track ; the error in each ϕ is about 1·5°. The angles between the projections of the secondaries on to the plane perpendicular to the line of flight of A are denoted by θ_{12} etc.

Summary of Data on the τ-Meson Decay

(1)	Track number	A	1	2	3
(2)	ϕ (deg.)	—	127·5	137	91·5
(3)	θ (deg.)	—	$\theta_{12}=32$	$\theta_{23}=158$	$\theta_{31}=170$
(4)	Estimated ionization ($\times$ minimum)	>8	<2	3–5	<2
(5)	Calculated ionization ($\times$ minimum)	12·5	2·1	4·6	1·8
(6)	Estimated momentum range (Mev/c)	100–131	98–127	53–68	110–142
(7)	Calculated momentum (Mev/c)	108 ± 13	105 ± 15	57 ± 10	118 ± 18

Using the data in the table, the mass of particle A can be estimated in the following manner, assuming it to be a τ-meson and the three secondary particles to be π-mesons. Particle 1 stopped in 1·6 cm of lead and therefore had a momentum of less than 127 Mev/c. Assuming conservation of momentum at the decay and using the upper limit for the momentum of particle 1, upper limits for the momenta of particles A, 2 and 3, can be obtained and are given in row (6) of the table. Track 3 is long and well illuminated and has an estimated ionization of less than twice the minimum value ; its momentum is therefore greater than 110 Mev/c. Thus lower limits for the momenta of the other three particles can be obtained ; these values are also given in row (6) of the table. By using the momentum ranges for all the particles in the relativistic form of the conservation of energy equation, it is found that the mass of the unstable particle lies within the range (960–1020) m_e. It is thus consistent with the known mass of the τ-meson. The errors in each of the mass limits due to angle measurements are unlikely to be greater than about 15 m_e.

If it is now assumed that particle A was a τ-meson of mass 975 m_e, then the momenta of the secondary particles and of particle A can be calculated. The values are given in row (7) of the table and the corresponding calculated ionizations are in row (5). The agreement between the visual ionization estimates and the calculated values is very good, and it may be concluded that the event in the gas was produced by a τ-meson.

The origin of the interaction with which the τ-meson is associated has been determined to within (1–2) mm by tracing back the tracks of several of the penetrating shower particles. The line-of-flight of the τ-meson is copunctal with this origin. The path length of the τ-meson in the lead plate was $(2{\cdot}5\pm0{\cdot}2)$ cm and its energy at creation was (107 ± 7) MEV. It appears, therefore, that the τ-meson was produced directly in the high energy interaction and is probably not the secondary of a short-lived particle. This confirms the conclusion of Ceccarelli *et. al.* (1952) who observed a τ-meson in a photographic emulsion which emerged directly from a star. The interaction in which the slow τ-meson was produced contained 10–15 penetrating particles most of which were probably mesons, thus the total energy of the interaction was probably greater than 20 BEV.

The τ-meson lived for $(7{\cdot}8\pm1{\cdot}0)\times10^{-10}$ sec in the illuminated volume of the chamber and is the longest lived yet reported. The potential traversal time, or the time the τ-meson would have taken to traverse the space between the lead plates if it had not decayed, is $(1{\cdot}6\pm0{\cdot}2)\times10^{-9}$ sec. These times have been measured from fiducial surfaces drawn just below the upper plate and just above the lower plate in the manner suggested by Wilson and Butler (1952). No direct estimate of the lifetime of the τ-meson has yet been made but Herz (1953) has found a lower limit of 10^{-9} sec, based on observations of three decays at rest in photographic emulsions.

REFERENCES

ANNIS, M., and HARMON, N. F., 1952, *Phys. Rev.*, **88,** 1202.
BARKER, K. H., SARD, R. D., and SOWERBY, M. G., 1952, *Phil. Mag.*, **44,** 46.
BROWN, R. H., CAMERINI, U., FOWLER, P. H., MUIRHEAD, H., POWELL, C. F., and RITSON, D. M., 1949, *Nature, Lond.*, **163,** 82.
CECCARELLI, M., DALLAPORTA, N., MERLIN, M., and ROSTAGNI, A., 1952, *Nature, Lond.*, **170,** 454.
HERZ, A. J., HODGSON, P. E., and TENNENT, R. M., 1953, *Phil. Mag.*, **44,** 85.
LEIGHTON, R. B., and WANLASS, S. D., 1952, *Phys. Rev.*, **86,** 426.
VAN LINT, V. A. J., and TRILLING, G. H., 1953, *Phys. Rev.*, in the press.
WILSON, J. G., and BUTLER, C. C., 1952, *Phil. Mag.*, **43,** 993.

CXXXVII. CORRESPONDENCE

Note on a Paper by K. H. Tzou

By J. B. Hughes
Department of Mathematics, University College of North Wales, Bangor*

[Received July 28, 1953]

In a paper on the "Relativistic Hamiltonian System of a Particle and Relativistic Heisenberg's Equation", Tzou (1948) introduces the more symmetrical relativistic form of the Hamiltonian equations

$$\frac{dx^\mu}{d\tau}=\frac{\partial \mathscr{H}}{\partial \pi_\mu},\quad \frac{d\pi_\mu}{d\tau}=-\frac{\partial \mathscr{H}}{\partial x^\mu} \qquad (\mu=1,\ 2,\ 3,\ 4) \quad . \quad . \quad . \quad (1)$$

and also the relativistic modification of Heisenberg's equation†

$$\frac{dQ}{d\tau}=[Q,\mathscr{H}] \quad . \quad . \quad . \quad . \quad . \quad . \quad . \quad . \quad . \quad (2)$$

where $Q=Q\,(x^\mu,\pi_\mu)$.

In § 4 of Tzou's paper the motion of a free electron is discussed (along similar lines to those of Dirac (1947 a)) and it is stated that the results have some deviation from those obtained by Dirac (1947 a) using the non-relativistic Heisenberg equation. The results, however, are equivalent as will be shown in this note.

For a free electron $\mathscr{H}$ has the operational form

$$\mathscr{H}=-c\sqrt{(-\pi_\mu\pi_\mu)} \quad . \quad . \quad . \quad . \quad . \quad . \quad . \quad . \quad (3a)$$

and the constant value $$\mathscr{H}=-m_0c^2. \quad . \quad . \quad . \quad . \quad . \quad . \quad . \quad . \quad (3b)$$

This gives us the wave equation

$$\mathscr{H}\psi=-c\sqrt{(-\pi_\mu\pi_\mu)}\,\psi=-m_0c^2\psi. \quad . \quad . \quad . \quad . \quad . \quad (4)$$

If we write $$\mathscr{H}=-ic\,\beta^\mu\pi_\mu \quad . \quad . \quad . \quad . \quad . \quad . \quad . \quad (5)$$

eqn. (4) becomes $$(i\beta^\mu\pi_\mu-m_0c)\psi=0 \quad . \quad . \quad . \quad . \quad . \quad . \quad . \quad (6)$$

where the β^μ are operators satisfying

$$\beta^\mu\,\beta^\nu+\beta^\nu\,\beta^\mu=2\delta^{\mu\nu}. \quad . \quad . \quad . \quad . \quad . \quad . \quad . \quad (7)$$

Then $$\frac{dx^\mu}{d\tau}=[x^\mu,\mathscr{H}]=-ic\,\beta^\mu. \quad . \quad . \quad . \quad . \quad . \quad . \quad (8)$$

Therefore we see that β^μ is the 4-vector (or world) velocity operator corresponding to the μ-component of world velocity. Tzou, however, does not treat the time component of this vector, β^4, as an operator, but as a scalar; and it is on account of this that the apparent deviation of his results from Dirac's results appears.

---

* Communicated by R. A. Newing.

† Tzou (1948) writes this $dQ/d\tau=[\mathscr{H}\,,\,Q]$, and uses γ_μ in place of π_μ for the 4-vector momentum.

Equation (6) is the same as Tzou's eqn. (18) and therefore leads to Tzou's eqn. (31) for the world-velocity of the free electron

$$\frac{dx^\mu}{d\tau}=-c^2\pi_\mu\mathscr{H}^{-1}+\frac{\hbar c}{2}\left(\frac{d\beta^\mu}{d\tau}\right)_0\exp\left(-\frac{2i}{\hbar}\mathscr{H}\tau\right)\mathscr{H}^{-1}. \quad . \quad . \quad (9)$$

Tzou now compares this result with Dirac's result [which is for dx^j/dt $(j=1,\ 2,\ 3)$], by assuming the classical relativistic relation $dt/d\tau=[1-(v^2/c^2)]^{-1/2}$ which enables one to write eqn. (8) as

$$\left(1-\frac{v^2}{c^2}\right)^{-1/2}\frac{dx^\mu}{dt}=-ic\beta^\mu$$

and with $\mu=4$,

$$\beta^4=-\left(1-\frac{v^2}{c^2}\right)^{-1/2}.$$

This makes β^4 a scalar, instead of an operator. It is clearly wrong, for β^4, then, does not satisfy the necessary condition $(\beta^4)^2=1$.

The relation between dt and $d\tau$, appropriate to this problem, is obtained from eqn. (9) with $\mu=4$ $(x^4=ict)$

$$ic\frac{dt}{d\tau}=-c^2\pi_4\mathscr{H}^{-1}+\frac{\hbar c}{2}\left(\frac{d\beta^4}{d\tau}\right)_0\exp\left(-2i\frac{\mathscr{H}}{\hbar}\tau\right)\mathscr{H}^{-1}. \quad . \quad (10)$$

By treating β^4 as an operator we can reproduce Dirac's result starting from eqn. (6).

Multiplying eqn. (6) by $-\beta^4$ gives

$$(-i\beta^4\beta^\mu\pi_\mu+\beta^4m_0c)\psi=0$$

or

$$(i\beta^j\beta^4\pi_j+p_4+\beta^4m_0c)\psi=0 \quad (j=1,\ 2,\ 3) \quad . \quad . \quad . \quad . \quad (11)$$

since*

$$\pi_\mu=(p_1,\ p_2,\ p_3,\ ip_4).$$

If we write

$$\alpha^j=i\beta^j\beta^4, \qquad \rho^3=\beta^4$$

eqn. (11) is the same as Dirac's wave-equation for the free electron (Dirac 1947 b)

$$(\alpha^jp_j+p_4+\rho^3m_0c)\psi=0 \quad (j=1,\ 2,\ 3)$$

(clearly the α^j's and ρ^3 satisfy the necessary commutation relations).

Put $\mu=4$ in eqn. (8)

$$ic\frac{dt}{d\tau}=-ic\beta^4$$

$$\beta^4=-dt/d\tau$$

and, remembering that $(\beta^4)^2=1$, we get

$$\frac{d}{dt}=\left(\frac{dt}{d\tau}\right)^{-1}\frac{d}{d\tau}=-\beta^4\frac{d}{d\tau} \quad . \quad . \quad . \quad . \quad . \quad . \quad . \quad (12)$$

and

$$\frac{dx^j}{dt}=-\beta^4\frac{dx^j}{d\tau}=ic\,\beta^4\beta^j$$

$$=-c\alpha^j \quad . \quad . \quad . \quad . \quad . \quad . \quad . \quad . \quad . \quad (13)$$

which agrees with Dirac's result and shows that $\boldsymbol{\alpha}=(\alpha^1,\ \alpha^2,\ \alpha^3)$ is the 3-vector (or space) velocity operator.

---

* In Tzou's notation this would be $\pi_\mu=(p_1,\ p_2,\ p_3,\ p_4)$.

By eqn. (12)

$$i\hbar\frac{d\alpha^j}{dt}=-i\hbar\beta^4\frac{d\alpha^j}{d\tau}=-i\hbar\beta^4 i\left(\frac{d\beta^j}{d\tau}\beta^4+\beta^j\frac{d\beta^4}{d\tau}\right). \quad . \quad . \quad . \quad (14)$$

Since

$$i\hbar\frac{d\beta}{d\tau}=\beta^\mu\mathscr{H}-\mathscr{H}\beta^\mu$$

and

$$\beta^\mu\mathscr{H}+\mathscr{H}\beta^\mu=-2ic\,\pi_\mu$$

then

$$\frac{i\hbar}{2}\frac{d\alpha^j}{dt}=c\pi_j-\alpha^j ic\pi_4$$

$$=c\pi_j+\alpha^j H \quad . \quad . \quad . \quad . \quad . \quad . \quad . \quad . \quad . \quad (15)$$

for $\pi_4=ip_4=iH/c$, where H is Dirac's relativistic Hamiltonian.

Now π_μ commutes with $\mathscr{H}$ so $d\pi_\mu/d\tau=0$ and we get

$$\left.\begin{aligned}\frac{d\pi_j}{dt}&=-\beta^4\frac{d\pi_j}{d\tau}=0,\\ \frac{dH}{dt}&=\frac{c}{i}\frac{d}{dt}\pi_4=ic\beta^4\frac{d\pi_4}{d\tau}=0,\end{aligned}\right\} \quad . \quad . \quad . \quad . \quad (16)$$

so that by differentiating eqn. (15) with respect to t

$$\frac{i\hbar}{2}\frac{d^2\alpha^j}{dt^2}=\frac{d\alpha^j}{dt}H \quad . \quad . \quad . \quad . \quad . \quad . \quad . \quad . \quad (17)$$

which is Dirac's differential eqn. for α^j.

Equations (13) and (17) together reproduce Dirac's results, thus showing that these results are not changed by using the relativistic Heisenberg equations.

References

Dirac, P. A. M., 1947 a, *Quantum Mechanics*, 3rd edition (Oxford), § 69; 1947 b, *Ibid.*, § 67.

Tzou, K. H., 1948, *Phil. Mag.*, **39**, 790.

Angular Distributions of Gamma Rays from ^{19}F (p, $\alpha\gamma$) ^{16}O

By J. E. Sanders*

Cavendish Laboratory, Cambridge†

[Received August 31, 1953]

Measurements of the angular distributions of the 6·14 mev (γ_1) and the combined 6·91 and 7·11 mev ($\gamma_2+\gamma_3$) radiations at the 874 kev resonance of the reaction ^{19}F (p, $\alpha\gamma$) ^{16}O have already been reported (Sanders 1952). Separation of the γ_1 from the ($\gamma_2+\gamma_3$) radiation was achieved by using a deuterium-filled gridded ion chamber as the gamma ray detector and analysing the photoproton pulses on a multi-channel kicksorter.

* Communicated by the Author.

† Now at A.E.R.E., Harwell.

Observations of the intensities of the γ_1 and $(\gamma_2+\gamma_3)$ radiations were made at various angles θ between the incident proton beam and the direction of emission of the radiation.

Similar observations have now been made at the resonances at 935 and 1381 kev. CaF_2 targets of between 10 and 20 kev thickness were bombarded by the proton beam of the Cavendish electrostatic generator. If the results are fitted to expressions of the form $I(\theta)=1+a\cos^2\theta$, the values found for the coefficient a are those shown in the accompanying table.

Resonance	$a(\gamma_1)$	$a(\gamma_2+\gamma_3)$
935 kev	$0{\cdot}00\pm0{\cdot}05$	$0{\cdot}0\ \pm0{\cdot}1$
1381 kev	$-0{\cdot}14\pm0{\cdot}03$	$0{\cdot}58\pm0{\cdot}13$

The results at 935 kev are in agreement with the isotropic angular distribution of the total gamma radiation at this resonance (Day *et al.* 1950) and with the assignment 1^+ to the compound state of ^{20}Ne involved (Seed and French 1952).

Combining the distributions at the 1381 kev resonance using the intensity ratio $\gamma_1/(\gamma_2+\gamma_3)$ at $\theta=90°$ of 8·7 found in the present work, the angular distribution of the total radiation will be $I(\theta)=1-0{\cdot}06\cos^2\theta$, in good agreement with the measurements of Day *et al.* On the basis of the near-isotropy of the total radiation, it has been suggested (Chao 1950) that the compound state of ^{20}Ne involved is a 1^+ state. The anisotropy of the component radiations revealed by the measurements described here makes this assignment unlikely, while a 2^- state would be consistent with the observed distributions.

References

Chao, C. Y., 1950, *Phys. Rev.*, **80,** 1035.
Day, R. B., Chao, C. Y., Fowler, W. A., and Perry, J. E., 1950, *Phys. Rev.*, **80,** 131.
Sanders, J. E., 1952, *Phil. Mag.*, **43,** 630.
Seed, J., and French, A. P., 1952, *Phys. Rev.*, **88,** 1007.

The Velocities of Fundamental Particles

By L. L. Whyte

Difficulties in the theory of particles may be connected with the role of time (Heisenberg 1951, Whyte 1952). The application to the various particles of the concept of velocity should therefore be re-examined.

The presence of a linear velocity is a necessary inference only where two events have been observed which are localized and distinct both in space and in time : the departure and arrival of an entity which may be one

particle or the head of a pulse. This condition is not met in any of the experiments which purport to determine the velocities of particles lighter than nucleons.

For example, all the ' determinations of electron velocity ' (Thomson, Wiechert, Kirchner, Perry and Chaffee, Dunnington, etc.) used stationary conditions, i.e. continuous electron beams and static or periodic deflecting fields, and did not isolate two distinct events. Such experiments cannot discriminate between *oscillation or vibration periods* of an extended system and *transit times* of localized entities. The space and time coordinates of the departure and arrival of a particle and the presence of a transit time cannot be inferred from observations using static or periodic fields for they provide too little information, a fact inadequately recognized in the quantum-mechanical discussions. Moreover no electronic apparatus now in use provides compelling evidence for transit times varying with the voltage, for none meets the above condition.

The only type of experiment which can justify the concept of electron velocity is one replacing static or periodic fields by *separate signals, localized both in space and in time, of the departure and the arrival of a particle* or of the head of a pulse. Such signals can be provided by the use of mechanical rotors, deflectors charged at successive moments by a single pulse, pairs of counters recording single particle lags, or similar arrangements. It may now be possible to apply such methods to electrons, positrons, and mesons, and it is of importance that this should be done.

Experiments meeting the above condition have been carried out with neutrons and atomic or molecular beams, for example by using inertial motion in a rotating system, and the velocity concept confirmed. But this proves nothing regarding lighter particles, whose properties are in several respects different.

Recent publications on Geiger counters have employed the phrases: " transit time of an electron " (Stevenson 1952), " over most of its path an electron is moving at nearly constant velocity " (Ramsey 1952), though referring to overall time lags (relaxation times) of processes involving many electron paths and collisions. This looseness of expression obscures the fact that no measurements have yet been made which must be interpreted as transit times of electrons.

I wish to thank Dr. D. Gabor for helpful discussions.

References

Heisenberg, W., 1951, Paper in *Göttingen Festschrift.*
Ramsey, W. E., 1952, *Rev. Sci. Instrum.*, **23**, 95.
Stevenson, A., 1952, *Rev. Sci. Instrum.*, **23**, 93.
Whyte, L. L., 1952, *Brit. J. Phil. Sci.*, **3**, 243, 349.

The Excitation Function for the Reaction ^{9}Be(p, p2n)^{7}Be

By D. C. Salter and L. Bird
Atomic Energy Research Establishment, Harwell, Berks.

[Received September 11, 1953]

The excitation function for the reaction ^{9}Be(p, p2n)^{7}Be has been investigated for proton energies up to 155 mev. The internal proton beam of the Harwell cyclotron was scattered by a thin tungsten target and refocused on to a ' stacked foil ' target of beryllium and carbon plates ($\frac{1}{2}$ in. $\times \frac{1}{2}$ in. $\times \frac{1}{8}$ in.) and brass absorbers, which was placed in a position diametrically opposite the tungsten target and below the median plane of the cyclotron magnet. This method of irradiation, first used by Hintz and Ramsey (1952), selects a narrow band of proton energies from the normal wide spectrum of the internal beam. The carbon plates were used to monitor the proton flux through the stack by means of the ^{12}C(p, 3p3n)^{7}Be reaction, for which the excitation function is known (Dickson and Randle 1951).

The energy spectrum from the 0·005 in. thick tungsten scatterer at a radius of $47\frac{7}{8}$ in. had been investigated previously (Dickson and Salter 1953), and so the radial position of the ' stacked foil ' target for maximum intensity of the scattered beam was already known. The upper and lower limits of energy of the protons entering the stack were 156·8 and 155·3 mev respectively ; they were calculated from the radial positions of the scatterer and the targets ($47\frac{9}{16}$ in. to $47\frac{1}{16}$ in.), and the mean magnetic field along the scattering path. The range–energy curves of Aron, Hoffman and Williams (1949) were used to calculate the effective energies, and the spread of energies, of the protons traversing each plate. The range straggling of the protons was not an important source of energy spread.

For the irradiation, the height of the main beam was adjusted to $\frac{1}{2}$ in. using a ' chopper target ', and the stack was set 2 in. below the median plane of the beam, so that no part of the beam could strike either the stack or its attachments. The stack was irradiated for $2\frac{1}{4}$ hours and the active targets were loaded into identical sample holders, which completely enclosed them.

The decay of each target was followed for fifty days using a scintillation counter with a sodium iodide crystal ; at the end of this period the background count was less than 65% of the lowest target count observed. After a few days the logarithmic decay plots became straight lines, showing a half-life of approximately 53 days, characteristic of ^{7}Be decay (Segrè and Wiegand 1949). A source of ^{7}Be, chemically extracted from carbon after cyclotron irradiation, was counted each day with the active targets to check the performance of the counter. Since the same active isotope, ^{7}Be, was being counted in the beryllium and carbon targets in identical geometry, the absolute efficiency of the counter was not needed.

The errors shown in the figure are relative, and arise from errors in the $^{12}C(p, 3p3n)^{7}Be$ excitation function and statistical counting errors. In addition to these, there is an overall uncertainty of 8%, due to uncertainties in the ^{11}C half-life, the ^{7}Be branching ratio and the γ-ray efficiency ratio of the Geiger counter used in the $^{12}C(p, 3p3n)^{7}Be$ work.

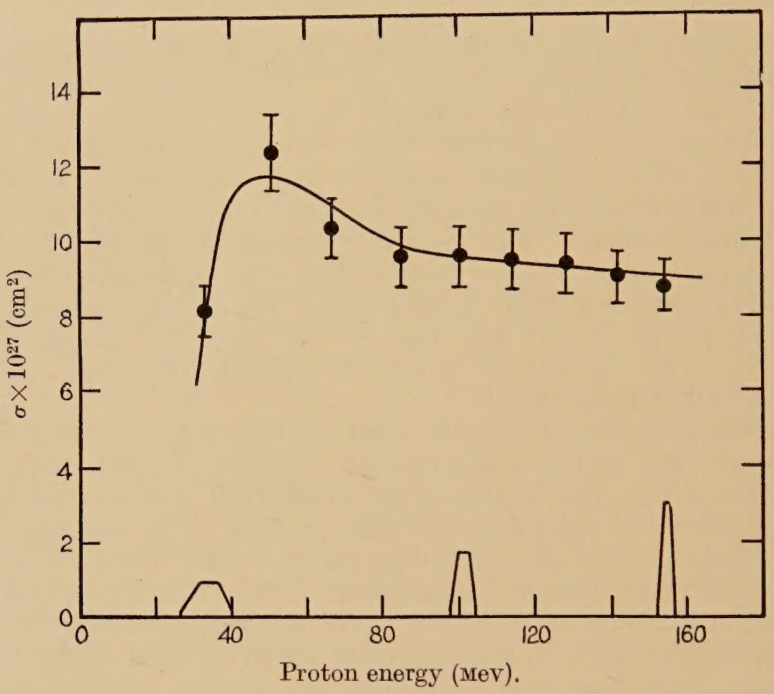

Excitation function for the $^{9}Be(p, p2n)^{7}Be$ reaction. The energy spectra for three beryllium targets are shown at the bottom of the graph.

The curve is in excellent agreement with the one point previously reported (Randle, Dickson and Cassels 1951) and should be of use for the monitoring of high energy proton bombardments of beryllium targets.

We should like to thank Mr. J. M. Dickson for his advice and interest throughout the experiment, and Dr. A. Blainey for providing the beryllium targets.

References

Aron, W. A., Hoffman, B. G., and Williams, F. C., 1949, *U.S. Atomic Energy Commission Reports*, A.E.C.U. 663.
Dickson, J. M., and Randle, T. C., 1951, *Proc. Phys. Soc.* A, **64**, 902.
Dickson, J. M., and Salter, D. C., 1953, *Brit. J. Appl. Phys.*, **4**, 175.
Hintz, N. M., and Ramsey, N. F., 1952, *Phys. Rev.*, **88**, 19.
Randle, T. C., Dickson, J. M., and Cassels, J. M., 1951, *Phil. Mag.*, **42**, 665.
Segrè, E., and Wiegand, C. E., 1949, *Phys. Rev.*, **75**, 39.

The Angular Distribution of the α-Particles from the ^{7}Li(p, α) *Reaction*

By D. K. Cartwright, L. L. Green and J. C. Willmott
University of Liverpool*

[Received September 24, 1953]

The angular distribution of the ^{7}Li(p, α) reaction has been the subject of several studies in recent years (Martin *et al.* 1949, Talbott *et al.* 1951, Hirst and Uebergang 1951).

The angular distribution of the α-particles is of the form

$$Y(\theta)=Y90(1+\cos^2\theta+B\cos^4\theta)$$

and the value of B at various energies is still rather uncertain. In the course of the setting up and checking of a piece of apparatus to study angular distributions we had occasion to investigate this reaction.

The α-particles were detected in a proportional counter which subtended a solid angle of 0·15% at the target, and the targets were less than 20 kev thick. The bombarding energy was electronically stabilized to 1 kv and the stabilizer was calibrated using the ^{19}F(p–γ) resonances (Lauritsen *et al.* 1950). The statistical errors on each count were of the order of 1% (about 20,000 counts in both the proportional counter, and a monitor counter at 90° to the beam). Counts were taken on both sides of the forward direction, and forward and backward at 90°.

The results of A and B obtained by means of a ' least squares ' analysis, together with their probable errors, P_A and P_B, are shown in the table for three different bombarding energies ; also shown are the results of Talbott *et al.* and Hirst and Uebergang in this energy region.

Author	Energy (kev)	A	P_A	B	P_B
a	600	1·22	0·08	−0·34	0·09
b	600	1·46	0·20	−0·13	—
		1·63	0·21	−0·27	—
c	610	1·39	0·05	−0·12	0·07
a	700	1·58	0·09	−0·31	0·10
b	700	1·83	0·29	−0·27	—
c	710	1·72	0·04	−0·18	0·05
a	800	1·85	0·08	−0·31	0·09
b	800	2·02	0·15	−0·22	—
c	800	2·08	0·05	−0·20	0·08

a—Talbott, Busala and Weiffenbach (1951).
b—Hirst and Uebergang (1951).
c—Present authors.

* Communicated by Professor H. W. B. Skinner.

Hirst and Uebergang do not give probable errors for B, but they should be of the same order as for A, and certainly not smaller. It will be seen that the probable errors of the results presented here are smaller by a factor of two to five than those of Hirst and Uebergang, who also used an electrical counting method. On the other hand, although the probable errors of Talbott *et al.* are only slightly larger than ours, these authors state that their errors are probably rather optimistic, as their results are compounded from several runs, the results of different individual runs showing wide variations. Hence the results presented here define the values of B, and of A, more closely, in this energy region, than heretofore.

We are grateful to Professor H. W. B. Skinner for helpful discussions. One of us (D.K.C.) thanks the Department of Scientific and Industrial Research for a maintenance grant.

References

Hirst, F., and Uebergang, R., 1951, *Aust. J. Sci. Res.* A, **4,** 284.

Lauritsen, W. F., Morrison, O., and Fowler, W. A., 1950, *Rev. Mod. Phys.*, **22,** 4, 291.

Martin, L. H., Bowers, J. C., Dunbar, D. N. F., and Hirst, F., 1949, *Aust. J. Sci. Res.* A, **2,** 25.

Talbott, F. L., Busala, A., and Weiffenbach, G. C., 1951, *Phys. Rev.*, **82,** 1.
